Structural and Kinetic Analysis of Carbon Fixation and Sucrose Metabolism in Sugarcane

Kristy Meyer

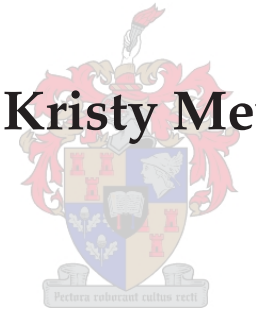

Thesis presented in partial fulfilment of
the requirements for the degree of Master of
Science (Biochemistry) at the University of
Stellenbosch

Supervisor: Prof J.M. Rohwer
Co-Supervisor: Prof J.-H.S. Hofmeyr
March 2008

Declaration

I, the undersigned, hereby declare that the work contained in this thesis is my own original work and has not previously in its entirety or part been submitted at any university for a degree.

_____

Signature

_____

Date

Summary

The aim of this study is the theoretical investigation of carbon fixation in sugarcane leaves. Sugarcane has a well known reputation for accumulating sucrose in the stalk to levels as high as 650 mM, almost a fifth of the plant's fresh weight. Although this is an efficient accumulating mechanism, there is an even more efficient 'carbon pump' found in C4 plants. This is a well documented carbon concentrating mechanism and one of the first to be studied. However scientists are still trying to understand the carboxylating mechanism and the regulation thereof. It has been speculated that this mechanism is at its saturation level and elevating carbon dioxide will have little or no effect on further carbon fixation. Futher, studies suggest that the sucrose accumulating sink is able to regulate photosynthesis. Therefore a regulatory mechanism should exist from the sink to carbon fixation in order for such regulation to occur. The work in this thesis therefore lays the foundation for investigating regulation of photosynthesis.

The field of systems biology is the study of cellular networks by assembling models. Pathways are considered as systems and not merely collections of single components. This allows the interaction of pathway metabolites and the regulation that they have on one another to be studied. The questions asked pertaining to a pathway, will determine the types of model analysis. Structural analysis is useful for studying stoichiometric models, determining characteristics like energy consumption, futile cycles and valid pathways through a system at steady-state. Kinetic analysis on the other hand, gives insight into system dynamics and the control exerted by the system components, predicting time-course and steady states.

In this thesis we begin to investigate photosynthesis in sugarcane leaves and the role it has in accumulating sucrose in the plant. Firstly, a structural model was developed incorporating carbon fixation, sucrose production in the leaf and

subsequent transport of sucrose to the storage parenchyma and accumulation. The model was analysed using elementary mode analysis, showing that there are twelve routes for producing sucrose with no pathway being more energy efficient than any other. Further, it highlighted a futile cycle transporting triose phosphates and phosphoglycerate between the two photosynthetic compartments in the leaf. In the storage parenchyma, many more futile cycles were revealed, many of them energetically wasteful. Three other sets of elementary modes describe sucrose's destination in either the vacuole or use in glycolysis or fibre formation, each with a different amount of required energy equivalents. The fourth set describes how sucrose cannot be converted to fibre precursors without also being used for glycolyis building blocks.

Secondly, a kinetic model of carbon fixation in the leaf was assembled with the primary goal of characterising this moiety-conserved cycle. This included the collation of kinetic data, incorporating volumes of the compartments and the areas of the location of the transporters into the model. This model was then analysed using metabolic control analysis. The model was able to predict metabolite concentration in the pathway at steady-state which were compared to those found experimentally. However, modifications need to be made to the model before further analysis is done so that the model predicted values match the experimental values more accurately. Time course analysis and response coefficients were also calculated for the carbon fixation cycle.

The work in this thesis therefore paves the way for understanding photosynthesis and its regulation in sugarcane leaves. Such work has the potential to pinpoint genetic engineering target points, allowing for better hybrid selection and propagation.

Opsomming

Die doel van hierdie studie was om die vaslegging van koolstof in die blare van suikerrietplante te ondersoek. Suikerriet is goed bekend vir die akkumulasie van sukrose in die stronk tot vlakke van 650nm, 'n vlak gelykstaande aan nagenoeg een vyfde van die plant se totale gewig. Alhoewel hierdie 'n effektiewe akkumuleringsmeganisme is, is daar 'n meer effektiewe 'koolstofpomp' teenwoordig in C4 plante. Die meganisme is 'n goed gedokumenteerde meganisme vir koolstof akkumulasie. Alhoewel dit een van die vroegste bestudeerde meganismes is, is wetenskaplikes steeds besig om die karboksilerings meganisme en regulering daarvan te ontrafel. Daar word gespekuleer dat die meganisme by 'n punt van versadiging verkeer en dat verhoogde vlakke van koolstofdioksied weinig of geen effek sal hê nie op koolstofvaslegging. Verdere studies wys dat fotosintese gereguleer kan word deur sukrose akkumulasie. As gevolg hiervan moet daar 'n meganisme bestaan wat koolstofvaslegging reguleer. Die werk saamgevat in herdie tesis poog om 'n fondasie te lê vir die teoretiese studie van hierdie regulatoriese meganisme.

'n Belangrike aspek van die veld van stelsels-biologie is die studie van sellulêre netwerke deur middel van wiskundige en rekenaar modelle. Metaboliese paaie word beskou as geïntegreerde netwerke en nie bloot as versamelings van individuele komponente. Dit laat die studie toe van die interaksie tussen metaboliese paaie en van die regulatoriese effek van metaboliete opmekaar. Hoe die modelle se gedrag geanaliseer word hang af van die vrae wat gevra word. Strukturele analise is geskik vir die studie van stoichiometriese modelle van kenmerke soos energieverbruik, futiele sikluse en geldige paaie van 'n stelsel in die bestendige toestand. Kinetiese analise aan die ander kant, verskaf insig oor die beheer wat uitgeoefen word deur verskillende komponente in die sisteem en voorspel tydsafhanklike gedrag sowel as bestendige toestandsgedrag.

Die tesis begin met 'n ondersoek ten opsigte van fotosintese in die blare van suikerriet en die rol wat dit speel in die algemene akkumulasie van sukrose in die plant. Eerstens is 'n strukturele model ontwikkel wat koolstofvaslegging, sukrose produksie in die blaar, sowel as die vervoer en akkumulasie daarvan in die parenchiem beskryf. Die model is deur analise van elementêre modusse. Die analise het getoon dat daar twaalf paaie van sukrose produksie is, maar dat geen een van die twaalf paaie meer effektief as die ander is nie. Die analise het ook getoon dat daar 'n futiele siklus is wat triose fosfate en fosfogliseraat vervoer tussen die twee fotosintetiese kompartemente in die blaar. In die parenchiem, wat as stoorplek vir sukrose gebruik word, is daar heelwat meer futiele sikluse ontdek waarvan 'n hele aantal energie vermors. Drie ander stelle elementêre modusse beskryf sukrose se bestemming as die vakuool, vir gebruik in glikolise of vir die produksie van vesel. Die drie bestemmings benodig verskillend energie ekwivalente. Die vierde stel modusse beskryf hoe sukrose nie na boustene vir vesel omgeskakel kan word sonder om ook as boustene vir glikolise te dien nie.

Tweedens is 'n kinetiese model van koolstofvaslegging in die blaar ontwikkel met die primêre doel om die gekonserveerde siklus te karakteriseer, om die kinetiese data te orden en te ondersoek, sowel as om volumes aan die verskillende kompartemente te inkorporeer. Die model is geanaliseer deur gebruik te maak van metaboliese kontrole analise. Die model kon die metabolite konsentrasies in die pad in die bestendige toestand voorspel. Hierdie waardes was vergelykbaar met die wat eksperimenteel verkry is. Daar word egter aanbeveel dat die model aangepas word sodat dit eksperimentele waardes meer akkuraat kan voorspel. Tydafhanklike analise en reponskoëffisiënte is ook bereken deur gebruik te maak van die model.

Die werk in die tesis baan dus die weg vir 'n dieper begrip van fotosintese en die regulerende rol daarvan in suikerrietplant-blare. Hierdie tipe ondersoeke kan lei tot spesifikasie van teikens vir genetiese manipulasie wat gebruik kan word om beter hibriede te selekteer en te kweek.

List of Figures

List of Tables

List of Abbreviations

Metabolites

ALA	Alanine
ASP	Aspartate
CO_2	Carbon Dioxide
DHAP	Dihydroxyacetone Phosphate
E4P	Erythrose 4-Phosphate
FBP	Fructose-1,6-Bisphosphate
F6P	Fructose-6-Phosphate
BPG	1,3 Bisphosphoglycerate
PGA	Phosphoglycerate
HCO_3^-	Hydrogen Carbonate
MAL	Malate
OAA	Oxaloacetate
PA	Pyruvate
RuBP	Ribulose-1,5-Bisphosphate
R5P	Ribose 5-Phosphate
SBP	Sedoheptulose 1,7 Bisphosphate
S7P	Sedoheptulose 7-Phosphate
PEP	Phosphoenolpyruvate
Ru5P	Ribulose-5-Phosphate
TRP	Triose Phosphate
Xu5P	Xylulose 5-Phosphate

Enzymes

ADK	Adenylate Kinase
ALAT	Alanine Aminotransferase
ALD	Aldolase
ASAT	Aspartate Aminotransferase
AWI	Cell Wall Bound Invertase
CA	Carbonic Anhydrase
FBP	Fructose 1,6-bisphosphatase
FRK	Fructokinase
GAPDH	Glyceraldehyde 3-phosphate dehydrogenase
HK	Hexokinase
PGK	Glycerate 3-Phosphate Kinase
NPMDH	NADP-Malate Dehydrogenase
NPME	NADP-Malic enzyme
NI	Neutral Invertase
PEPCase	Phosphoenolpyruvate Carboxylase
PFK	Phosphofructokinase
PFP	Pyrophosphate:Fructose 6-phosphate Phosphotransferase
PPI	Phosphopentose Epimerase
PPK	Pyruvate Phosphate Dikinase
PPP	Pyrophosphatase
PPPE	Ribulose 5-Phosphate 3-Epimerase
PRK	Phosphoribulokinase
RPI	Ribose 5-Phosphate isomerase
Rubisco	Ribulose 1,5-bis phosphate carboxylase-oxygenase
SBPase	Sedoheptulose 1,7-bisphosphatase
SPS	Sucrose-phosphate Synthase
SPase	Sucrose phosphorylase
SuSy	Sucrose Synthase
TPI	Triose Phosphate Isomerase
TRK	Transketolase
UDP PPase	UDP-glucose pyrophosphatase
UDPGDH	UDP-glucose dehydrogenase

General Abbreviations

CC	Calvin Cycle
EM	Elementary Mode
ExPA	Extreme Pathway Analysis
FBA	Flux Balance Analysis
MCA	Metabolic Control Anaylsis
PCR	Photosynthetic Carbon Reductive Cycle
SDA	Supply-Demand Analysis

For My Father

In Loving Memory of Betty Meyer.

And certainly not least of all
To Dad, Mom, Lindi and Julie.

Acknowledgements

- Professor Johann Rohwer
  Thank you for always having an open door, for your advice and insight. Also, thank you for always calming me down and giving me inspiration.
- Professor Jannie Hofmeyr
  Thank you for your valuable input.
- Lafras Uys
  Thank you for your advice, guidelines and patience.
- Dr Julian Westoll
  You have helped me in so many ways, thank you!
- Amy Baier
  You have always been there, thank you!
- National Bioinformatics Network
  Thank you for your support in the form of a Master's bursary.

Contents

Chapter 1

Introduction to the Sugarcane Project

The essence of the 'sugarcane project' is a theoretical study of sucrose metabolism in sugarcane. Both industry and pure biochemistry research have focused on this efficient photosynthesising plant. A high sucrose yield in sugarcane is important industrially as the demand for sucrose needs to meet the supply and because prices are set according to the amount produced per year. The already established industry bases its yield on year to year conditions – depending on temperature, soil conditions and location of the plantation. However, biochemically, scientists look to the enzymes present in the plant and the effect they have on the overall yield of the plant. Understanding the sucrose accumulating mechanism in this instance would not only have implications for sugarcane and increasing its yield but possibly also for other food and biofuel crops. Experimentally, plants such as sugarcane are useful subjects of study. Compartmentation of pathways between the mesophyll and bundle sheath cells allows scientists to isolate a compartment with a specific pathway in mind (e.g. the Calvin cycle exists in the bundle sheath stroma only). These data thus collected from these isolated pathways are incredibly valuable to theoretical scientists looking to characterise a pathway and predict how it works.

In the field of computational systems biology, models are assembled that can mimic cellular networks such as signal transduction pathways, gene regulatory networks and metabolic pathways. Data that characterise the interaction of enzymes with their substrates and products in a pathway are collected and assembled into a model that can predict functions, roles and outcomes of a subject pathway. For example, the work by Rohwer and Botha [96] emphasised theoretical futile cycling and its control in sugarcane medium mature tissue. The model pre-

diction that 22% of futile cycling occurs in sugarcane culm is supported by the experimental evidence, showing 20% futile cycling [127]. This foundational work in the storage parenchyma was extended by Uys [119], to include storage of sucrose in the vacuole, together with sucrose degradation for fibre formation and glycolysis. The model predicted that futile cycling decreases as internode maturity increases and that sucrose is not stored in the storage parenchyma cytoplasm which has also been shown experimentally [127]. This work has now laid the foundation for the investigation of the source of sucrose and whether increasing the source concentration might increase the sink accumulation.

The work in this thesis begins to shed light on the process of photosynthesis in the leaf, the origin of sucrose in the plant. This is not only the first step in understanding the carboxylating mechanism but also aids in understanding the regulation of sucrose from when it is produced in the leaf until storage in the paranchyma vacuoles. It is questionable whether producing a model will be able to predict the control of carbon fixation and whether this flux can be upregulated to the extent that sucrose accumulation will in fact increase too. However, predicting such outcomes would have an insightful and profitable impact on the genetic engineering of sugarcane, biochemically and industrially.

The work described in this thesis has the following aims:

- building a structural model to characterise photosynthesis and sucrose accumulation,
- assessment of the above model using structural analysis,
- construction of a kinetic model characterising carbon fixation in the leaf, and
- analysis of the steady-state using metabolic control analysis.

This thesis consists of five chapters. Chapter 2 gives an overview of sugarcane in the plant kingdom and its photosynthesising pathways, whereas Chapter 3 outlines strategies for modelling and analysing plant metabolism. This review work is then used to assemble and analyse a structural model composed of carbon fixation and sucrose accumulation in Chapter 4. A more detailed look at the kinetics of carbon fixation in the leaf is presented in Chapter 5, and in Chapter

6, the structural and kinetic models are concluded and discussed, together with proposed future work.

Chapter 2

Sugarcane in the Plant Kingdom

This Chapter serves to place *Saccharum officarium* (sugarcane), the subject of our study, into the context of the plant kingdom (Sections 2.1 & 2.2). It further gives insight into sugarcane's ability to produce sucrose, which contributes to its well-known reputation of a high sucrose yield (Sections 2.2.1 - 2.2.3). Produced sucrose is transported from the leaves to the rest of the plant for utilisation or storage (Sections 2.2.4 & 2.2.5). These pathways and metabolites are featured in the models described in Chapters 4 and 5.

The plant kingdom consists of three plant types, i.e. C3, C4 and CAM plants (Figure 2.1). Carbon fixation is essential for the growth and photosynthate production of any plant. The types of plants are therefore categorised according to the carboxylating mechanism. The most abundant, C3 plants, have one carboxylating mechanism which fixes carbon in a single cell type via the Calvin cycle. CAM plants are less common than C3 plants but are similar to C4 plants in their approach to fixing carbon. Both have two carboxylating mechanisms but differ in their approach in using them. In C4 plants, the two carboxylation steps occur between two different cell types, whereas CAM plants separate the process over time. This partitioning of carbon between two cell types allows C4 plants to concentrate carbon in the bundle sheath up to 30-75 μM, whereas C3 plants can only acumulate as little as 7-8 μM within their single cell type [60].

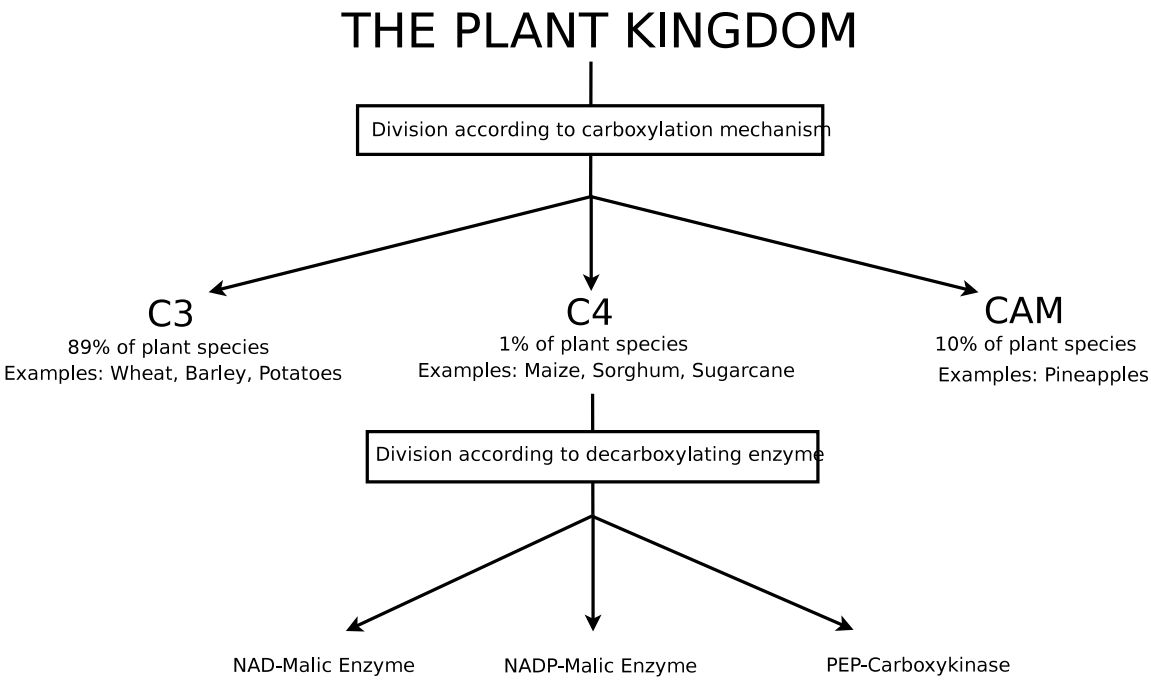

Figure 2.1: The Plant Kingdom showing where C4 plants occur. C4 plants are classified by their decarboxylating mechanism resulting in three subtypes. Sugarcane falls in the subtype, NADP-ME.

2.1 C4 Plants

C4 species are aptly named due to the initial fixation products being dicarboxylic (C4) compounds. Within C4 plants, C3 compounds are carboxylated in one cell type and transported to another cell type to be decarboxylated and are then shuttled back. This partitioning of carbon gives C4 plants the ability to concentrate carbon to levels many times higher than ambient levels, especially under tropical conditions [60]. The following criteria are required to be considered a C4 plant but are also responsible for the C4 plants ability to accumulate carbon: (i) Kranz anatomy, the arrangement of photosynthetic cells, must exist (Section 2.2), (ii) C4 acids should be the initial product of carboxylation, (iii) fixation of CO_2 must be in the light and (iv) the decarboxylated carbon is fed into the Calvin cycle [104]. Soros and Dengler [107] further describe requirements as: (i) "two types of photosynthetic cells", (ii) "orientation of photosynthetic cells", (iii) "pathway length between the photosynthetic cells" and (iv) "structural modifications limiting carbon leakage".

The above modifications seen within the C4 species allow C4 plants to be classified in the category of the most efficient photosynthesising species. C4 plants are unique in that they are usually characterised by high photosynthetic and growth rates as well as the highest carbon to sucrose ratio [70]. That is, a large portion of the carbon taken up by C4 plants is allocated to the production and accumulation of sucrose, substantially more than other plants. Within this group, the species can be subtyped according to the decarboxylating mechanism in the plant (Figure 1). There are three subtypes:

- NAD-malic enzyme (NAD-ME, e.g. *Panicum miliaceum*)
- Phosphoenolpyruvate carboxykinase (PEP-CK, e.g. *Urochloa panicoides*)
- NADP-malic enzyme (NADP-ME, e.g. *Zea mays, Saccharum officarium*)

Since the focus of this work is sugarcane, only NADP-ME plants are considered in further detail here.

2.2 NADP-ME Plants

NADP-ME plants are named according to their decarboxylating enzyme contained in the bundle sheath chloroplast. The two photosynthetic tissue types are the mesophyll and bundle sheath cells (Figure 2.2). Carbon first enters the plant via stomata, and it is then fixed by phosphoenolpyruvate carboxylase, the first carboxylating enzyme in the mesophyll cytoplasm. Shuttles in C4 plants serve to transport fixated carbon from the mesophyll to the bundle sheath cells. NADP-ME decarboxylates the shuttle metabolites which then feeds the carbon to the second carboxylating enzyme, Rubisco (Calvin cycle).

One of the most efficient photosynthetisers within C4 plants is sugarcane. Sugarcane is so efficient that nearly 20% of its fresh weight can be accumulated as sucrose [63]. Sucrose levels as high as 650 mM have been found in sugarcane stalks [94] and approximately 70% of the world's sucrose is produced from sugarcane. The ability of the plant to concentrate carbon lies within the biochemical and anatomical adaptations found within the anatomy of the C4 plants. The two types of photosynthetic cells are never more than one cell apart and have a concentric flower-shaped arrangement known as Kranz anatomy (Figure 2.2) [107]. This partitioning allows sugarcane to have physiological features such as high

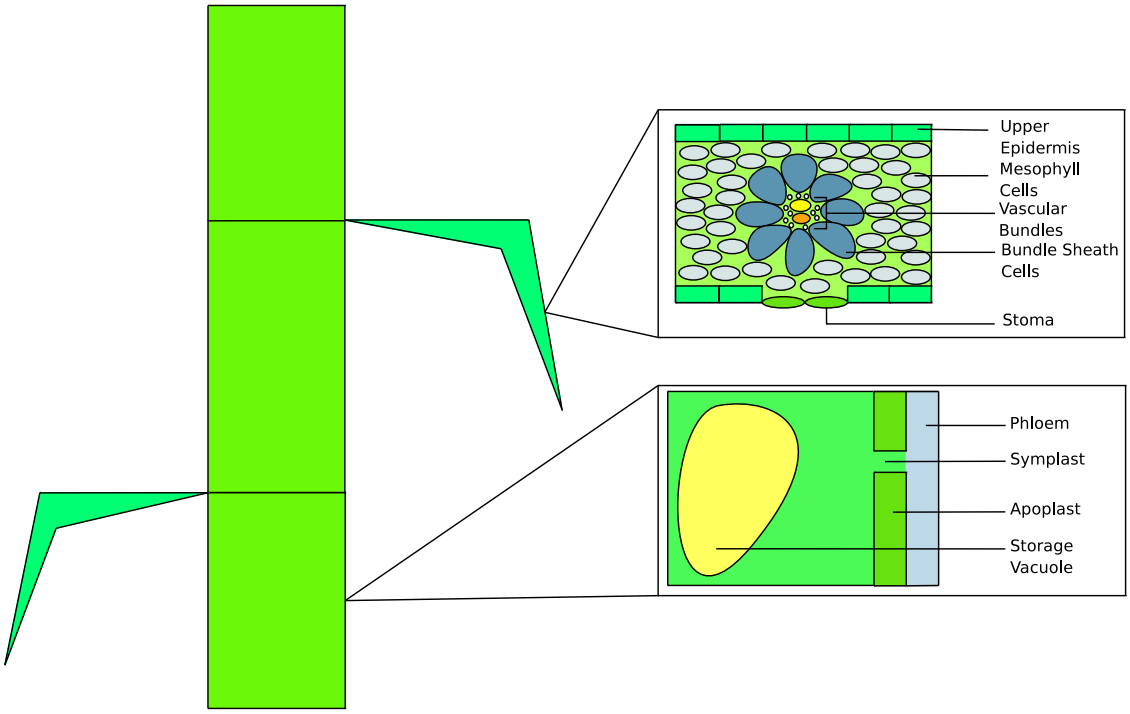

Figure 2.2: The anatomy of sugarcane. There is one leaf per internode. The leaf contains mesophyll cells and bundle sheath cells, surrounding the vascular bundles. Within the stalk is the storage parenchyma which consists of the phloem feeding photosynthate symplastically or apoplastically into the storage parenchyma cytosol.

light saturated photosynthesis rates, the absence of effects by oxygen during photosynthesis and the almost negligible photorespiration [25]. However, in order to grasp how this efficient photosynthesiser works, one needs to look at the components of this system to understand the photosynthate accumulating mechanism. The overall reaction for the mechanism is the uptake of carbon to produce photosynthate via photosynthesis in the leaf. The photosynthate is then transported via the phloem into the stalk for storage or utilisation (Figure 2.3).

2.2.1 Photosynthesis

The leaf is the site of photosynthesis (Figure 2.2). Photosynthesis is the light driven process of carbon fixation and photosynthate production. However, within photosynthesis are two types of reactions, light and dark reactions. Light reactions produce ATP and NADPH, whereas the dark reactions consume ATP and

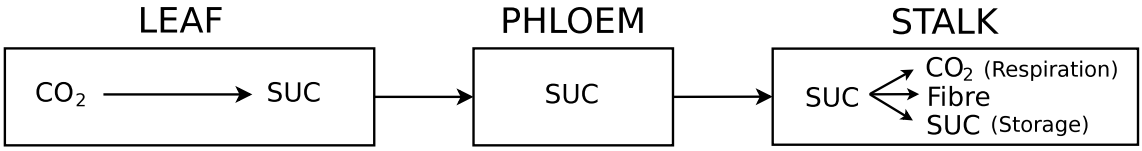

Figure 2.3: The net reaction of photosynthesis to the production of photosynthate, which is then transported to the stalk for accumulation or utilization.

NADPH, requiring 5 ATP and 2 NADPH for every 1 CO_2 fixed. The terms "light" and "dark" may be somewhat misleading though, as they do not refer to night and day but rather to light dependence and independence.

Light Reactions The light reactions occur within photosystems (PS) I and II in the thylakoid membrane. PSI and PSII allow the photoreduction of $NAPH^+$ to produce NADPH [37]. PSII is connected to cytochrome b_6f complex which is connected to PSI. Electrons flow through the protein complexes via mobile electron carriers generating NADPH from the oxidation of H_2O. The overall reaction is

$$2NADP^+ + H_2O \rightleftharpoons 2NADPH + O_2 + 2H^+$$

where PSII generates O_2 and PSI generates NADPH [120].

Dark Reactions The dark reactions consist of the fixation of carbon dioxide to produce photosynthate. Carbon fixation in the C4 pathway occurs via two shuttles in sugarcane, the malate/pyruvate (MAL/PA) and alanine/aspartate (ALA/ASP) shuttle (Chapter 4), serving to increase the level of carbon entering the Calvin cycle. The current level of atmospheric carbon dioxide is viewed as a limiting step in photosynthesis [122]. With the shuttles found in sugarcane, the shortcomings of low atmospheric carbon dioxide levels are overcome and photosynthesis is said to be near saturation. Hence, a rise in atmospheric levels of CO_2 should have little or an insignificant impact on C4 photosynthesis [122].

Together, the shuttles can concentrate the levels of carbon in the bundle sheath chloroplast to 75μM, many fold higher than ambient levels [60]. However, these levels can be influenced by a number of factors [60]:

- temperature, influencing the solubility of CO_2;

- the intercellular CO_2 partial pressure;
- the diffusion of C4 metabolites from the mesophyll cells;
- the decarboxylation process;
- the carboxylation via Rubisco; and
- the leakage of CO_2 from the bundle sheath cells.

The shuttles and anatomy play a large role in sustaining high carbon levels. However, the partitioning of carbon and elevated levels of carbon also play a role in sugarcane's high photosynthetic rates.

2.2.2 Carbon Partitioning

Carbon is partitioned between mesophyll and bundle sheath cells, which are each further compartmentalised into cytoplasm and chloroplasts. This aids in sugarcane photosynthesis by:

- preventing inhibition of decarboxylation,
- preventing loss of carbon,
- preventing photorespiration,
- allowing $\sim 10\times$ higher levels of carbon than ambient levels, and
- continuation of photosynthesis under stress conditions.

Inhibition of decarboxylation The majority of carbonic anhydrase (CA) occurs in the mesophyll cytoplasm where CO_2 equilibrates with HCO_3^-. Studies by Burnell and Hatch [9] on *Zea mays* show that approximately only 1.6% of the total amount of CA resides in the bundle sheath cells. The partitioning of CA from the bundle sheath chloroplast ensures that only CO_2 in its disolved gaseous state can exist in this compartment [9, 11]. In sugarcane, HCO_3^- is found to be inhibitory to the decarboxylation process in the bundle sheath chloroplasts [53].

Carbon loss The amount of CO_2 fixated depends on the irradiance where photosynthesis is at its optimal peak near full sunlight [70]. The level of fixed carbon can be maintained in the bundle sheath chloroplast as the bundle sheath cell is said to be gas tight, therefore minimising CO_2 loss.

Prevention of photorespiration and continuation of photosynthesis High levels of CO_2 are important for 2 reasons: (i) inhibiting photorespiration and (ii) continuation of photosynthesis when stomata are closed. The relationship between the anatomical adaptation and the biochemistry of the pathway form a very delicate balance for concentrating CO_2 and protecting the plant against the harmful effects of Rubisco's oxygenase reaction as well as the coupled photorespiration [16, 67]. High levels of CO_2 inhibit the oxygenase activity of Rubisco and hence photorespiration [60] to the point where in sugarcane it is said to be negligible [25]. If photorespiration were to occur, it would minimise carbon fixation to the point where it would almost become insignificant [60]. This suppression therefore allows C4 plants to have a higher productivity potential than C3 plants, but the drawback is the additional ATP per CO_2 fixed required by C4 plants. Secondly, high levels of carbon mean that although the stomata may be closed during water loss conditions, photosynthesis can still occur [70].

Futher prevention of photorespiration There are two types of chloroplasts found within the leaf, granal and agranal. Granal chloroplasts, found in the mesophyll, contain PSI and PSII, whereas agranal, found in the bundle sheath, only have PSI. This adaption exhibited by the bundle sheath chloroplast also prevents photorespiration. The lack of PSII means that no O_2 is generated within the bundle sheath chloroplast. Rubisco, the carboxylating enzyme within the Calvin cycle, has an affinity for both O_2 and CO_2. Therefore, if O_2 were to occur within the bundle sheath chloroplasts, it would have devastating effects on photosynthesis. Further, the lack of PSII means that no NADPH is generated within the bundle sheath chloroplast, which is required by the Calvin cycle in producing triose phosphates for photosynthate production.

Although compartmentation allows high levels of carbon accumulation, limits photorespiration and loss of carbon in the bundle sheath of chloroplast, the processes require movement of metabolites. Due to the lack of PSII within bundle sheath chloroplasts, reducing equivalents can either be delivered to the bundle sheath chloroplast via the MAL/PA shuttle or metabolites can be transported to mesophyll cells.

2.2.3 Transport

Transport is vital for carbon fixation in C4 plants. Due to the Kranz anatomy, the movement of metabolites between the two cell types has been dubbed 'co-operative photosynthesis' by Karpilov (1970). The rate of transport between the two cell types is comparable to the rate of photosynthesis, approximately 5 μmol min^{-1} (mgChl)$^{-1}$ [123]. Two types of transport can occur, i.e. intercellular and intracellular.

Intercellular This is the transport of metabolites between the mesophyll and bundle sheath cells. Predominantly malate (MAL), pyruvate (PA), aspartate (ASP) and alanine (ALA) are shuttled between the cell types. However, 3-phosphoglycerate (PGA) and triose phosphates (TRP) can also diffuse between the cell types as well as between the cytoplasm and chloroplast (more in intracellular transport). MAL and ASP move from the mesophyll to the bundle sheath, upon which they are decarboxylated to PA and ALA respectively and move back to the mesophyll. The MAL/PA shuttle does not only deliver carbon between the two cells, but also serves a secondary role. It is able to deliver reducing equivalents via the decarboxylation process in the bundle sheath chloroplasts, which are then used for the production of TRP in the Calvin cycle, directly linking the decarboxylation phase and the Calvin cycle [10].

The interface between the mesophyll and bundle sheath needs to be dynamic enough to allow the transport of the necessary metabolites whilst not allowing a large loss of inorganic carbon from the bundle sheath [123]. Rapid flux between the cells is made possible by the many plasmodesmata as well as the high concentrations of the transported metabolites [32, 39]. Intercellular transport primarily occurs via the plasmodesmata and no apparent symplastic connection has been found [83]. Theoretical calculations based on plasmodesmata frequency by Osmond [85] report that MAL and PA diffusion fluxes require a concentration gradient of 10^{-3} to 10^{-2}M [85, 39] and the loss of carbon to be as high as 10% [25, 39]. Weiner *et al.* [123] however report new findings to suggest that as much as 30% of inorganic carbon delivered to the bundle sheath is leaked back into the mesophyll cells. To maintain the rate of photosynthesis (at 3 μmol min^{-1} (mgChl)$^{-1}$), a 2 mM gradient needs to be maintained for the diffusion of MAL from the mesophyll to bundle sheath cells [123].

Due to the nature of the diffusion through the plasmodesmata, large concentration gradients of metabolites are seen between the mesophyll and bundle sheath cells. Depending on the cell type and the metabolite, these gradients are maintained by the uptake of MAL and PA into the respective chloroplasts. That is, the bundle sheath is continually taking up MAL, hence there is a low level of MAL in the bundle sheath cytoplasm. Likewise, a low level of PA is seen within the mesophyll cytoplasm and chloroplast. Both these instances are due movement via specific transporters across the chloroplasts [3].

Intracellular The transport of metabolites across the chloroplast membrane is an important function in maintaining the rate of photosynthesis. Intracellular transport differs depending on the metabolite and its location. Specific transporters within the C4 species transport metabolites such as PGA, phosphoenolpyruvate (PEP), TRP, MAL, oxaloacetate (OAA) and PA. Within the chloroplast, the inner membrane is permeable to CO_2 but is impermeable to ions, whereas the outer membrane is permeable to small molecules. Therefore, due to the inner membrane forming a functional barrier between the cytoplasm and stroma, the chloroplast transports metabolites and ions in opposite directions [45]. Three transporters exist within C4 plants:

- Dicarboxylate transporter
- Phosphate transporter
- ATP transporter

The Dicarboxylate Transporter transports the C4 acids, MAL and OAA, across the chloroplast membranes. However, the MAL transporter in the bundle sheath chloroplast has yet to be characterised. Studies in spinach chloroplasts indicate that this transporter is different from dicarboxylate transporters in C3 chloroplasts [45]. It was originally thought that MAL and OAA were transported by the same by translocator [22]. Due to the equilibrium constant of the malate dehydrogenase catalysed reaction ($K_{eq} = 3 \times 10^{-4}$) [123], the cellular concentration of MAL needs to be many-fold higher than OAA, making it unlikely that they share a translocator [22]. Dicarboxylate transport can also occur as a counter-exchange which is not necessarily coupled. Unpublished data by Lehner and Heldt cited in

[45] show that the rate of co-transport can be two orders of magnitude lower than counter-transport. Many of these transporters are also light activated. Flugge *et al.* [21] show that light plays a role in increasing the V_{max} but not the K_m for PA uptake in maize bundle sheath chloroplast [21, 81].

The Phosphate Transporter is an inorganic phosphate translocator. It is regarded as different to that found in C3 due to the additional capacity to transport PEP [80]. The transporter is found in both the mesophyll and bundle sheath chloroplasts transporting PGA and TRP. Light appears to affect the maximum activity of the mesophyll phosphate transporter and not that found in the bundle sheath [80]. It is is highly specific in that it requires P_i or a three carbon molecule which has a phosphate esterified on the end. The phosphate translocator is also temperature sensitive and can be up to five-fold more active at $20^{\circ}\mathrm{C}$ than at $4^{\circ}\mathrm{C}$ [45].

The ATP Transporter is highly specific for ATP. However, it can also transport ADP, AMP, UTP and other nucleotides, but at a much lower rate. Even when transporting ATP, it is still two-fold slower than the phosphate transporter. The hypothesised role of this transporter is to provide ATP to the dark phase in the chloroplast [45].

The transport and diffusion of metabolites are essential for maintaining metabolites levels in different compartments and allowing effective functioning of the C4 pathway. The overall function is carbon fixation to sucrose precursors, leading to the most important metabolite, sucrose. In the initial step in Figure 2.3, the leaf fixes CO_2 to produce sucrose. The next step is the transport of sucrose.

2.2.4 Phloem Loading and Unloading

Sucrose is the primary photosynthate in sugarcane [31]. C4 plants have an effective and efficient manner of transporting sucrose from the leaves. Due to the anatomy of sugarcane (Section 2.2), sucrose does not have to travel far in order to diffuse into the phloem for transport [36]. The sucrose moves into the phloem and is driven by a concentration gradient [7]. Once sucrose reaches its destination, it is unloaded from the phloem and enters the storage parenchyma apoplastically or symplastically (Chapter 4). This then leads to the final step in Figure 2.3, i.e.

the utilization of sucrose in the storage parenchyma.

2.2.5 Storage Parenchyma

Sucrose entering the storage parenchyma has three destinations (Figure 2.3). Firstly, the storage parenchyma contains many vacuoles which occupy up to 90% of the total volume and sucrose is mainly accumulated here against a sucrose concentration gradient [98]. Alternatively, sucrose is broken down to triose phosphates to be used in respiration, or hexose phosphates to be used for fibre formation (Chapter 4).

2.3 Concluding Remarks

This Chapter has presented an overview of sucrose metabolism in sugarcane whereas Chapter 3 gives background to the analysis tools required in later Chapters. In Chapter 4, the focus is on metabolite reactions and the structural analysis of the stoichiometry model, whereas in Chapter 5, a more in depth focus is placed on the enzymes of carbon fixation and their kinetic analysis.

Chapter 3

Modelling of Cellular Systems

In trying to understand the functioning of the cell, scientists have traditionally taken it apart, thinking that if the cellular components are understood, the whole will be understood as well. However, it is increasingly being recognised that this is not sufficient and that it is also necessary to address the interaction and regulation of the components in the physiological context of the entire system [103, 105]. In the field of computational systems biology, the individual information from each component is collected and built into a model to describe cellular processes with the hope of eventually being able to accurately represent an entire cellular system [61, 109]. The following outlines a few reasons why systems are modelled as a whole.

3.1 Reasons For Modelling

Understanding a phenomenon Core models are developed to understand a particular phenomenon. In these models, the level of detail is simplified and an arbitrary parameter set is given so that only the systemic properties can be observed, which are due to a particular model structure or arrangement.

Mimicking experimental behaviour Detailed models are built to mimic behaviour seen experimentally. In the case of kinetic models of metabolism, enzymes are modelled explicitly. This allows scientists to work in a 'virtual laboratory' without the technicalities and expense of running experiments [91] where the subject model can be manipulated and the behaviour monitored accordingly. These models aid in predicting behaviour in a system including (i) valid path-

ways in a network, (ii) enzymatic control and regulation within a system, (iii) oscillations, (iv) signal transduction and (v) gene regulation. Built on this is the collation of these models in the pursuit of building a complete cellular system dubbed the in Silicon Cell Project [106]. Databases of these models include: JWS online (http://jjj.biochem.sun.ac.za) or Biomodels (http://www.ebi.ac.uk/biomodels/).

Highlighting areas of interest Models also allow the identification of areas of interest. These include (i) identifying genetic manipulation target points (ii) highlighting unexpected features/functions of a network and (iii) formulating testable hypotheses [108].

Therefore the investigator's questions and the level of detailed information required in order to answer the questions determine the type of model assembled. These include, in increasing level of detail:

- Phenomenological models
- Structural models
- Kinetic models

3.2 Types of Models

Phenomenological This is a general model that does not take kinetic data of the individual components into account. Instead, formulae are applied to characterise a general observable property of a system. Although most of these models are unable to be derived from theory, they do however use laws and principles associated with theories. This approach merely allows the data to extrapolated and the model therefore makes a prediction but does not explain the model. Models, revelant to plant physiology that have been characterised using this approach include: the C4 pathway [121], structure and allometry of plant vascular systems [126] and photosynthesis [62, 71]. However, for the purpose of this thesis, these models will not be further discussed.

Structural A structural model is a quantitative approach, built using only the stoichiometries of the reactions. By investigating the topology of a given net-

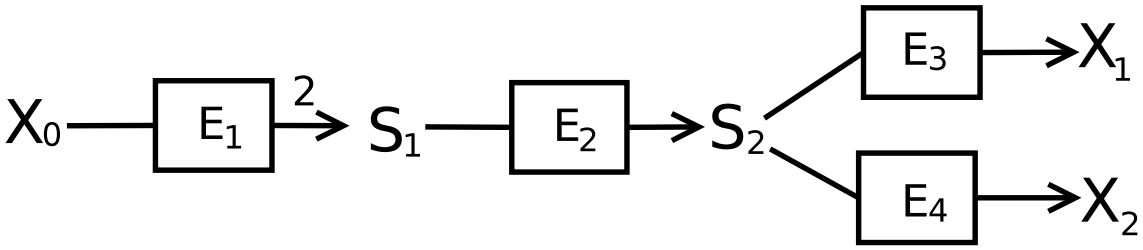

Figure 3.1: A simple pathway illustrating the conversion of X_0 to either X_1 or X_2.

work, one can determine its properties using structural analysis. Aspects that are highlighted in a model include futile cycles and valid pathways at steady-state. Structural models revelant to this thesis are (see Section 3.3.4): the Calvin [90, 91] and TCA cycle [109].

Kinetic A kinetic model is a mechanistic based approach where the behaviour of each species in a system is characterised by a set of differential equations [110]. Models are built using parameters, variables, enzyme kinetics and rate equations to establish the flux through the system and the concentrations of the variable species [77]. Kinetic models that are revelant to this thesis include (Section 3.3.4): the Calvin cycle [88], sucrose accumulation [96, 119] and C4 photosynthesis [54].

3.2.1 Development of Models

Development of models has been discussed in [1, 77, 86]. The following simple network is used to describe the model components (Figure 3.1).

External metabolites which are either the source or sink, are illustrated as 'X' and assumed to be independent of the system's enzymes, having constant concentrations to allow steady-state conditions. Metabolites between the external metabolites are illustrated as variables, 'S'. The enzymes catalysing the reactions are illustrated as 'E'. Enzymes in the system are characterised using rate laws to describe their behaviour and integration in a system. The most common known kinetic law is the Michaelis-Menten equation. However, this is only accurate for uni-subtrate and uni-product enzymes and therefore falls short of describing multiple binding enzymes [12]. It further fails to account for cooperative enzymes or allosteric modifiers. Therefore many more laws have been developed to accu-

rately describe these attributes, including the irreversible [46] and reversible [29] Hill and Monod, Wyman and Changeux [76] equations. More recently, generic equations have been shown to accurately describe the kinetics of enzymes with unknown binding mechanisms [29, 97].

The set of differential equations that make up the model can be presented in the matrix form:

$$\frac{d\boldsymbol{S}}{dt} = N \cdot \mathbf{v} \tag{3.1}$$

where **S** and **v** are the m- and n-dimensional vectors of metabolite concentrations and reaction rates respectively. N describes the stoichiometry matrix consisting of m rows and n columns to illustrate the number of internal metabolites and reactions respectively. Therefore, defining this for the network seen in Figure 3.1, the topology is described by matrix N, e.g.,

E_1	E_2	E_3	E_4	
-1	0	0	0	X_0
2	-1	0	0	S_1
0	1	-1	-1	S_2
0	0	1	0	X_1
0	0	0	1	X_2

Using equation 3.1, time-course analysis can be done. However, if the differential equation for S_1 and S_2 in equation 3.1 are set to zero, the steady-state of the system can be calculated for metabolite concentrations and fluxes and structural analysis of the system can be done.

Structural analysis is performed if kinetic data is limited with regard to enzyme kinetics. This analysis therefore investigates the stoichiometry of the system. Alternatively, if the former is available, interaction and regulation of enzymes within the system can be calculated using metabolic control analysis. Although the type of analysis that one can perform is largely determined by the available data, the purpose of these analysis tools is to allow scientists to answer questions about a system under investigation. Further, these analysis tools can also help determine whether a model is accurate and valid to represent a system (Section 3.3.3).

3.3 Analysis of Models

Structural and kinetic models each have their own types of analysis associated with them, which are reviewed briefly below.

3.3.1 Structural Analysis

Structural models can be analysed in terms of:

- calculating extreme pathways [128]
- flux balance analysis [61]
- elementary modes [100, 101, 102]

Extreme Pathways Extreme Pathway Analysis (ExPA) is a constraint-based modelling approach, using stoichiometry of the system alone. ExPA and flux balance analysis (FBA) are similar types of analyses that determine the flux distribution of a given pathway. They are also similar in that both are non-decomposable and each set that is defined is unique for the system [93, 99, 103]. However, ExPA determines all the possible steady-state pathways in a network whereas FBA determines the distribution of the flux at steady-state. Added to this, extreme pathways are found in a convex solution cone, are thought of as a subset of elementary modes and cannot be represented as a non-negative linear combination of any of the other pathways [87]. ExPA is useful in describing a system's robustness and flexibility as well as functional properties [103].

Flux Balance Analysis (FBA) is also a constraint-based modelling approach which allows the identification of flux distribution that maximises a stated objective function. However, the disadvantage is that the solution of the analysis is only as good as the constraints defining it. A model is built using the enzyme reactions, metabolites of a network as well as the stoichiometry and flux for each enzyme reaction. To date, this traditional approach to FBA has been extended to incorporate regulation, explicit incorporation of thermodynamics and alternative classes of objective functions [61, 93].

Elementary Mode Analysis Elementary modes are non-decomposable subsets of reactions that can carry a steady-state flux in a pathway [102]. It is an effective

tool for (i) identifying futile cycles, (ii) identifying valid routes through a pathway and (iii) calculating ATP consumption in a metabolic pathway. Elementary modes are therefore able to indicate for example whether there is a more energy efficient pathway for producing sucrose in sugarcane leaves. Further, they are also an indication of the richness of metabolic functions [89].

As elementary mode analysis is performed in Chapter 4, an example of such analysis is given using Figure 3.1. If the enzymes in the reaction pathway are reversible, three modes exist:

1. $X_0 \rightleftharpoons S_1 \rightleftharpoons S_2 \rightleftharpoons X_1$,
2. $X_0 \rightleftharpoons S_1 \rightleftharpoons S_2 \rightleftharpoons X_2$ and
3. $X_1 \rightleftharpoons S_2 \rightleftharpoons X_2$.

However if the pathway enzymes are irreversible, then only two modes exist:

1. $X_0 \longrightarrow S_1 \longrightarrow S_2 \longrightarrow X_1$ and
2. $X_0 \longrightarrow S_1 \longrightarrow S_2 \longrightarrow X_2$.

Calculating Elementary Modes METATOOL is an automated method for calculating elementary modes, basis vectors and enzyme subsets for a specified network topology [89]. It is written in C and is able to run on UNIX and MS-DOS platforms. The program requires an ASCII file which includes the reaction equation, internal and external metabolites, and the reversible and irreversible enzymes. The program outputs an ASCII file which include the following: the stoichiometry and null-space matrix, the total number of reaction and metabolites, the enzyme subsets in matrix and list form, the enzyme subset stoichiometry and the elementary modes. The elementary modes are calculated using a complex algorithm based on the Gauss-Jordan method for solving linear equations. This algorithm requires only the reaction equations and their reversibility information. The algorithm implemented by METATOOL is also implemented by ELMO in Turbo-pascal (Hilgetag), EMPATH in smalltalk (J. Woods, Oxford) and METAFLUX in MAPLE (Klaus Mauch, Stuttgart) [100]. METATOOL is open-source software and can be downloaded from ftp://bmsdarwin.brookes.ac.uk/-pub/software/ibmpc/metatool [89].

3.3.2 Kinetic Analysis

Each reaction in a pathway is given a Ordinary Differential Equation (ODE) which is used to characterise the behaviour of an enzyme. These ODEs can then be integrated and used to analyse a system. The following types of analysis can be performed on kinetic models

- Time-course Analysis
- Steady-state Analysis
- Metabolic Control Analysis (MCA)
- Parameter Scans
- Supply-Demand Analysis

to analyse models.

Time-course Analysis Time course analysis is the integration of ODEs to produce a time-course showing the change in a system's variables from time zero to steady-state or whatever final state the system is approaching. This is particularly interesting and useful, as one can for example determine the effect of the initial concentration of a starting metabolite on the rest of a system's initial metabolite concentrations that have been set to zero (Chapter 5).

Steady-state Analysis In steady-state analysis, the defined ODEs can also be solved for the variable's value at steady-state. This can then be also used to carry out a sensitivity analysis (metabolic control analysis). A system in steady-state carries a flux however the metabolite concentration remains constant with time. This analysis therefore determines the effect of its parameters, topology, stoichiometry and reactions rates on its steady-state.

MCA Metabolic control analysis determines the sensitivity of a system's fluxes and variable metabolite concentrations at steady-state [12, 47, 58]. It calculates the degree of control shown by enzymes on the system's variables when a pertubation is made and the system settles to a new steady-state. It can be calculated locally or globally in a system. Locally, elasticity coefficients are a change in the local enzyme's rate when either its substrate, product or parameter is varied.

Global properties can be calculated as response and control coefficients. Response coefficients are the change in a system's flux when a small perturbation is made to a parameter. Control coefficients are the amount of control an enzyme has to cause an effect on a system i.e. how sensitive is the entire system to a slight change in a specific enzyme [48].

Parameter Scans Parameter scans allow a modeller to visualise the effect of a parameter on a variable/s over a large change in the parameter value (decided by the modeller). It gives insight into the boundaries or effects of a parameter on a variable in the system. This is similar to response coefficients but the boundaries of the change in the parameter can be substantially larger.

Supply-Demand Analysis Supply-demand analysis is a quantitative approach to determine the integration of source and sink in a system. It therefore allows the behaviour and regulation of a system to be described in terms of elasticities of the supply and demand. The source (supply) and sink (demand) in a system interact via a linking metabolite. For example, in sugarcane, sucrose is produced in the leaf and transported to the storage parenchyma for use. Metabolic supply-demand analysis therefore would determine the effect of the leaf (supply) and the storage parenchyma (demand) on the linking metabolite, sucrose, as well as the flux linking the two [48].

3.3.3 Validation

Validation allows the modeller to determine the accuracy of the model developed, i.e. whether the system's behaviour is adequately captured. Further, it addresses the question whether the model can reproduce the variable values and steady-state fluxes seen experimentally [96].

Many of these analyses have been applied to models of plant metabolism. Below we describe a few examples and the insight gained from the analysis.

3.3.4 Examples of Plant Modelling Studies

Within the structural framework, we focus on:

- the Calvin cycle

- the Tricarboxylic Acid (TCA) cycle

Within the kinetic framework, the following will be discussed:

- sucrose accumulation
- the Calvin cycle

3.3.5 Structural Analysis

The Calvin cycle is the carboxylating pathway found in the chloroplast in C3 plants. However the chloroplast also consists of the oxidative pentose phosphate pathway. The pathways have many similarities but differ in regard to the thioredoxin system. The thioredoxin system reduces or oxidises disulfide bonds thereby regulating the oxidation state — and hence activity — of certain proteins. Therefore this system ensures that specific enzymes within the Calvin cycle are up-regulated whereas specific enzymes in the oxidative pentose phosphate pathway are down-regulated in light conditions. However, under dark conditions, the converse is true. With this in mind, Poolman *et al.* [91] conducted studies on the Calvin cycle and oxidative pentose phosphate pathway and their effect on starch degradation under light and dark conditions. Using elementary mode analysis, the following conclusions were drawn from the model [91]

1. triose phosphates cannot be produced from the degradation of starch,
2. starch degradation aids in CO_2 assimilation but cannot replace it entirely on its own,
3. the oxidative pentose phosphate pathway together with the thioredoxin system is able to produce sugar phosphates and NADPH in the dark,
4. therefore both sugar phosphates and NADPH are available during light and dark conditions,
5. the Calvin cycle and oxidative pentose phosphate pathway should be seen as complementary pathways which are used according to light intensity by the thioredoxin system to produce NADPH and sugar phosphates.

TCA cycle Steuer *et al.* [109] studied the TCA cycle which is found in the leaf mitochondria and plays a large role in biosynthesis. As discussed above, structural and kinetic analysis are two different types of modelling approaches that can be applied to a given system. Due to the drawbacks of both methods, Steuer *et al.* [109] suggest an alternate method for studying the TCA cycle. They dubbed it a 'structural kinetic model'. It is a method that uses a parametric representation of the Jacobian matrix to quantitatively analyse a metabolic model without using an explicit set of differential equations. It is able to indicate (i) the stability of steady-states (ii) bifurcations (iii) oscillatory regions. Elementary flux mode analysis was also applied to the model. Six elementary modes were found and describe the modes through this anabolic pathway. The structural kinetic model showed the effect of the metabolite concentrations on the stability of the model. In this case, OAA and PA had the biggest impact on the stability of the system meaning that the lower the concentrations, the more stable the model is. Therefore, Steuer *et al.* [109] conclude that this alternate model is an efficient tool in identifying values that ensure maximal stability of a system.

3.3.6 Kinetic Analysis

Sucrose Accumulation Rohwer and Botha [96] built a kinetic model to determine the control of futile cycling and sucrose accumulation in medium-mature tissue in sugarcane. It was hypothesised that increased sucrose futile cycling reduced the accumulation of sucrose and so, if control of futile cycling could be determined, accumulation of sucrose could be increased by targeting reactions with largest control on futile cycling. The model confirmed the experimental finding that 22% of sucrose produced is broken down again by futile cycles (neutral invertase). The following reactions controlling futile cycling were identified: (i) an increase specific cytoplasmic glucose and fructose uptake (ii) an increase vacuolar sucrose uptake activity (iii) a decrease in neutral invertase acivity.

However, many simplifications were made in this model:

1. The vacuole was not modelled explicitly due to a lack of data on the metabolite pools and transport steps,
2. Cofactors were clamped as relevant reactions lacked detail,
3. Only internode 5 was modelled, as representing medium-mature tissue,

4. The average of the isoforms of an was implicitly modelled,
5. Fibre formation was not included,
6. Many values (maximal activities and kinetic constants) were estimated due to lack of available experimental data.

This model was further developed by Uys [119] to include varying degrees of tissue maturity (internodes 3-10) and carbon partitioning to the vacuole, glycolysis and fibre formation. Also, the isoforms of sucrose synthase and fructokinase were included explicitly. The model predicted that (i) the futile cycling of sucrose decreases with internode maturity (ii) there is little change in the control of the flux split between sucrose accumulation and breakdown with internode maturity and (iii) sucrose is transported from the cytosol and stored in another compartment [119].

The Calvin Cycle MCA has been applied to the Calvin cycle of C3 plants (transgenic and wild type tobacco). It has long been thought that Rubisco controls carbon fixation in C3 plants. However it has been suggested that sedoheptulose-1,7-bisphosphatase (SBPase) can alter the carbon fixation and partitioning of photosynthate. Poolman *et al.* [90] therefore conducted studies on the effect of SBPase activity on light saturated assimilation rates (A_{sat}) and starch levels for different leaves (from internodes 8, 10, 12, 14, 16). The older leaves generally showed higher rates of SBPase activity and starch levels in the wild type. However, transgenic plants showed highest A_{sat}, SBPase activity and starch levels in the more mature leaves. Using metabolic control analysis, the control coefficient (CCs) of SBPase activity on either carbon assimilation or storage of starch was determined. The study therefore suggested that two steady states exist for any model (with one set of parameters) which Poolman *et al.* [90] termed 'fast' or 'slow' states. The fast steady state has positive control coefficients but the slow steady state's are negative. These steady-states are dependent on which leaves they are found, therefore more mature leaves show positive CCs and the younger leaves show negative CCs. The study suggests that the Calvin cycle is able to switch between these states and the switch can induced by several factors. However, it is mostly affected by the concentration of inorganic phosphate in the chloroplast. The switching between the states in the differing maturity of leaves is thought to be dependent on the requirements of the leaves. The more mature leaves are carbon sources, therefore exhibiting a high carbon demand (for atmospheric carbon),

whereas the younger leaves are carbon sinks (requiring an import of sucrose). The amount of P_i and type of steady-state present is dependent on whether the leaf is acting as a source or a sink. The study was therefore able to conclude that SBPase is able to some degree control carbon assimilation and starch storage in the Calvin cycle in C3 plants [90].

3.4 Software

The above modelling and analysis is made possible by the abundant availability of software for modelling of cellular systems. Simulation tools include

- SBW http://www.sys-bio.org/research/sbwIntro.htm [50],
- Gepasi (http://www.gepasi.org/) [75],
- Copasi (http://www.copasi.org) [49],
- Virtual Cell (http://www.nrcam.uchc.edu/login/login.html) [69],
- PySCeS (http://pysces.sourceforge.net/) [84]
- BioSpice (http://biospice.lbl.gov/home.html) [4],
- MCell (http://www.mcell.psc.edu) [111, 112],
- StochSim (https://sourceforge.net/projects/stochsim/) [65] and
- E-Cell (http://www.e-cell.org) [115].

However, a more specific focus on PySCeS will be taken as this is the tool employed in this work.

3.4.1 Python Simulator for Cellular Systems

The Python Simulator for Cellular Systems (PySCeS) [84] allows the study and analysis of reaction networks within cellular systems. It is a modelling tool which has been developed and maintained by our group. PySCeS is a high-level modelling interface which runs on top of the combination of Python and SciPy. One can therefore simulate complex systems without knowledge of advanced programming languages and low-level numerical algorithms (http://pysces.sourceforge.net).

The first step in using PySCeS, is to create an input file specifying reactions, reaction equations, stoichiometry, parameters and variables of a given model (A.1 & B.1). The program may then be run interactively using the Python console or executed in a script-based fashion. Once a model is loaded as an input file, PySCeS is able to solve Ordinary Differential Equations (ODEs) with the ODE solvers (HYBRD, FINTSLV and NLEQ2). If one ODE solver fails to find a solution, another ODE solver can be called. Some of the analyses that can be performed include: Metabolic Control Analysis (MCA), time-course analysis and Supply-Demand Analysis to determine the control of enzymes in a system and relationship between the supply and demand block respectively. Further, as a structural analysis tool, PySCeS can interface with METATOOL [89] and therefore calculate elementary modes [84].

Python is an incredibly powerful, high level, object-orientated programming language. It acts as a glue, interfacing with other languages like C++, Java and Perl. It has extensive standard libraries that aid in software development and facilitate modules and packages enabling code reuse. The syntax is easy and readable which makes code many times shorter than other languages. However, Python sometimes falls short in that some code takes longer to run than other languages. It is open source software that is able to run on Windows or Linux based systems and is available for download (http://www.python.org).

SciPy is a numerical library for Python containing many mathematical algorithms, which are used in this case for analysing cellular systems. It depends on NumPy (see below) and has many high-level science modules (ODE solvers, optimizations, numerical integration, etc.). It is open source and available for download (http://www.scipy.org).

NumPy is another numerical library used by Python as a multi-dimensional array package. NumPy includes algorithms for Fourier transformations and basic linear algebra functions (http://numpy.scipy.org/).

SBML Over the years, different software programs have emerged for modelling systems but unfortunately they bring with them incompatibility and a lack of

standardised format of models [51]. Therefore Systems Biology Markup Language (SBML) was developed which is based on eXtensible Markup Language (XML) [8] as a standardized method of writing, specifying and collating metabolic models. The components of an SBML model include (i) reactions, (ii) parameters, (iii) species, (iv) compartments, (v) unit definitions and (vi) rules. It is an effective tool allowing models to be shared and evaluated by the same standard, creating a format for models that can therefore be used with a number of types of software. This allows models to be defined in a machine-readable format so that they can still be used beyond the lifespan of the software they were developed with.

3.5 Complications Faced When Modelling

Some complications that can arise when modelling are: (i) lack of available kinetic data for substrates, products and inhibitors, (ii) limited validation data, (iii) enzyme binding mechanisms that have not been described or studied, (iv) modelling of compartments and (v) modelling moiety-conserved cycles. These are discussed below and then applied in Chapter 4 and 5.

i. Lack of Kinetic Data Often a system has not been studied in sufficient detail to provide kinetic data (K_m, K_i, V_{max}). In this instance, a structural model can be built until such time kinetic data becomes available. Structural models therefore pave the way for kinetic models.

ii. Limited Validation Data Within kinetic modelling, the model predicted values need to be compared to those found experimentally to determine the accuracy of a model. However, often the experimental data (fluxes, metabolite concentrations and control coefficients) is not available and therefore the model cannot to be validated. In such cases, a structural model can be developed until such time that validation data becomes available.

iii. Unknown Binding Mechanisms Often studies have not characterised binding mechanisms of enzymes. However, recent work from our group has shown that generic equations are able to overcome these shortcomings [97]. These equations can mimic the effects of random, ordered and ping-pong mechanism without having to describe the binding mechanism of the enzyme. The only requirement is that the equation is able to describe the enzyme's response in a network

as a function of substrate and product concentration. In our work, to describe the simple non-cooperative reaction

$$\text{A + B} \longrightarrow \text{P + Q}$$

the following simplified equation can be used:

$$v = \frac{\frac{V_\text{f}}{KaKb}(ab - \frac{pq}{K_\text{eq}})}{(1 + \frac{a}{Ka} + \frac{p}{Kp})(1 + \frac{b}{Kp} + \frac{q}{Kq})}$$

where v is the rate, V_f the maximal rate of the enzyme, $\text{K}_a/K_b/K_c/K_d$ are the half saturation constants and the lowercase letters are the concentrations of the respective metabolites.

iv. Modelling of Compartment Volumes When modelling a cellular pathway, one is often confronted with a change of compartment. However, modelling compartments that differ in volume can be error prone and tedious. A simple solution to this is to model the metabolites in mole amounts. Therefore to determine the steady-state concentration, the mole amount may be divided by the volume that the metabolite is found in. This method was applied to the kinetic model of carbon fixation in Chapter 5.

v. Modelling moiety conserved cycles Many reactions supply and consume ATP, ADP and AMP. A helpful tool often applied to modelling such moiety conserved cycles are forcing functions. In this case, ATP, ADP and AMP are calculated as ratios of the total amount of adenylates. It is assumed that the total adenylate concentration remains constant and the adenylates are therefore modelled as expressions of K_{eq} (of adenylate kinase) and total adenylate concentration. The "charged" adenylate pool is then referred to as 'P' to denote [2ATP] + [ADP], $\text{K}_{eq} = \frac{[AMP][ATP]}{[ADP]^2}$ and the total adenylate pool where C_A = [ATP]+[ADP]+[AMP] [114]. The following equations allow the concentration of the vacuolar adenylate forms to be calculated:

$$\text{[ATP]} = \frac{P - 4K_{eq}P - C_A + \sqrt{P^2 - 4K_{eq}P^2 - 2PC_A + 8K_{eq}PC_A + C_A^2}}{2 - 8K_{eq}},$$

$$\text{[ADP]} = \frac{C_A - \sqrt{P^2 - 4K_{eq}P^2 - 2PC_A + 8K_{eq}PC_A + C_A^2}}{1 - 4K_{eq}},$$

$$\text{and [AMP]} = \frac{K_{eq}[ADP]^2}{[ATP]}$$

Forcing functions were used for example, in the study by Rohwer and Botha [96] to describe the hexose equilibrium block and by Teusink *et al.* [114] to describe the adenylate pool in yeast.

3.6 Concluding Remarks

With all this in mind, we set about constructing a structural model (Chapter 4) and kinetic model (Chapter 5) of sucrose metabolism in sugarcane. In Chapter 4, we extended the kinetic model described by Rohwer and Botha [96] and Uys [119] to a plant-scale structural model. Chapter 5 then describes a kinetic model of carbon fixation in sugarcane leaves.

Chapter 4

A Plant-Scale Structural Model in Sugarcane

The aim of this Chapter is to construct a plant-scale structural model characterising sucrose production and accumulation in sugarcane. A structural model was built for three reasons. Firstly, structural models require stoichiometry alone. This is useful when kinetic data is limited or enzyme binding mechanisms have not been characterised. Secondly, modelling such a system kinetically would be impractical at this stage due to the size of the model. Each section would be more accurately modelled individually and reassembled for the complete system. Therefore, a structural model lays the foundation for a kinetic model. Thirdly, a structural model allows one to answer specific questions pertaining to the relationships within a system. These include: (i) energy requirements of a system, (ii) validity of pathways in a system and (iii) favoured pathways in a system.

This model is built consisting of the pathways required for the production (leaf) and utilization (stalk) of sucrose in sugarcane (Section 4.1). The structural model is assembled (Section 4.3) and the difficulties of the assembly discussed (Section 4.3.1). Structural analysis is performed (Section 4.4) and the findings are discussed and concluded (Section 4.5 & 4.6).

4.1 Components of Sucrose Metabolism

The components of the model include carbon fixation, sucrose production, phloem loading and unloading, sucrose accumulation and consumption (Figure 4.1). Car-

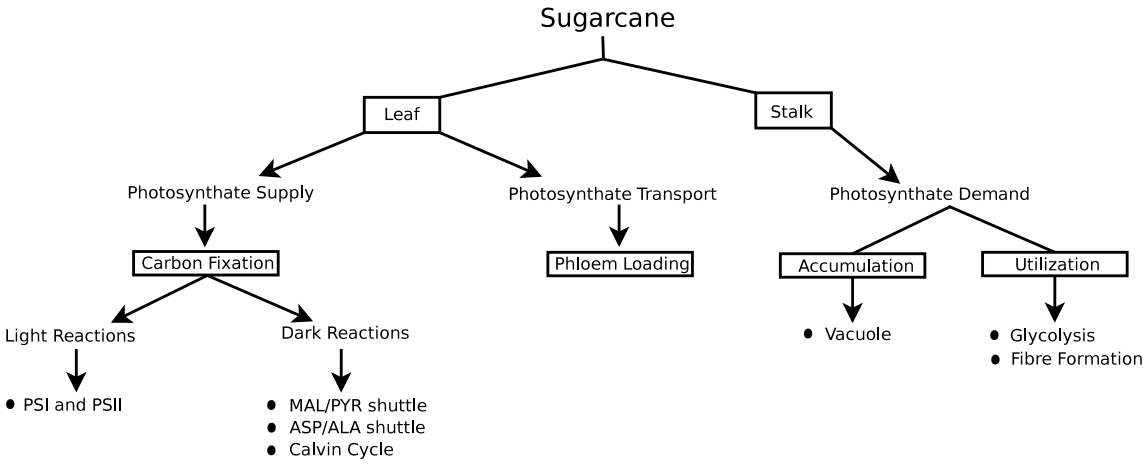

Figure 4.1: Components of the Structural Model. The pathways are outlined in Chapter 2.

bon fixation occurs by the C4 cycle (Section 2.2.1), producing sucrose in either the mesophyll or the bundle sheath cells [70] and loaded into the phloem [7]. Sucrose is unloaded into the storage parenchyma and either accumulated in the vacuole or used for fibre formation and glycolysis in the storage parenchyma [127].

4.1.1 Carbon Fixation

The main aim of C4 cycle is the net transport of carbon into the bundle sheath chloroplast [41]. Carbon is incorporated into the mesophyll cells via the carboxylation of PEP to OAA. The fate of OAA can either be MAL or ASP depending on the C4 species [60] and the presence of malate dehydrogenase and aminotransferases [34]. MAL and ASP are the key carbon carrying metabolites found in the two shuttles in sugarcane (Figure 4.2). The primary shuttle is the MAL/PA shuttle and the secondary shuttle is the ASP/ALA shuttle.

The uptake of CO_2 via stomata, the equilibration of CO_2 to HCO_3^- and the conversion of PEP and HCO_3^- to OAA is common to both shuttles (Figure 4.2, purple line). In the MAL/PA shuttle, MAL from mesophyll chloroplast is transported into the mesophyll cytoplasm and diffuses into the bundle sheath cytoplasm. MAL moves into the chloroplast where it is decarboxylated by NADP-malic enzyme (Section 2.2) to produce PA. PA, a C3 skeleton, is transported over the chloroplast membrane into the bundle sheath cytoplasm. It diffuses into the

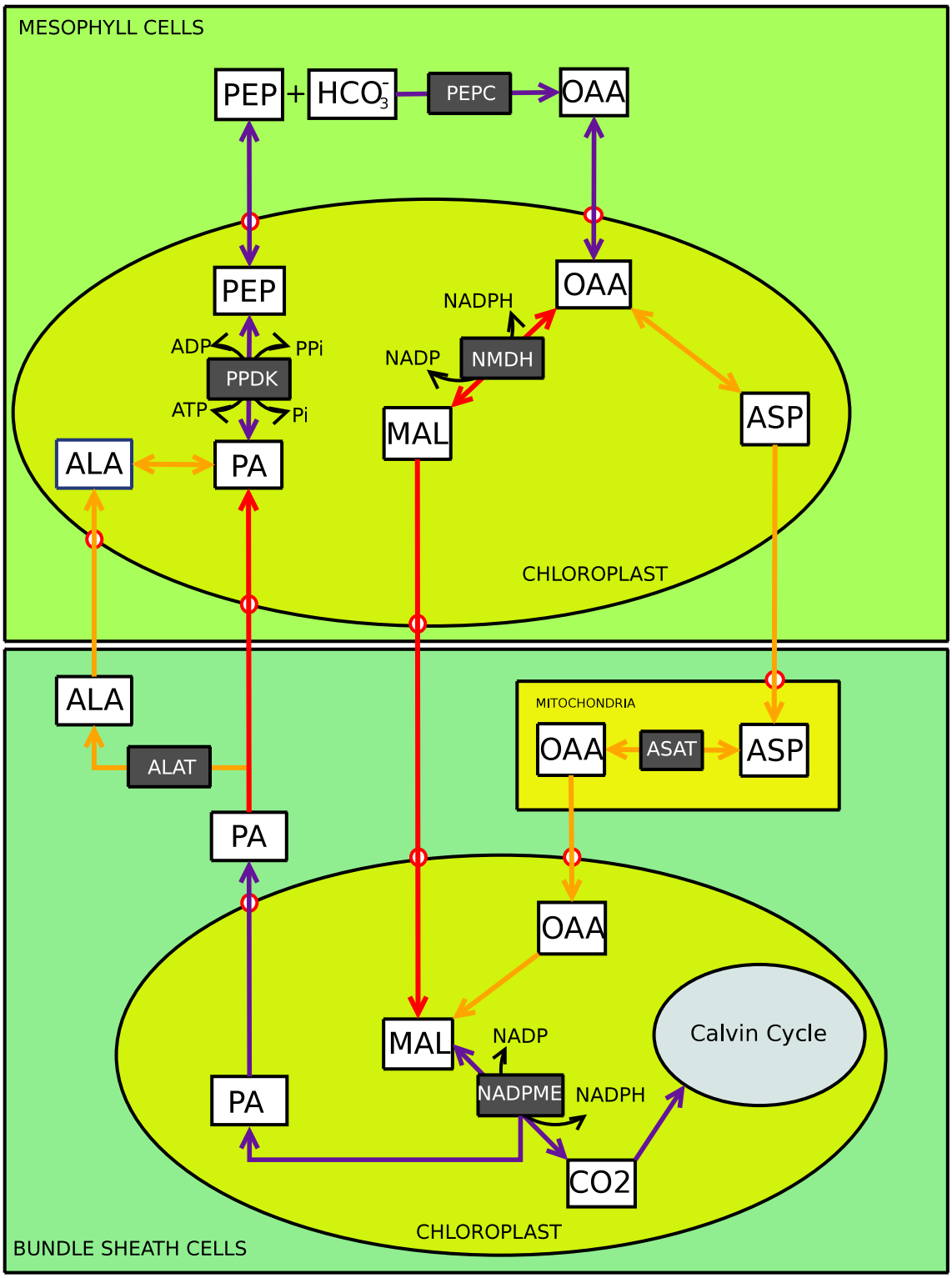

Figure 4.2: The C4 pathway illustrating the MAL/PA and ASP/ALA shuttle in sugarcane. CO_2 is taken up into the mesophyll cells. PEP is carboxylated to OAA which feeds into either of the shuttles. MAL or ASP is transported to the bundle sheath cells where decarboxylation occurs with CO_2 entering the Calvin cycle. The white blocks represent metabolites and the gray blocks are enzymes. Abbreviations on viii-x.

mesophyll cytoplasm and enters the mesophyll chloroplast (red line). PA is converted to PEP and once again primed to assimilate more carbon, another step that is common to both shuttles. However, the ASP shuttle transports ASP from the mesophyll chloroplast to the bundle sheath mitochondria where it is converted back to OAA. OAA is transported into the chloroplast and converted to MAL, whereupon it is decarboxylated to PA. PA is transported from the chloroplast and converted to ALA. ALA diffuses from the bundle sheath cytoplasm into the mesophyll cytoplasm and taken up into the chloroplast and converted to PA [17] (orange line).

In summary, both shuttles alternate between C3 and C4 compounds to move carbon from one cell type to another in order to decarboxylate their metabolites in the bundle sheath chloroplast. It is this alternating mechanism between two cell types that increases the concentration of carbon dioxide in this bundle sheath chloroplast compartment. The CO_2 then enters the Calvin cycle, the second carboxylation step in C4 plants (Section 2.1).

4.1.2 The Calvin Cycle

The Calvin cycle occurs within the bundle sheath chloroplasts in C4 plants. This is where the metabolism of carbon begins. Carbon is taken up to produce TRP which are either used within the cycle to receive more carbon or are made available for the production sucrose (Figure 4.3). The cycle has three phases totaling 13 reactions (catalysed by 11 enzymes) in the stroma of chloroplasts [17]. The phases are carboxylation, reduction and regeneration.

The carboxylation phase is the conversion of three Ribulose-1,5-bisphosphate (RuBP) with three accumulated carbons to produce six PGA. This reaction is catalysed by Rubisco which has a high affinity for CO_2 but an even higher affinity for O_2 (Section 2.2.2).

The reduction phase is the reduction of six PGA to six TRP with the expense of six ATP and six NADPH. The majority of ATP and NADP is consumed here with only one other step consuming three ATP in the production of RuBP. The

ATP and NADPH harvested from the light phase of photosynthesis [24]. The ATP consuming reaction is PGA kinase and the NADPH consuming reaction is NADP-glyceraldehyde phosphate dehydrogenase [10].

The regeneration phase consumes six triose phosphates to prime the cycle to produce RuBP to receive more carbon via Rubisco. The cycle alternates between 4C, 5C, 6C and 7C molecules in preparation to produce RuBP. Two TRPs produce fructose-1,6-bisphosphate (FBP) which is dephosphorylated to fructose-6-phosphate (F6P). F6P combines with another TRP to make xylulose-5-phosphate (Xu5P) and erythrose-4-phosphate (E4P). E4P together with TRP produces sedoheptulose-1,7-bisphosphate (SBP) which is dephosphorylated to sedoheptulose-7-phosphate (S7P). S7P and TRP then produces Xu5P and ribose-5-phosphate (R5P). Two Xu5P are consumed to two ribulose-5-phosphate (Ru5P). Alternatively, one R5P is converted to one Ru5P. In total, three Ru5P are produced, together with three ATP, to yield three RuBP via ribulose 5-phosphate kinase [10].

In short, to run the Calvin cycle, 3 CO_2 + 3 RuBP enter the cycle to produce 6 TRP, consuming 6 ATP and 6 NADPH. These 5 TRP are utilised within the cycle, consuming 3 ATP in the last step to produce 3 RuBP. Therefore, 5 ATP and 2 NADPH molecules are used per CO_2 consumed by the Calvin cycle [60, 91]. The sixth TRP represents the gain in fixed carbon.

Figure 4.3 shows three transporters. Phosphate translocators allow the transport of PGA and TRP into and out of the chloroplasts (Section 2.2.3 & 4.1.3). The movement of these metabolites across the chloroplasts is important for two reasons. But firstly, the role of chloroplast needs to be highlighted.

4.1.3 Chloroplasts

Chloroplasts are the photosynthetic machinery which generate ATP and NADPH. They are organelles which have an outer and inner membrane and contain the stroma where all the cell's photosynthetic reactions happen (i.e. the Calvin Cycle.) It also contains the thylakoids which consist of stacked disk shaped sacs called grana that interconnected by stromal lamellae [120].

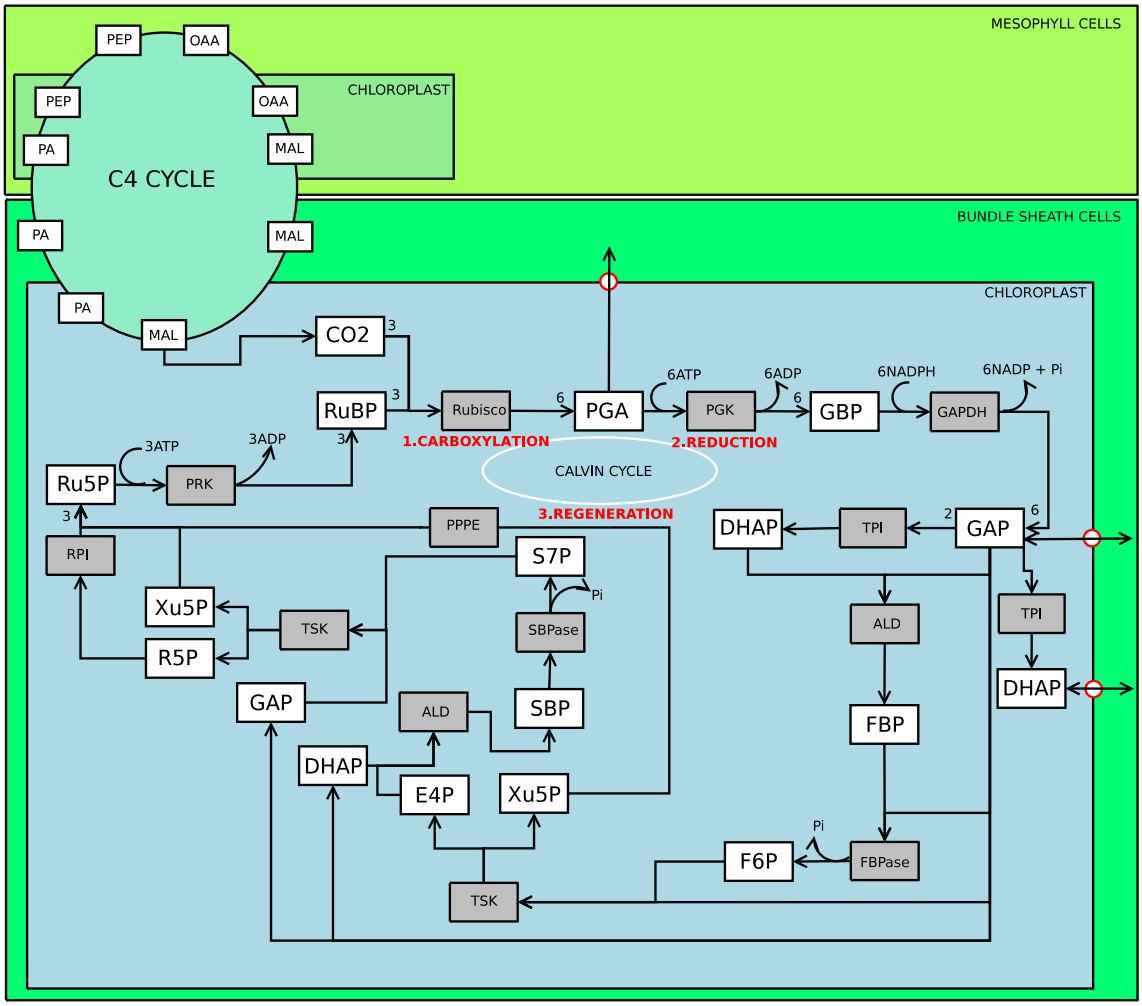

Figure 4.3: The Calvin Cycle. The C4 cycle concentrates the level of CO_2 in the bundle sheath chloroplast which enters the Calvin Cycle. It consists of 3 phases, (i) carboxylation, (ii) reduction and (iii) regeneration. Glycerate 3-phosphate and the triose phosphates can be transported from the chloroplast for the exchange for inorganic phosphate.

There are two types of chloroplasts, i.e. granal and agranal. The mesophyll chloroplasts are granal meaning both PSI and PSII are present and hence they generate both ATP and NADPH. On the other hand, the bundle sheath chloroplasts are agranal, meaning they do not contain PSII and therefore cannot produce NADPH (Section 2.2.1).

The reason we see differents types of chloroplasts is due to the nature of sugarcane (Section 2.2.2). The second decarboxylating enzyme, Rubisco, has an affinity for both O_2 and CO_2. Hence if O_2 were generated via PSII, both CO_2 and O_2 would compete for Rubisco's active site and possibly allow photorespiration to occur (if O_2 levels are sufficiently high enough). Therefore in the bundle sheath chloroplast, only CO_2 exists and hence no O_2 occupies Rubisco [9].

The reason for the movement of metabolites not only across chloroplasts, but also across cell types, is as follows. Firstly, the lack of PSII in the bundle sheath chloroplast forces PGA to follow alternate paths to receive reducing equivalents. Therefore, PGA moves from the bundle sheath chloroplast to the mesophyll chloroplast to receive reducing equivalents to be reduced to TRP. However, the mesophyll chloroplasts can effectively serve another role. When OAA together with NADPH is converted to MAL (Section 4.1.1), the reducing equivalent is also transported to the bundle sheath chloroplast via the MAL/PA shuttle to supply the reduction phase [44].

It is important that PGA is reduced to TRP as these serve as precursors to sucrose production. Almost half of the PGA produced from the Calvin Cycle in the bundle sheath chloroplast is transported to the mesophyll chloroplast for reduction [66]. TRP has two destinations. It may enter the mesophyll cytoplasm to be reduced to sucrose, or the predominant pathway is returning a minimum of two thirds to the bundle sheath chloroplast to replenish the Calvin Cycle's sugar phosphates [66]. TRP in the bundle sheath cytoplasm may also be used for sucrose production. However, sucrose is predominantly produced in the mesophyll cytoplasm [70].

4.1.4 Sucrose Production

Many studies have reported on sucrose production in the leaf. Initially, studies by Edelman and Schoolar [15] showed that chloroplasts contain sucrose producing enzymes and a sucrose efflux. They emphasized that the majority of sucrose efflux occurrs in the mesophyll chloroplasts and proposed a carrier-mediated system [15]. However, it has since been shown that sucrose is produced in the cytoplasm and starch is produced in the chloroplast [70]. The majority of sucrose is produced in the mesophyll cytoplasm and small amounts in the bundle sheath cytoplasm depending on the species [70]. TRP in the mesophyll and bundle sheath chloroplast is transported to the cytoplasm via the phosphate translocator. TRP is therefore the precursor for sucrose production where the sequence of reactions is:

$$\text{2TRP} \longrightarrow \text{FBP} \longrightarrow \text{HEXP} \longrightarrow \text{UDPGLC}$$
$$\text{UDPGLC+ HEXP} \longrightarrow \text{S6P} \longrightarrow \text{SUC}$$

There are two steps which produce P_i: (i) the conversion of SBP $\longrightarrow$ HEXP, and (ii) SUC6P $\longrightarrow$ SUC. The conversion of HEXP $\longrightarrow$ UDPGLC produces PP_i. The transport of both P_i and PP_i back into the chloroplast is essential for use within the phosphate transporter since inorganic phosphate drives the transport of TRP over the chloroplast membrane via the phosphate translocator [70].

The synthesis of sucrose in the mesophyll cytoplasm needs to be regulated so that a TRP gradient is maintained between mesophyll and bundle sheath cells which is essential for TRP to be transported back to the bundle sheath for the use in the Calvin cycle [70].

The sucrose in mesophyll cytoplasm diffuses into the bundle sheath cytoplasm, and together with the bundle sheath produced sucrose is loaded into the phloem.

4.1.5 Phloem Loading and Unloading

C4 plants have an effective and efficient manner of transporting sucrose from the leaves to the stalk. Due to the anatomy of sugarcane (Section 2.2.2), sucrose does not have to travel far in order to diffuse into the phloem for transport [36]. Distribution points within the sink include developing shoots, internodes and

roots [94]. However, in sugarcane, the predominant route is to enter the storage parenchyma cytosol either apoplastically or symplastically (Figure 4.4). Back flow of sucrose from apoplast into the phloem is prevented by the composition of the cell walls found around the vascular bundles [125]. However, in the symplast, sucrose is quickly transported to either the apoplast or vacuole to create a driving force of sucrose flow into the storage parenchyma [94, 98].

As sugarcane is able to accumulate high concentrations of sucrose in the stalk, the plant has mechanisms of overcoming high turgor pressures generated by the levels of sucrose. The following minimise the turgor pressure within the storage parenchyma: (i) sucrose is partitioned between the apoplast and symplast, (ii) hydrolysis of sucrose to glucose and fructose in both the apoplast and cytosol which are further metabolised to osmotically inert products, and (iii) the movement of sucrose from the cytosol to the vacuole.

However, even with the breakdown of sucrose between the compartments, the predominant metabolite in both the apoplast and symplast is still sucrose with smaller amounts of fructose and glucose [125].

4.1.6 Storage Parenchyma

Although sucrose is hydrolysed to hexoses in the cytosol and apoplast to overcome high turgor pressures, it is also resynthesised to sucrose, creating a cycling effect between synthesis and degradation [27, 40]. Approximately 20% of sucrose is broken down and resynthesised again [96, 127]. However, the majority of sucrose enters the storage vacuole where it can accumlate to levels as high as 650 mM [94]. Here, sucrose can also be hydrolysed to hexoses which can move back into the cytosol [28]. The cytosolic hexoses may then be used as building blocks to hexose phosphates and these in turn used as precursors to glycolysis (triose phosphates) and fibre formation (UDP-glucose) [127]. Apart from using UDP-glucose for fibre formation, it together with fructose can also be used to synthesize sucrose in the parenchyma cytosol [40]. Therefore, sucrose entering the storage parenchyma has three destinations: (i) accumulation in the vacuole, (ii) glycolysis or (iii) fibre formation.

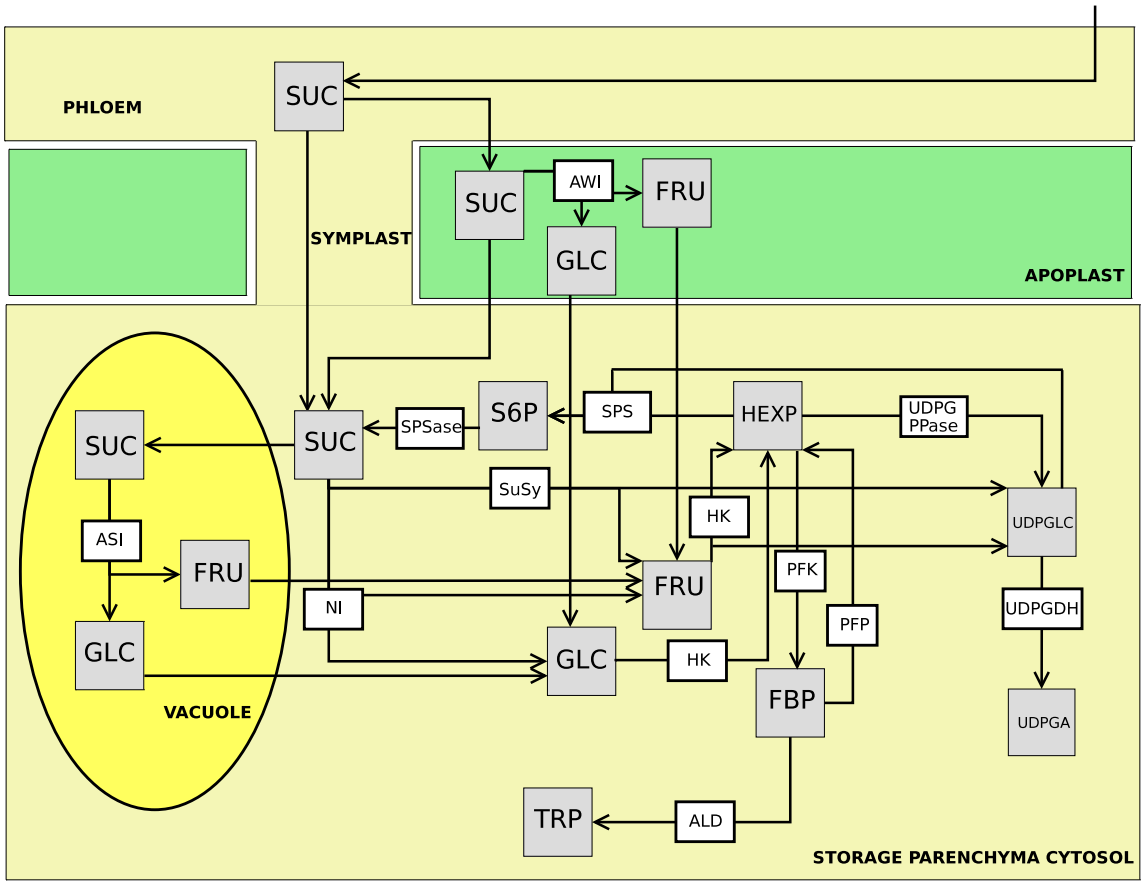

Figure 4.4: Phloem unloading and transport of sucrose to accumulation in the vacuole, respiration and glycolysis in the storage parenchyma. Abbreviations of the enzymes may be found under enzyme abbreviations.

4.2 Model Construction

The model was written in the form of a PySCeS [84] input file (Appendix A.1 & A.2) and run via Python on a MSI450 laptop running Mandriva Linux 2007.0. The elementary modes were calculated using METATOOL [89].

The model was assembled to characterize carbon fixation and sucrose production in the mesophyll and bundle sheath cells, phloem uploading, sucrose accumulation in the vacuole, respiration and fibre formation in the storage parenchyma. All source (supply) and sink (demand) metabolites as well as cofactors and protons were clamped. Starch production was not included in this model as it is produced during the day, broken down to sucrose at night and transported into the culm [70]. We only wanted to observe the net production, transport and accumulation of sucrose and not temporary storage in starch formation. We also did not include photorespiration in the leaves as this is thought to be negligible in sugarcane [25]. The storage parenchyma of the model was based on the kinetic model described by Uys [119].

4.2.1 Modifications to The Model

Simplifications In calculating elementary modes, every valid route in a system is given and due to the size of our model, this totalled 241 elementary modes. To simplify this, we made all transport steps irreversible to highlight the physiological relevant modes. To simplify the elementary mode analysis even further, we broke the model into two parts since there is only one connection point between the leaf and storage parenchyma via phloem loading. We were able to make these reductions as the elementary modes for the complete system would merely be a combination of those for the sub-parts.

Clamping of Sucrose in the Vacuole Figure 4.4 shows that sucrose enters the storage vacuole whereas fructose and glucose exit. However, the rates at which sucrose enters the vacuole and that at which fructose and glucose exit may not be equal, even when the rest of metabolism is at steady-state. Clamping an intermediate metabolite means that the flux towards and away from the metabolite can differ allowing sucrose to accumulate in the storage vacuole. Alternatively, if the metabolite were not modelled as a fixed species, it would imply that sucrose

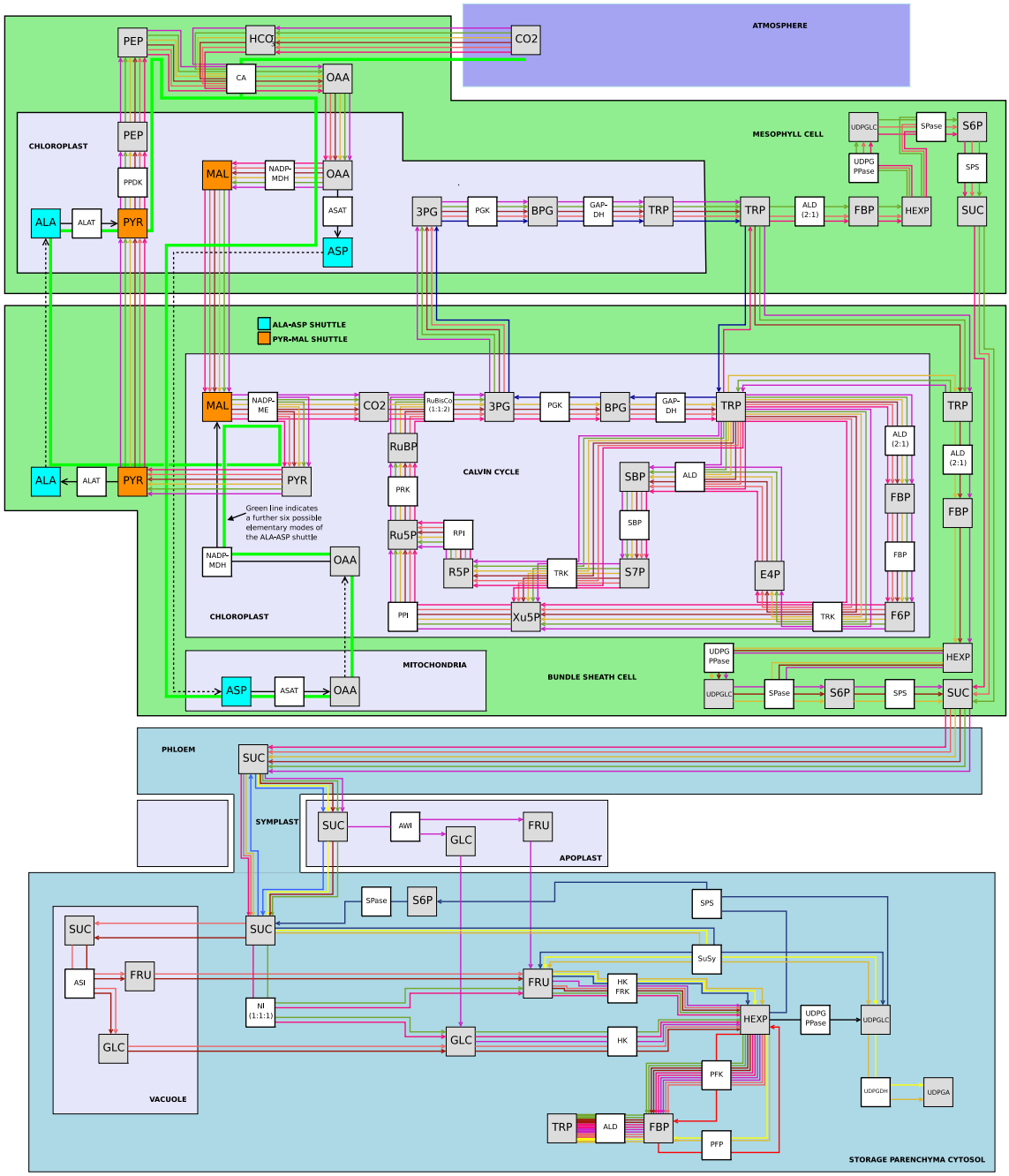

Figure 4.5: The complete plant-scale structural model showing the elementary modes for carbon fixation and sucrose production, phloem loading, sucrose accumulation and storage in sugarcane. Each line represents an elementary mode.

uptake and hexose export in the vacuole are always equal at steady-state. Clamping an intermediate metabolite increases the number of elementary modes as the metabolite is then able to function as an additional source or sink in the pathway.

4.3 Model Analysis

We found that in total there are 241 elementary modes which span across 10 compartments. The model contains 72 reactions and transport steps which consist of 110 metabolites and cofactors (Figure 4.5). Once the modifications to the model were made, we found 13 and 33 elementary modes existing in the leaf and storage parenchyma respectively.

4.3.1 The Leaf

There are 13 elementary modes that exist in the leaf (Figure 4.5). Twelve of these describe the shuttling of carbon to the production of sucrose in the mesophyll or bundle sheath cells. These twelve elementary modes can be broken down further, six modes for each shuttle. However, only the six of the MAL/PA shuttle are discussed as this is the predominant shuttle in sugarcane. Also, the set of elementary modes for both shuttles are identical. The analysis shows that the net reaction for these modes is

$$12\ CO_2 \longrightarrow \text{Sucrose}$$

with the consumption of 60 ATP, 24 NADPH and 1 UTP.

As stated, six of the elementary modes run through the MAL/PA shuttle and enter into the Calvin cycle. However, their destination routes differ from this point. Three describe the production of sucrose in the mesophyll cells whereas the other three describe sucrose production in the bundle sheath. In the mesophyll, sucrose can be produced from PGA or TRP which are transported from the bundle sheath chloroplast (Figure 4.6, elementary mode 6, 9, 12). The other three describe the routes either from PGA or TRP; to the production of sucrose in the bundle sheath cells (elementary mode 3, 7, 13). Two elementary modes are especially interesting. These modes describe how the elementary mode enters the Calvin cycle up to PGA. PGA is the transported into the mesophyll chloroplast for the reduction phase and TRP is transported back into the Calvin cycle, missing the step between

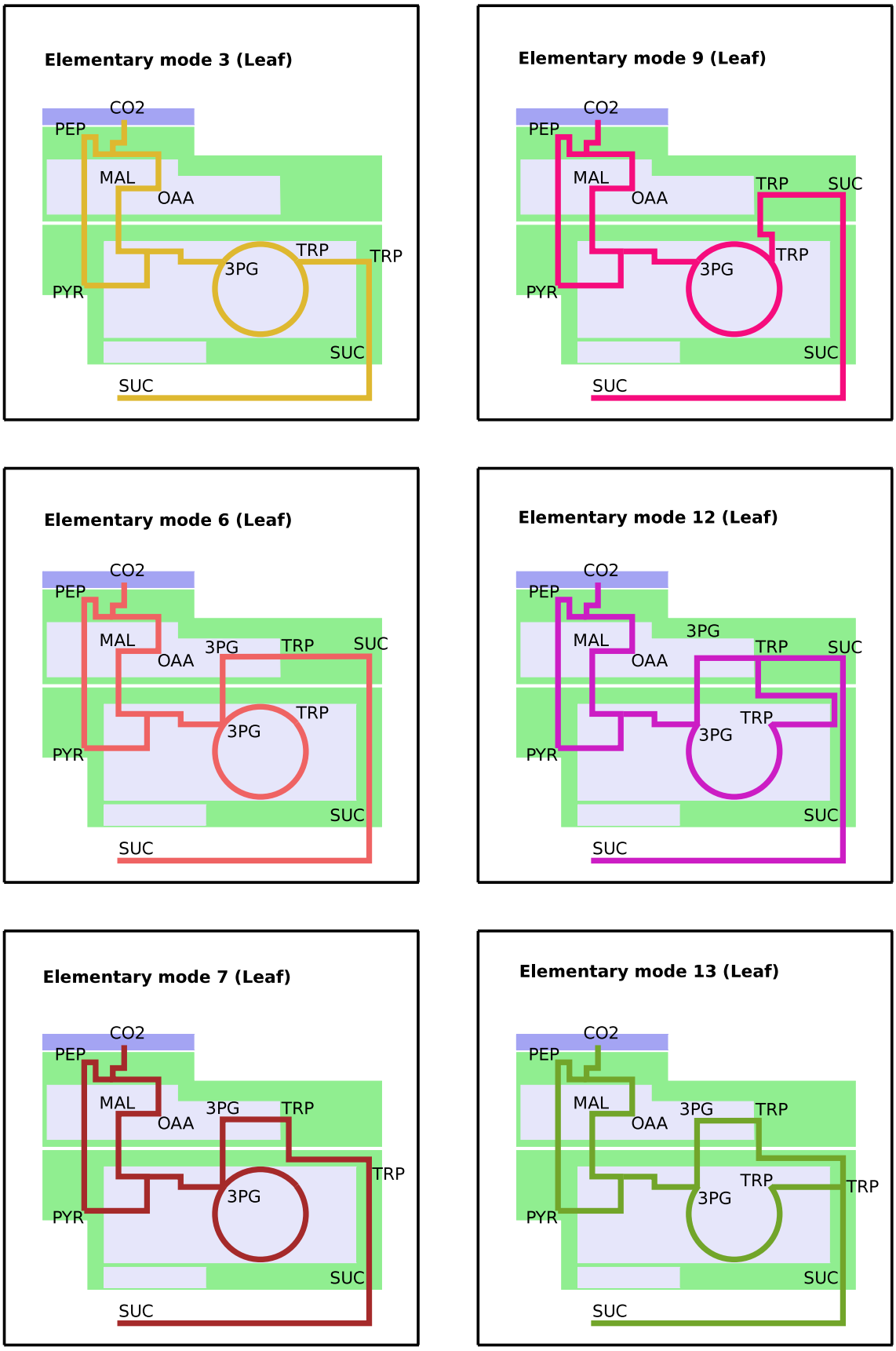

Figure 4.6: The six modes describing the pathway via the MAL/PA shuttle to produce sucrose in the sugarcane leaf.

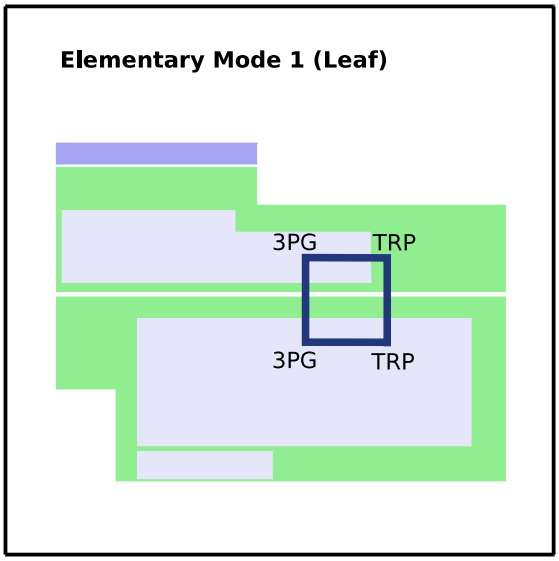

Figure 4.7: The futile cycle describing the transport of PGA from the bundle sheath chloroplast to the mesophyll chloroplast where it is converted to TRP and transported back to the bundle sheath chloroplast.

PGA $\longrightarrow$ GBP $\longrightarrow$ TRP in the bundle sheath chloroplast (elementary mode 12,13).

The thirteenth mode describes a futile cycle that shuttles PGA from the bundle sheath chloroplast to the mesophyll chloroplast for the reduction to TRP where TRP is then transported back to the bundle sheath chloroplast. TRP is then converted back to PGA, completing the futile cycle (Figure 4.7). The full net reactions for the leaf may be found in A.3.

4.3.2 The Storage Parenchyma

Once sucrose is uploaded into the phloem, it has three destinations. There are 24 elementary modes to describe sucrose's fate to either accumulation in storage vacuole, respiration or fibre formation (Table 4.1, Figure 4.8). Eight modes describe the breakdown of sucrose to TRP, two sets of four, differing in the energy required for each reaction to proceed (elementary modes 22, 23, 24, 25 (set one) and 25, 26, 27, 28, 29 (set two)). Set one require 4 ATP whereas set two require 2 PPi and 2 ATP but they are equal in energy expenditure. However, the source of the sucrose differs. Six elementary modes illustrate the breakdown of sucrose to fibre precursors, one set comprising of two elementary modes requiring 4 NAD^+,

Elem. mode	Net Reaction	Requirements
2	No net reaction	None
4	No net reaction	ATP
5	No net reaction	PPi
6,9,10	No net reaction	ATP,UTP
7,14,17	No net reaction	2ATP,UTP
1,3	$Suc_{phl} \longrightarrow Suc_{vac}$	None
8	$Suc_{vac} \longrightarrow Suc_{phl}$	ATP,UTP
11	$Suc_{phl} \longrightarrow Suc_{vac}$	ATP,UTP
13	$Suc_{vac} \longrightarrow Suc_{phl}$	2ATP,UTP
19	$Suc_{phl} \longrightarrow Suc_{vac}$	2ATP,UTP
16	$Suc_{vac} \longrightarrow$ 2UDPGA	$4NAD^+$,2ATP,2UTP
12,15	$Suc_{phl} \longrightarrow$ 2UDPGA	$4NAD^+$,ATP,UTP
18,20,21	$Suc_{phl} \longrightarrow$ 2UDPGA	$4NAD^+$,2ATP,2UTP
22	$Suc_{vac} \longrightarrow$ 4TRP	4ATP
23,24,25	$Suc_{phl} \longrightarrow$ 4TRP	4ATP
26	$Suc_{vac} \longrightarrow$ 4TRP	2PPi,2ATP
27,28,29	$Suc_{phl} \longrightarrow$ 4TRP	2PPi,2ATP
30,32	$Suc_{phl} \longrightarrow$ UDPGA + 2TRP	$2NAD^+$,2ATP
31,33	$Suc_{phl} \longrightarrow$ UDPGA + 2TRP	$2NAD^+$,PPi,ATP

Table 4.1: Elementary Modes in Storage Parenchyma. Suc_{phl} is sucrose in the phloem whereas Suc_{vac} is sucrose in the vacuole. Numbers in bold are the elementary modes that are depicted in Figure 4.8. Th full reactions may be found in A.3 & A.4.

ATP and UTP. The other set of four, require NAD^+, 2 ATP and 2 UTP but also divided by the compact of sucrose location. Then there are four elementary modes showing the breakdown of sucrose to fibre and glycolysis precursors. Elementary modes 30 and 32 require 2 NAD^+ and 2 ATP whereas elementary modes 31 and 33 consume 2 NAD^+, ATP and PPi. Both have sucrose in the phloem as the source. These total the 24 elementary modes describing sucrose's fate, there are a further 9 futile cycles (elementary modes 2, 4, 5, 6, 7, 9, 10, 14, 17), differing in energy requirements. There are also six elementary modes illustrating the movement of sucrose between the different compartments (elementary modes 1, 3, 8, 11, 13, 19). Two of these (elementary modes 1, 3) have no energy requirements, a further two requiring ATP and UTP (elementary modes 8, 11) and the last two requiring 2 ATP and UTP. The full net reactions for the storage parenchyma may be found in A.4.

4.4 Discussion

As seen from the results above, structural analysis is an effective tool for identifying valid routes at steady state, futile cycles and ATP requirements. In total, in the leaf, one futile cycle and 12 sucrose-producing routes were identified, yielding a total of 13 valid routes. By investigating the requirements of the net reactions of the sucrose-producing routes, we were able to deduce that there is no single more energy efficient sucrose producing pathway. In the storage parenchyma, there are three futile cycles and 14 pathways routes of sucrose breakdown, totally 17 valid routes. Ten of these describe the utilisation of sucrose for glycolysis and respiration. By exploring the requirements of these ten pathways, it becomes evident that no single pathway is more efficient pathway for the breakdown of sucrose to TRP.

In the leaf, both carboxylating shuttles have 6 identical sucrose producing routes. Four of these utilise the respective shuttle, the Calvin cycle and sucrose-producing pathway in either the mesophyll or bundle sheath cytoplasm. However, the remaining two are identical to the above except in the way they utilize the Calvin cycle. It becomes evident that the Calvin cycle can span over two cell types, with the reduction phase (PGA $\longrightarrow$ GBP $\longrightarrow$ TRP) being able to occur in the mesophyll. The reduction of PGA to TRP in the bundle sheath chloroplast also occurs

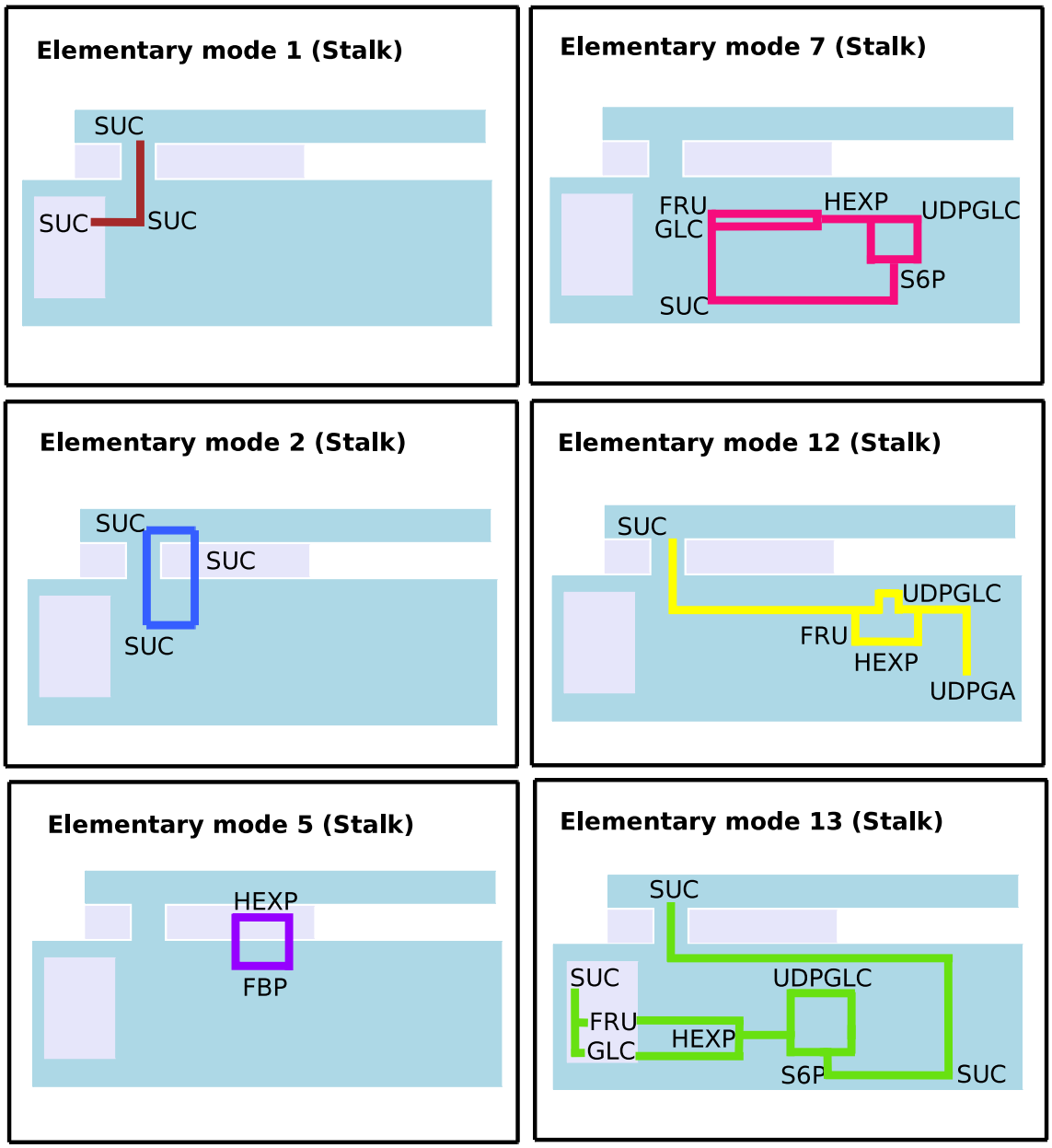

Figure 4.8: Elementary modes describing sucrose accumulation and storage in the sugarcane parenchyma.

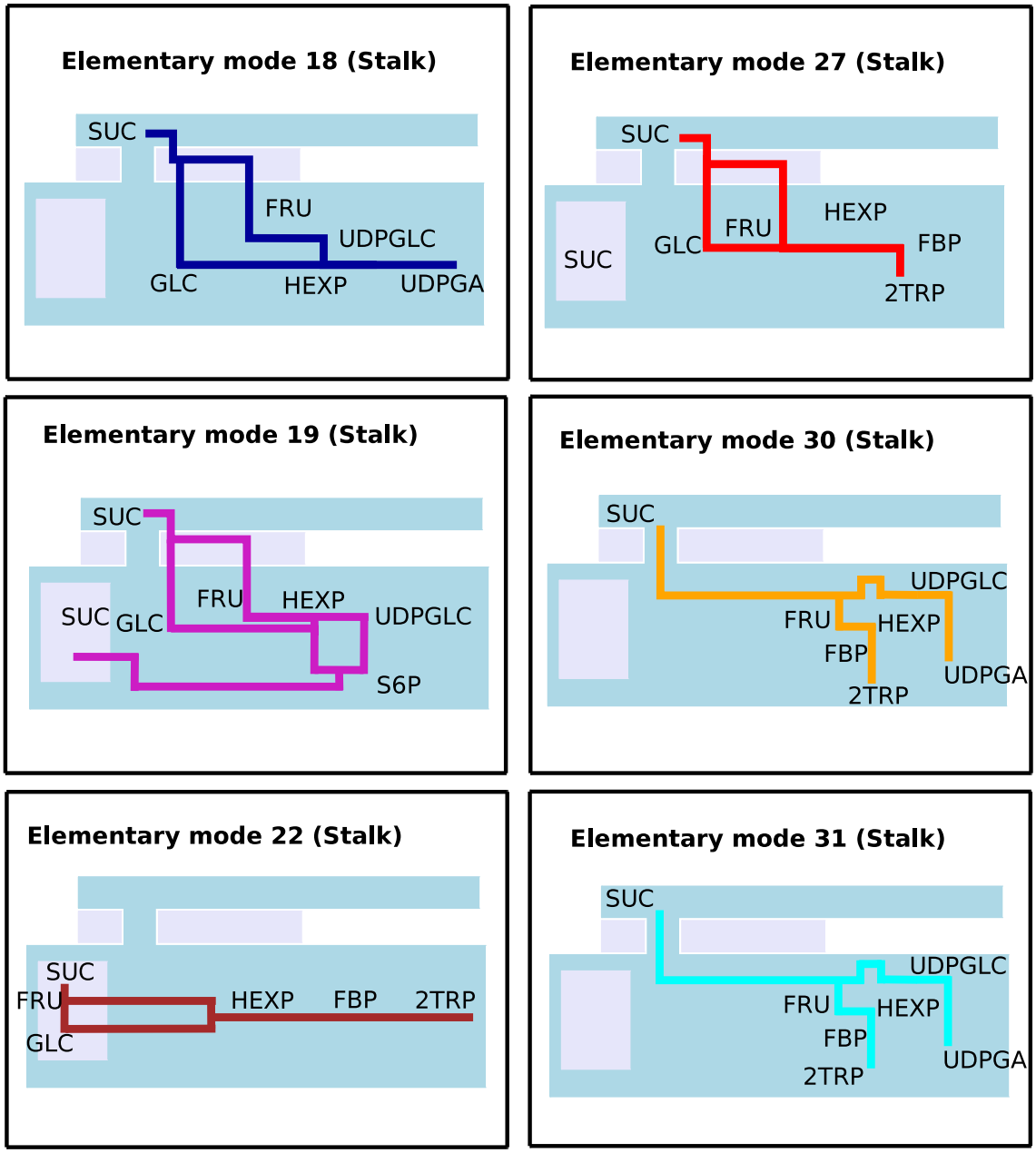

Figure 4.9: Elementary modes describing sucrose accumulation and storage in the sugarcane parenchyma

in the mesophyll chloroplast because of the lack of reducing equivalents in the bundle sheath chloroplast. This therefore allows the Calvin cycle to span across two different cell types.

The reduction phase in the mesophyll further allows a futile cycle. PGA is exported from the bundle sheath chloroplast to the mesophyll chloroplast for the reduction of PGA to TRP. TRP is imported back to the bundle sheath chloroplast for use in the Calvin cycle therefore closing the cycle. The futile cycle illustrates the NADPH requirements of the Calvin cycle, to reduce PGA to TRP and indicates the bundle sheath chloroplast PSII deficiency. PGA is exported from the bundle sheath chloroplast to utilise the PSII in the mesophyll chloroplast. Up to half the total PGA is transported into the mesophyll chloroplast for reduction to TRP [66]. Once reduced, a minimum of two thirds of TRP moves back to the bundle sheath chloroplast to replenish the Calvin Cycle's sugar phosphates. Alternatively, TRP can be used for sucrose production in the bundle sheath cytoplasm. The remaining TRP in the mesophyll cytoplasm is used for sucrose production. The ratio of [PGA]/[TRP] is approximately five-fold higher in the bundle sheath than in the mesophyll. A low level of mesophyll [PGA]/[TRP] means that the level of mesophyll [ATP][NAD(P)H][H^+]/[ADP][NAD(P)H][Pi] needs to relatively high in order to drive the reduction of PGA to TRP in the mesophyll [66].

The reason we see this migration of PGA to the mesophyll chloroplast is because of the lack of PSII in the bundle sheath chloroplast. The bundle sheath chloroplasts lack PSII because of the generation of O_2 from this photosynthetic centre. Rubisco, the carboxylating enzyme in the Calvin cycle, has an affinity for both O_2 and CO_2. Therefore, the lack of PSII allows only CO_2 to compete for Rubisco and hence photorespiration is said to to be negligible in sugarcane [25].

The MAL/PA shuttles also bring reducing equivalents into the bundle sheath chloroplast. The decarboxylation process produces NADPH which then provides approximately half the amount of the NADPH required for the reduction of glycerate 3-phosphate (PGA) in the Calvin cycle [10]. Therefore the decarboxylation process is coupled to the reduction of PGA [10, 37].

In the storage parenchyma, when investigating the elementary modes, the fate

of sucrose is evident. Sucrose may be broken down to fructose and glucose in the apoplast or between symplast and cytoplasm. The content of glucose and fructose is more apparent in the younger internodes' apoplast and symplast with a minimal amount of sucrose. Hexoses, more so glucose, are suggested to be found in younger internodes to be used as precursors to cellulose production and glycolysis [94]. In more mature internodes, up 76% of the total solutes in apoplast and symplast is sucrose [125]. From our analysis, it is evident that there are futile cycles present between the symplast and cytoplasm and within the apoplast. The cycling between sucrose and hexoses has been shown by Whittaker *et al.* [127] but the amount of breakdown of sucrose to glucose and fructose in the storage parenchyma depends on the internode maturity or the photosynthetic supply [73, 127]. Younger internodes show a higher sucrose degradation whereas sucrose synthesis is more apparent in more mature internodes. However, environmental conditions have also been shown to play a role in the fate of sucrose in the storage accumulation. Colder climates and nutrient deficiencies appear to favour sucrose accumulation as opposed to fibre formation [36].

Eight of nine futile cycles calculated show to be energetically wasteful cycles. Experimental studies by Whittaker [127] and theoretical analysis by Rohwer and Botha [96] show futile cycling to be as high as 22% in sugarcane culm. The most wasteful of these are elementary modes 7, 14 and 17 using 2 ATP and UTP.

Six elementary modes show the interconversions of sucrose between the compartments. However, they are independent of each other. For example, elementary modes 8 and 11 are reverse reactions of each other yet they do not have to run simultaneously (Table 4.1). The same is true for elementary modes 13 and 19 however they are more energetically expensive. Elementary mode 1 however may be somewhat misleading. Although the analysis shows no requirements, the uptake of sucrose is via a H^+ symport which therefore requires energy. Transporters were not explicitly defined within our model hence elementary mode 1 appears to have no energy requirements.

Sucrose may also be broken down to hexose phosphates for utilisation for fibre formation or in glycolysis but this is minimal by comparison to the amount of sucrose accumulated by the vacuole [127]. For the production of fibre precur-

sors, there are two routes which are more energetically favourable with a further four having the same energy requirements. Eight elementary modes show that there is no single more energy efficient pathway to produce glycolysis precursors. However, there are also four elementary modes which illustrate that UDPGA, the fibre precursor, cannot be made unless carbohydrates are diverted to glycolysis and respiration. Two of these are energetically less expensive.

4.5 Concluding Remarks

Elementary mode analysis is an effective tool for highlighting functional aspects in a metabolic pathway that may not have been evident from mere inspection. It also aids in understanding reactions and the location of reactions, i.e. the futile cycling of PGA and TRP due to the lack of PSII in the bundle sheath. As we have seen, structural modelling allows the visualisation of the bigger picture as one begins to integrate the many cycles. For example, when studying the Calvin cycle on its own, one may forget the reduction phase in the mesophyll and hence the ability of the Calvin cycle to function across two cell types. Therefore, it is important to choose the type of analysis based on the type of questions one wants to answer concerning a system.

Kinetic analysis allows the investigation of the control in a system. As a result, areas that have the most influence on and which control a network can be highlighted. These highlights are therefore valuable tools for pinpointing targets that would cause a system to have a sensitive response should the system be altered. However, there are many current limitations in performing kinetic analysis on the above plant-scale structural model, these include:

- the lack of available kinetic data
- the size of the model including the many transport steps and compartments
- limited experimental evidence for validation

Although there are limitations to kinetic modelling for larger models, we decided to focus on a smaller section of the structural model. We therefore assembled a kinetic model of the MAL/PA shuttle. This model was then analysed using metabolic control analysis to determine the factors controlling this system

and possibly highlight areas of interest to scientists looking to increase the flux through the system.

Chapter 5

The Kinetic Model of Carbon Fixation in Sugarcane

The kinetic model described here consists of the uptake of carbon dioxide and fixation via the MAL/PA shuttle. We decided to add kinetic detail to this section of the structural model because:

- the Calvin cycle has been previously modelled [90];
- carbon is the backbone of sucrose and understanding the carbon concentrating mechanism is theoretically important, and
- we wanted to theoretically understand the regulation of photosynthesis, which can also be regulated by sink strength [73].

Although much is known about the enzymes and metabolites in C4 plants, not much is known about the overall mechanism of carboxylation and decarboxylation between the two cell types. Through this investigation we aim to establish where the control lies in the system using metabolic control analysis. Our group [96, 119] has built kinetic models to describe sucrose accumulation in the sugarcane culm (Section 3.3.4) and this kinetic model was built using the same principles.

This Chapter therefore outlines the pathway of the kinetic model (Section 5.1), the construction of the model (Section 5.2) and the model parameters (Section 5.3). The analysis of the model is given in Section 5.4 and the predicted results are given and discussed in Sections 5.5 & 5.6.

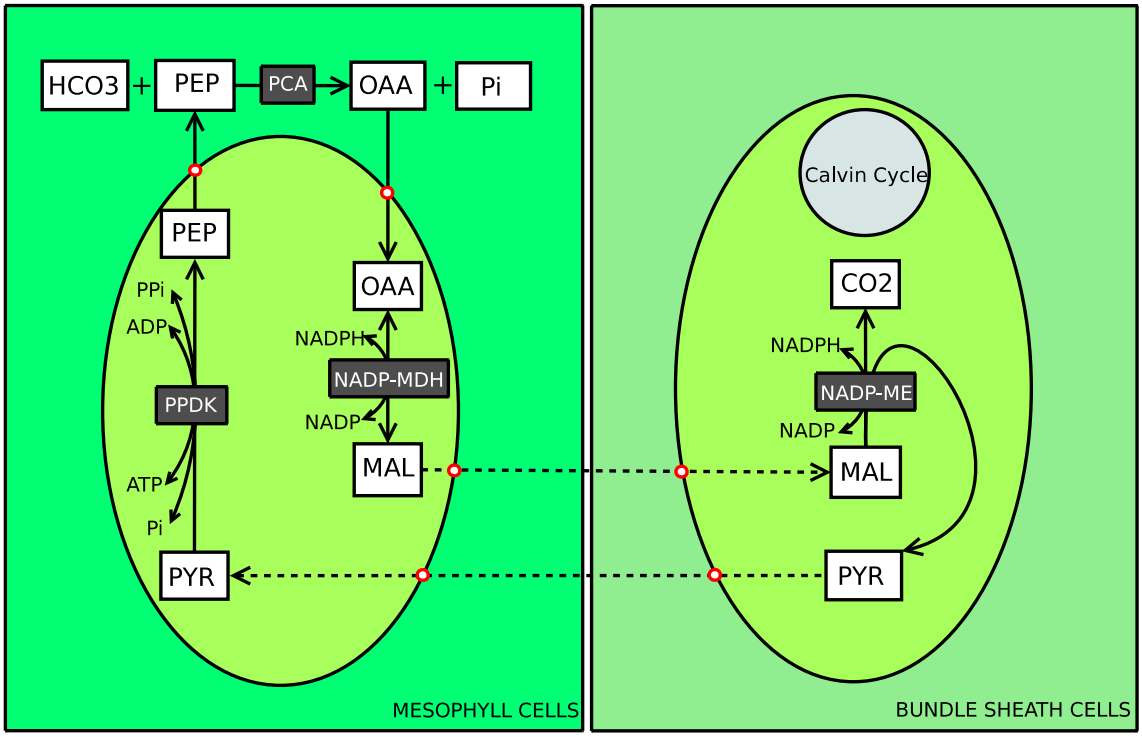

Figure 5.1: Kinetic Model of Carbon Fixation via the MAL/PA Shuttle. The gray blocks indicate enzymes and the white metabolites. Dotted lines indicate diffusion and red dots are transporters.

5.1 The Carbon Fixation Model

The stoichiometry of the basic model has been discussed in Section 4.1.1, showing the metabolites found in the MAL/PA shuttle. However, as the kinetic model focusses more on the dynamics of enzymes and transporters, a more in-depth view of each of the enzymes is needed (Section 5.3). The model shown in Figure 5.1 includes the enzymes and transporters as well as their localisation in the leaf.

5.2 Construction of the Model

In this study, we used generic equations to describe the behaviour of the enzymes in the carbon fixation pathway. As all the enzymes are non-cooperative, the simplified generic equation [97] based on random equilibrium binding of substrates and products was used.

Diffusion was modelled using a generic equation to characterise the movements of metabolites across the plasmodesmata. The equation describes the rate of movement multiplied by the concentration gradient of the metabolite across the two compartments:

$$v = k_d(m_A - m_B)$$

where k_d is the diffusion coefficient, m denotes the metabolite concentration and A/B refer to the compartment that the metabolite exists in.

In essence, the MAL/PA shuttle is a moiety-conserved cycle as there is no net gain of carbon. This means that the total metabolite concentration remains constant, showing mass-conservation. To incorporate this cycle into the model, together with the different compartment volumes found in the C4 pathway, the amounts of the metabolites were modelled as moles. Due to the conserved cycle, volumes changes were not included in the stoichiometry, rather each metabolite concentration in the rate equation was divided by the volume of the compartment relative to the location of the enzyme. Studies by Edwards *et al.* [19] show the ratio of mesophyll:bundle sheath to be 1.17:1 in *Saccharum officarium*, which is based on chlorophyll concentration [72]. The ratio of chloroplast volume to mesophyll cell volume is 1:2.7 [117]. Further, PEP in the mesophyll cytoplasm was the only metabolite modelled with an initial concentration. All other variables were set to

zero to determine the change in metabolites pools from time zero to steady-state. The transporters were modelled by dividing the V_{max} relative to the area of the chloroplast where they exist. The area ratio of the mesophyll to bundle sheath chloroplast was 1:1.11 which was calculated using the sphere volume and surface area formulae. The transporters are active transporters and therefore their equilibrium constants were set high (1×10^3) [120].

In the case of PEPCase, binding affinities of PA and OAA were not available. Therefore parameter scans were done to determine values that were realistic and suitable for the model. In other cases, parameter scans were conducted to determine the effect of the parameter on the system's variable. For a few of the transporters, the V_{max} values were changed slightly, within physiological ranges, and displayed in the relevant table (under the 'Comment' column). Increasing the V_{max} of transporters is permissible as the orginal values obtained are not truly comparable as they are obtained at different physiological conditions. In addition, the V_{max} selected fell well within accepted physiological ranges.

Fixed species in the input file include the external parameters, HCO_3^- in the mesophyll cytoplasm and CO_2 in the bundle sheath chloroplast. The cofactors (ATP, AMP, ADP, P_i, NADPH and $NADP^+$) were fixed as an initial step in the model. A more complete approach is discussed in Section 6.3.

5.3 Components of the model

Model components, including the enzymes responsible for each reaction, the transporters involved in moving metabolites across compartments, and diffusion steps are described below.

5.3.1 Phosphoenolpyruvate Carboxylase

$$PEP + HCO_3^- \longrightarrow OAA + P_i$$

PEP carboxylase (PEPCase; EC: 4.1.1.31) is primarily found in the mesophyll cytoplasm, irreversibly carboxylating PEP to OAA and inorganic phosphate therefore initiating the C4 cycle. This enzyme is light-regulated, activated by glucose-6-phosphate and glycine [116], and inhibited by MAL and OAA (which are con-

sidered to be non-competitive) [74, 79]. Cooperativity is evident under certain circumstances, in that PEPCase binds its substrates in a sigmoidal fashion at pH 7 (Hill coefficient is 2); yet at pH 8, the pH optimum [104], the binding appears to be hyperbolic, decreasing the K_m and increasing the V_{max} values [116]. Like the pH8 effect, when PEPCase is in the presence of glucose-6-P, the same hyperbolic binding is reported [116]. Further, the presence of Mg^{2+} is not necessary for the binding of PEP to PEPCase, but it increases the affinity of the PEPCase for PEP [2, 5, 82].

This reaction was modelled using an irreversible simplified generic rate equation based on random equilibrium binding of substrates and products [97].

$$v = \frac{\frac{V_f}{K_{mHCO_3}K_{mPEP}}(HCO_3 \times PEP)}{(1 + \frac{HCO_3}{K_{mHCO_3}} + \frac{OAA}{K_{mOAA}} + \frac{MAL}{K_{iMAL}})(1 + \frac{PEP}{K_{mPEP}} + \frac{P_i}{K_{mPi}})}$$

PEP Carboxylase	**Value**	**Reference**	**Comment**
$K_m HCO_3^-$	0.027 mM	[6]	
K_mPEP	8.7 mM	[23]	pH 7
K_mOAA	0.25 mM		assumption
K_mPA	0.6 mM		assumption
K_iMAL	0.97 mM	[74]	illuminated
V_{max}	27.5 μmol min^{-1} (mgChl)$^{-1}$	[38]	

5.3.2 Oxaloacetate transport into the mesophyll chloroplast

There is a very active OAA carrier in chloroplasts [67]. This transporter is light activated and is only slightly inhibited by MAL [35]. Studies conducted by Hatch [39] show an influx of OAA of 2.5 μmol min^{-1} (mgChl)$^{-1}$ in *Z. mays*.

This reaction was modelled using the simplified reversible generic equation based on the same assumptions as PEPCase.

$$v = \frac{\frac{V_f}{K_{mOAA_{cyt}}}(OAA_{cyt} - \frac{OAA_{chl}}{K_{eq}})}{(1 + \frac{OAA_{cyt}}{K_{mOAA_{cyt}}} + \frac{OAA_{chl}}{K_{mOAA_{chl}}} + \frac{MAL}{K_{iMAL}})}$$

Oxaloacetate transporter	Value	Reference	Comment
$K_m OAA_{cyt}$	53 μM	[35]	
$K_m OAA_{chl}$	53 μM	[35]	
K_iMAL	7.5 mM	[35]	
K_{eq}	1×10^3	-	active transport
V_{max}	1.4 μmol min^{-1} (mgChl)$^{-1}$	[35]	modelled as 1.5

5.3.3 NADP malate dehydrogenase

$$\text{OAA + NADPH} \rightleftharpoons \text{MAL + NADP}^+$$

NADP-malate dehydrogenase (NADP-MDH; EC: 1.1.1.82) converts OAA to MAL (MAL) while oxidising NADPH in the mesophyll chloroplast. Upon illumination, the enzyme becomes rapidly activated *in vivo* whereas it is deactivated when placed in the dark [57]. It has a maximum activity of 9.5 μmol min^{-1} (mgChl)$^{-1}$ [104] and a pH optimum of 8.5 [38].

This reaction was modelled using a simplified reversible generic equation based on the same assumptions as PEPCase.

$$v = \frac{\frac{V_f}{K_{mOAA}K_{mNADPH}}(OAA \times NADPH - \frac{MAL \times NADP^+}{K_{eq}})}{(1 + \frac{OAA}{K_{mOAA}} + \frac{MAL}{K_{mMAL}})(1 + \frac{NADPH}{K_{mNADPH}} + \frac{NADP^+}{K_{mNADP^+}})}$$

NADP-MDH	Value	Reference	Comment
K_mOAA	0.056 mM	[59]	*Z.mays*
K_mNADPH	0.024 mM	[59]	*Z.mays*
K_mMAL	32 mM	[59]	*Z.mays*
K_mNADP	0.073 mM	[59]	*Z.mays*
V_{max}	9.5 μmol min^{-1} (mgChl)$^{-1}$	[38]	
K_{eq}	3×10^4	[123]	*P.miliaceum*

5.3.4 MAL transport out of mesophyll chloroplasts

Day *et al.* [13] suggest an exchange diffusion carrier for the uptake of MAL into the chloroplast. Data are contradictory whether OAA and MAL use the same transporter (Section 2.2.3). OAA is also able to use the transporter, hence competitively inhibiting the uptake of MAL. Day *et al.* [13] further suggest that the

K_i of OAA is similar to the actual K_m for the uptake of OAA via the dicarboxylic carrier [13]. Although a V_{max} of 0.83 μmol min $^{-1}$ (mgChl)$^{-1}$ is given at 4°C, extrapolation of the data show a V_{max} of 50 μmol min^{-1} (mgChl)$^{-1}$ (OAA uptake is reported likely to be similar) at 30°C [13]. The values reported of the concentration of MAL in the mesophyll and bundle sheath cells include both the chloroplast and cytoplasm [21].

This reaction was modelled using a simplified generic equation based on the same assumptions as PEPCase.

$$v = \frac{\frac{V_f}{K_{mMAL_{chl}}}(MAL_{chl} - \frac{MAL_{cyt}}{K_{eq}})}{(1 + \frac{MAL_{chl}}{K_{mMAL_{chl}}} + \frac{MAL_{cyt}}{K_{mMAL_{cyt}}} + \frac{OAA}{K_{iOAA}})}$$

MAL Transport	**Value**	**Reference**	**Comment**
$K_m MAL_{chl}$	0.5 mM	[13]	
$K_m MAL_{cyt}$	0.5 mM	[13]	
K_iOAA	0.3 mM	[13]	
K_{eq}	1×10^3	-	active transport
V_{max}	0.83 μmol min^{-1} (mgChl)$^{-1}$	[13]	modelled as 0.7

5.3.5 MAL diffusion between mesophyll and bundle sheath

Diffusion of MAL occurs symplastically via plasmodesmata along the mesophyll and bundle sheath interface [83]. Weiner *et al.* [123] reported a diffusion constant of 5.1 μmol min^{-1} (mgChl)$^{-1}$ mM^{-1}. There is an apparent gradient of 43.2 mM between the mesophyll and bundle sheath, which does not limit photosynthesis [67, 123].

We used the equation as specified in Section 5.2.

$$v = k_d(MAL\_ms\_cyt - MAL\_bs\_cyt)$$

where the diffusion coefficient was set to 10.0 so as to not be rate-limiting in photosynthesis. Currently, the plasmodesmata are yet to be included in the model. Hence, parameters scans were used to determine a diffusion coefficient that would accurately characterise diffusion through the plasmodesmata.

5.3.6 Transport of MAL from bundle sheath cytoplasm to chloroplast

This transport step remains uncharacterised and is thought to be mediated by a specialised transporter, differing from the dicarboxylate transporter found in chloroplasts [104]. However, for modelling purposes, this transporter is treated like a dicarboxylate transporter. The data applied is from spinach [45].

This reaction was modelled using the simplified generic equation based on the same assumptions as PEPCase.

$$v = \frac{\frac{V_f}{K_{mMAL_{cyt}}}(MAL_{cyt} - \frac{MAL_{chl}}{K_{eq}})}{(1 + \frac{MAL_{cyt}}{K_{mMAL_{cyt}}} + \frac{MAL_{chl}}{K_{mMAL_{chl}}})}$$

MAL Transport	Value	Reference	Comment
$K_m MAL_{chl}$	0.4 mM	[45]	
$K_m MAL_{cyt}$	0.4 mM	[45]	
K_{eq}	1×10^3	-	active transport
V_{max}	0.31 μmol min^{-1} $(mgChl)^{-1}$	[45]	used 0.6

5.3.7 NADP-Malic enzyme

$$MAL + NADP^+ \rightleftharpoons PA + CO_2 + NADPH$$

NADP malic enzyme (NADP-ME; EC: 1.1.1.40) is light activated and primarily located in the bundle sheath chloroplasts [37, 10, 78]. It decarboxylates MAL to produce PA while reducing $NADP^+$. The level of CO_2 rises up to ten times that of atmospheric CO_2 [55, 26]. The released CO_2 is the primary substrate of Rubisco which is fed into the Calvin Cycle (CC) for carboxylation and carbon assimilation, thus inhibiting photorespiration. However, CO_2 and not HCO_3^- which is fed into the CC because of the lack of CA in the bundle sheath (Section 2.2.2) and because it is found to be inhibitory to the decarboxylation process in the bundle sheath chloroplasts [53]. The pH optimum is 8.3-8.5 (in maize) [18, 104] with saturating MAL [104]. Contradictions exist in the estimation of the loss of inorganic carbon from the bundle sheath back into the mesophyll. Research shows that approximately between 10% [104] and 30% [123] of inorganic carbon is leaked back into the mesophyll. PEPCase fixes the leaked CO_2 back into the C4 cycle.

This reaction was modelled using the simplified reversible generic equation based on the same assumptions as PEPCase.

$$v = \frac{\frac{V_f}{K_{mMAL}K_{mNADP^+}}(MAL \times NADP^+ - \frac{PA \times NADPH \times CO_2}{K_{eq}})}{(1 + \frac{MAL}{K_{mMAL}} + \frac{PA}{K_{mPA}} + \frac{CO_2}{K_{mCO_2}})(1 + \frac{NADP^+}{K_{mNADP^+}} + \frac{NADPH}{K_{mNADPH}})}$$

NADP-ME	**Value**	**Reference**	**Comment**
K_mMAL	0.12 mM	[52]	pH 8
K_mNADP	0.0046 mM	[52]	pH 8
K_mNADPH	0.045 mM	[129]	
$K_m CO_2$	1.1 mM	[60]	
K_iPA	0.04 mM	-	
K_{eq}	51 mM	[30]	
V_{max}	10.7 μmol min^{-1} (mgChl)$^{-1}$	[38]	

5.3.8 PA transport from chloroplast to cytosol in the bundle sheath cells

Unlike the transporter found in the mesophyll, the translocator in this region is not light activated [21, 81].

This reaction was modelled using the simplified generic equation based on the same assumptions as PEPCase.

$$v = \frac{\frac{V_f}{K_{mPA_{chl}}}(PA_{chl} - \frac{PA_{cyt}}{K_{eq}})}{(1 + \frac{PA_{chl}}{K_{mPA_{chl}}} + \frac{PA_{cyt}}{K_{mPA_{cyt}}})}$$

PA Transport	**Value**	**Reference**	**Comment**
$K_m PA_{cyt}$	0.6 mM	[81]	*Panicum miliaceum*
$K_m PA_{chl}$	0.6 mM	[81]	*Panicum miliaceum*
K_{eq}	1×10^3	-	active transport
V_{max}	0.055 μmol min^{-1} (mgChl)$^{-1}$	[81]	modelled as 0.8

5.3.9 Diffusion of pyuvate between bundle sheath and mesophyll cells

The transport of PA from the bundle sheath to mesophyll cells has a small gradient, appearing to oppose the flux of the metabolite. This is due to the accumulation of PA in the mesophyll chloroplast meaning that the combined amount of PA in the chloroplast and cytoplasm of the mesophyll has a higher concentration of PA than the bundle sheath's cytoplasm and chloroplast [67, 21].
We used the equation as specified in Section 5.2.

$$v = k_d(MAL\_ms\_cyt - MAL\_bs\_cyt)$$

where the diffusion coefficient was set to 10 so as to not be rate-limiting in photosynthesis.

5.3.10 Transport of PA from the mesophyll cytoplasm to chloroplast

The transport of PA into the chloroplast is proposed to be via a novel translocator in the envelope membrane. This translocator catalyses the light-dependent uptake of PA and exists as cotransport with H^+ [21, 81].

This reaction was modelled using the simplified generic equation based on the same assumptions as PEPCase.

$$v = \frac{\frac{V_f}{K_{mPA_{cyt}}}(PA_{cyt} - \frac{PA_{chl}}{K_{eq}})}{(1 + \frac{PA_{cyt}}{K_{mPA_{cyt}}} + \frac{PA_{chl}}{K_{mPA_{chl}}})}$$

PA Transport	Value	Reference	Comment
$K_m PA_{chl}$	0.85 mM	[21]	*Zea mays*
$K_m PA_{cyt}$	0.85 mM	[21]	*Zea mays*
K_{eq}	10^3	-	active transport
V_{max}	0.5 μmol min^{-1} $(mgChl)^{-1}$	[81]	

5.3.11 Pyruvate, Orthophosphate Dikinase

$$\text{PA + ATP + Pi} \rightleftharpoons \text{PEP + AMP + PPi}$$

Pyruvate,Orthophosphate Dikinase (PPDK; EC: 2.7.9.1) is the final enzyme of the C4 pathway. It catalyses the ATP- and Pi-dependent regeneration of PEP in the mesophyll chloroplasts. PPDK is reversible (although in this reaction, it is considered energetically unfavourable at pH 7 [113]), light regulated (up to 20 fold activation within minutes [104] and rate-limiting [118]. High levels of adenylate kinase and pyrophosphatase ensure that PPDK performs effectively in PEP synthesis [20]. The products of this enzyme are PA, PPi and AMP. Usually PPi is converted to 2Pi by pyrophosphatase and AMP consumes another ATP to generate 2ADP by adenylate kinase. Adenylate kinase is not thought to have a regulatory role in photosynthesis as it has a high V_{max} value and low substrate K_m values [33].

This reaction was modelled with the following equation based on the same assumptions as PEPCase.

$$v = \frac{\frac{V_f}{K_{mPA}K_{mATP}K_{mP_i}}(PA \times ATP \times Pi - \frac{PEP \times AMP \times PP_i}{K_{eq}})}{(1 + \frac{PA}{K_{mPA}} + \frac{PEP}{K_{mPEP}})(1 + \frac{ATP}{K_{mATP}} + \frac{AMP}{K_{mAMP}})(1 + \frac{P_i}{K_{mP_i}} + \frac{PP_i}{K_{mPP_i}})}$$

PPDK	Value	Reference	Comment
K_mPA	0.11 mM	[43]	Maize
K_mATP	0.009 mM	[43]	Maize
K_mPi	0.56 mM	[56]	Maize
K_mPEP	0.11 mM	[20]	
K_mAMP	13 μM	[56]	
K_mPPi	0.32 μM	[56]	
K_{eq}	2×10^{-4}	[42]	
V_{max}	6.5 μmol min^{-1} $(mgChl)^{-1}$	[39]	

5.3.12 Transport of PEP out of mesophyll chloroplasts

PEP is transported out of the mesophyll chloroplast via a phosphate transporter for the regeneration of OAA. The transporter is a PEP/Pi antiporter.

This reaction was modelled using the simplified generic equation based on the

same assumptions as PEPCase.

$$v = \frac{\frac{V_f}{K_{mPEP_{chl}} K_{mPi_{cyt}}}(PEP_{chl} \times Pi_{cyt} - \frac{PEP_{cyt} \times Pi_{chl}}{K_{eq}})}{(1 + \frac{PEP_{chl}}{K_{iPEP_{chl}}} + \frac{PEP_{cyt}}{K_{iPEP_{cyt}}})(1 + \frac{Pi_{cyt}}{K_{mPi_{cyt}}} + \frac{Pi_{chl}}{K_{mPi_{chl}}})}$$

PEP Transporter	**Value**	**Reference**	**Comment**
$K_m Pi_{cyt}$	0.045 mM	[104]	
$K_i PEP_{chl}$	0.086 mM	[104]	
$K_m Pi_{chl}$	0.5 mM	[104]	
$K_i PEP_{cyt}$	0.8 mM	[104]	
K_{eq}	1×10^3	-	active transport
V_{max}	1 μmol min^{-1} $mgChl^{-1}$	[80]	modelled as 10

5.3.13 The Concentration of the Fixed Species in the Model

Below are the parameter concentrations used in the model. HCO_3^- is the source of carbon whereas CO_2 is the sink. For the purpose of this model they are kept constant and modelled as external parameters. The rest of cofactors within the model and there concentrations are also mainained at a constant concentration.

[Metabolite]	(mM)	Ref
HCO_3^-	0.041	[68]
CO_2	0.7	[68]
NADPH_ms_chl	1.37	[117]
NADP_ms_chl	0.48	[117]
NADPH_bs_chl	0.29	[64]
NADP_bs_chl	0.21	[64]
ATP_ms_chl	0.85	[117]
AMP_ms_chl	0.15	[117]
Pi_ms_cyt	10.0	[117]
Pi_ms_chl	15.0	[117]
PPi_ms_chl	10.0	-

5.4 Analysis of the Model

Once the pathway was established, it was written in the form of a PySCeS [84] input file (Appendix B.1). Parameters, variables and enzyme kinetics were applied to the model and it was analysed using PySCeS. The analysis was performed on a MSI450 laptop computer running Mandriva Linux 2007.0. Parameters scans were performed and certain parameters were altered within physiological ranges. The model was analysed by (i) time course analysis, (ii) steady-state analysis, and (iii) metabolic control analysis.

5.5 Results and Interpretations

5.5.1 Time-course Analysis of Change in Metabolite Concentration

This study demonstrates the metabolite pools filling up from time zero to steady-state and the likely steady-state concentrations of metabolites found in this pathway. Due to the carbon fixation pathway being a conserved cycle, irrespective of which metabolite was initialised, the steady-state concentrations will be the same. Figures 5.2 & 5.3 show the metabolite pools filling when PEP in the mesophyll cytoplasm and PA in the bundle sheath chloroplast respectively are set to 4800 nmoles whilst the other metabolites are initialised as zero. A comparison of these values can be found in Appendix B.2.

5.5.2 Steady-State Analysis

Steady-state analysis presents the likely metabolite concentrations and flux value at steady-state in the system. The values in Table 5.1 represent the model predicted values, contrasted with the experimental values found in literature for each variable in the respective compartment. The results demonstrate large pools of MAL and PA in the mesophyll chloroplast as well as PA in the bundle sheath chloroplast. As a result, the pools of PEP in the mesophyll chloroplast as well as MAL in the bundle sheath cytoplasm are relatively low compared to those found experimentally. Reasons for these discrepancies will be given in the discussion. Although there is a contrast between the experimental and theoretical data presented, the data found theoretically is still in a physiologically plausible range.

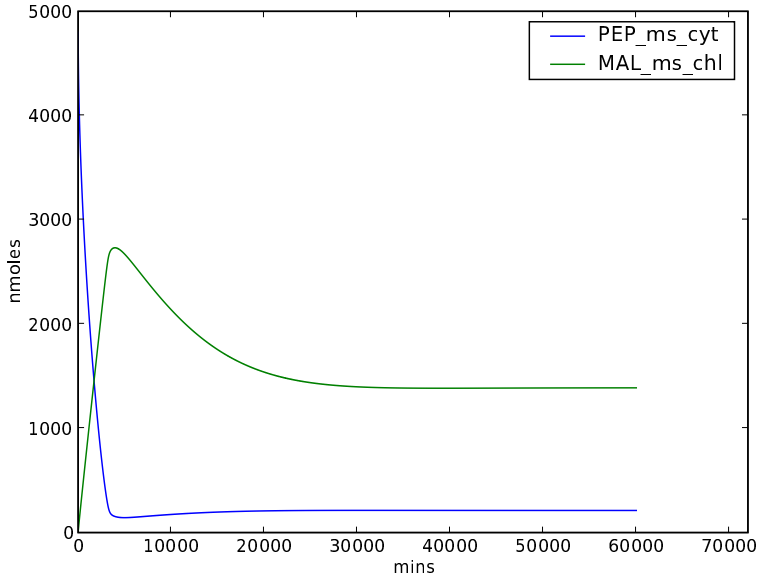

(a) Time-course studies of the filling of metabolite pools in the carbon fixation pathway. PEP's initial value is set to 4800 nmoles whereas the rest of the metabolites initial values are set to zero.

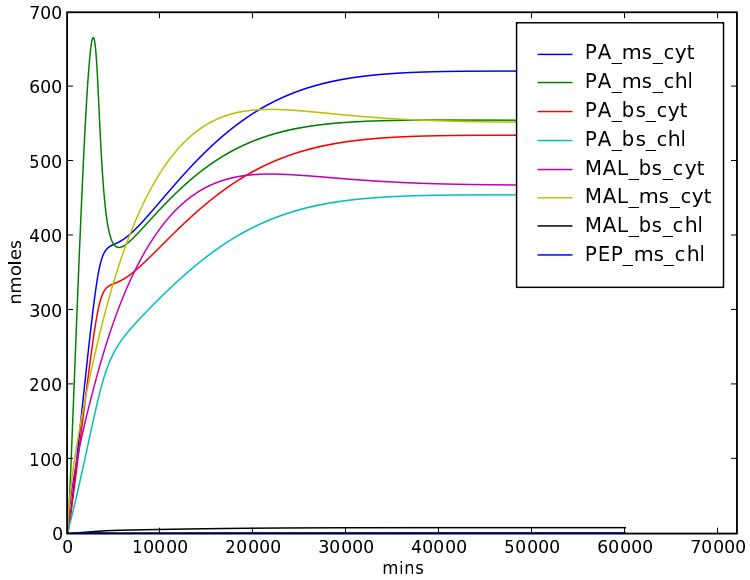

(b) Time-course studies of the filling of metabolite pools in the carbon fixation pathway. PEP's initial value is set to 4800 nmoles whereas the rest of the metabolites initial values are set to zero.

Figure 5.2: Time course studies of initialisation of PEP in the mesophyll cytoplasm and subsequent filling of metabolite pools.

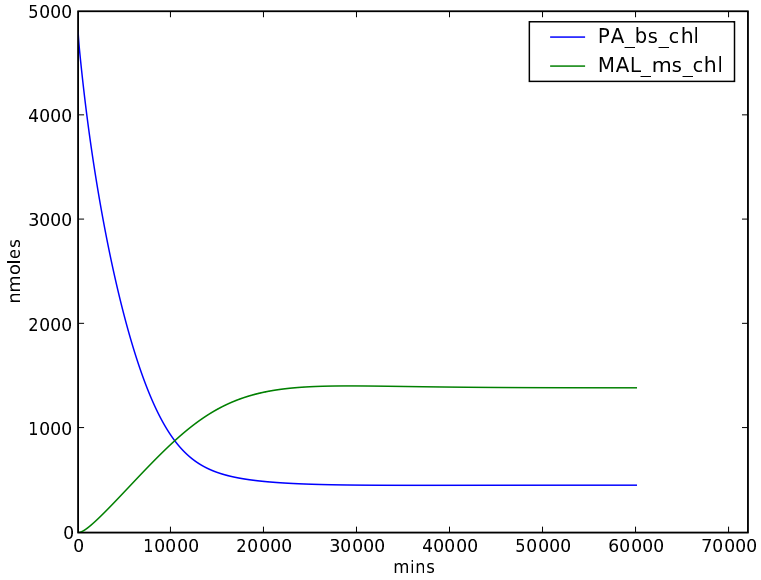

(a) Time-course studies of the filling of metabolite pools in the carbon fixation pathway. PA's initial value is set to 4800 nmoles whereas the rest of the metabolites initial values are set to zero.

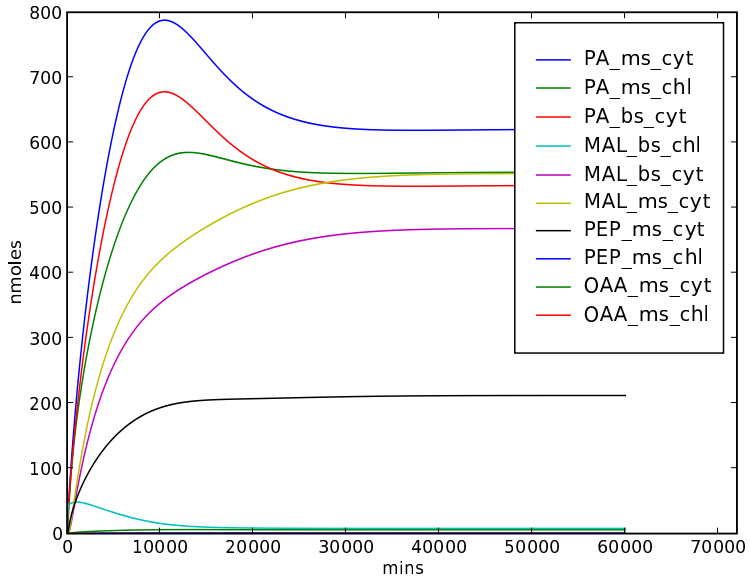

(b) Time-course studies of the filling of metabolite pools in the carbon fixation pathway. PA's initial value is set to 4800 nmoles whereas the rest of the metabolites initial values are set to zero.

Figure 5.3: Time course studies of initialisation of PA in the bundle sheath chloroplast and subsequent filling of metabolite pools.

Variable	Model Predicted Value (mM)	Experimental Value (mM)	Reference
PEP_ms_chl	0.03	-	
PEP_ms_cyt	2.68	-	
OAA_ms_cyt	0.07	-	
OAA_ms_chl	0.01	-	
MAL_ms_chl	47.45	35	estimation* from [21]
MAL_ms_cyt	6.99	17	estimation* from [21]
MAL_bs_cyt	6.93	10.5	estimation* from [67, 104]
MAL_bs_chl	0.32	1.5	estimation* from [124, 104]
PA_bs_chl	18.19	4	estimation* from [67]
PA_bs_cyt	7.92	2.3	estimation* from [67]
PA_ms_cyt	7.86	5	estimation* from [67]
PA_ms_chl	18.97	1.08 - 2.01	[3, 117]

Table 5.1: Experimental values (found in literature) and model predicted values of variables at steady-state. *Concentrations of metabolites are given for the mesophyll or bundle sheath cells without taking the chloroplast into account. However, some data only take chloroplast into account. Therefore, using these two sets of data, an estimation was made by subtracting the chloroplast value from the mesophyll or bundle sheath respectively.

Figure 5.4 illustrates the calculated flux control coefficients. The MAL transporter in the bundle sheath shows the highest of control in the system, followed by both the PA transporters, the MAL transporter in mesophyll, the PEP transporter and PEPCase.

As the model is a conserved cycle, the predicted flux will remain constant throughout the pathway. The steady-state flux in this system was found to be 0.604 nmoles/min.

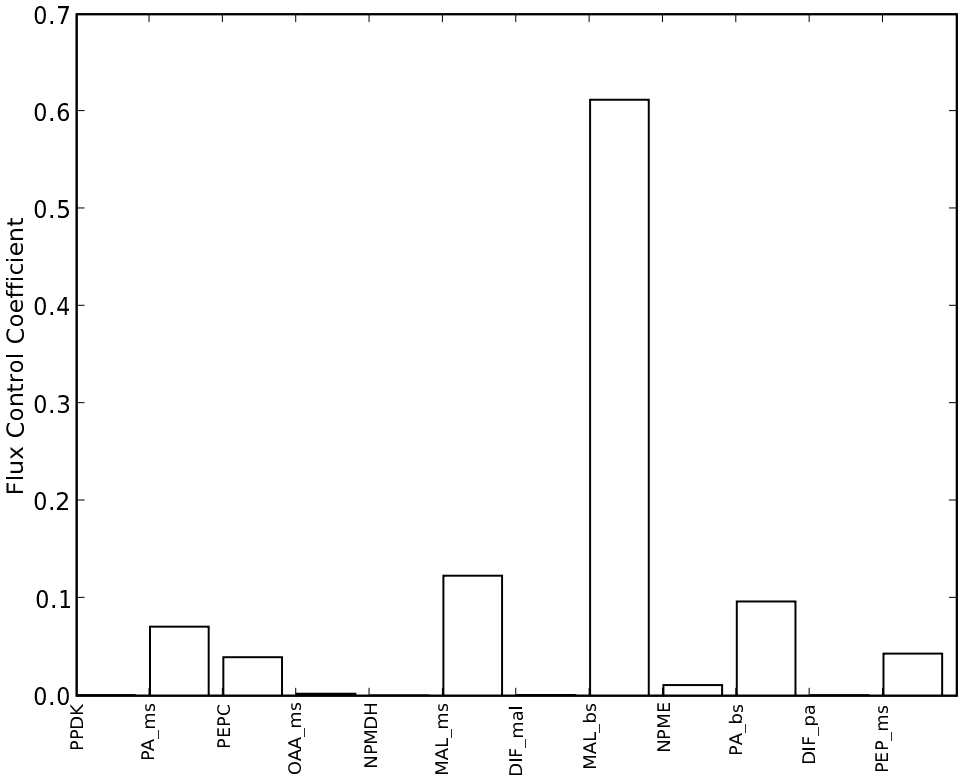

Figure 5.4: The flux control coefficients found in the carbon fixation pathway.

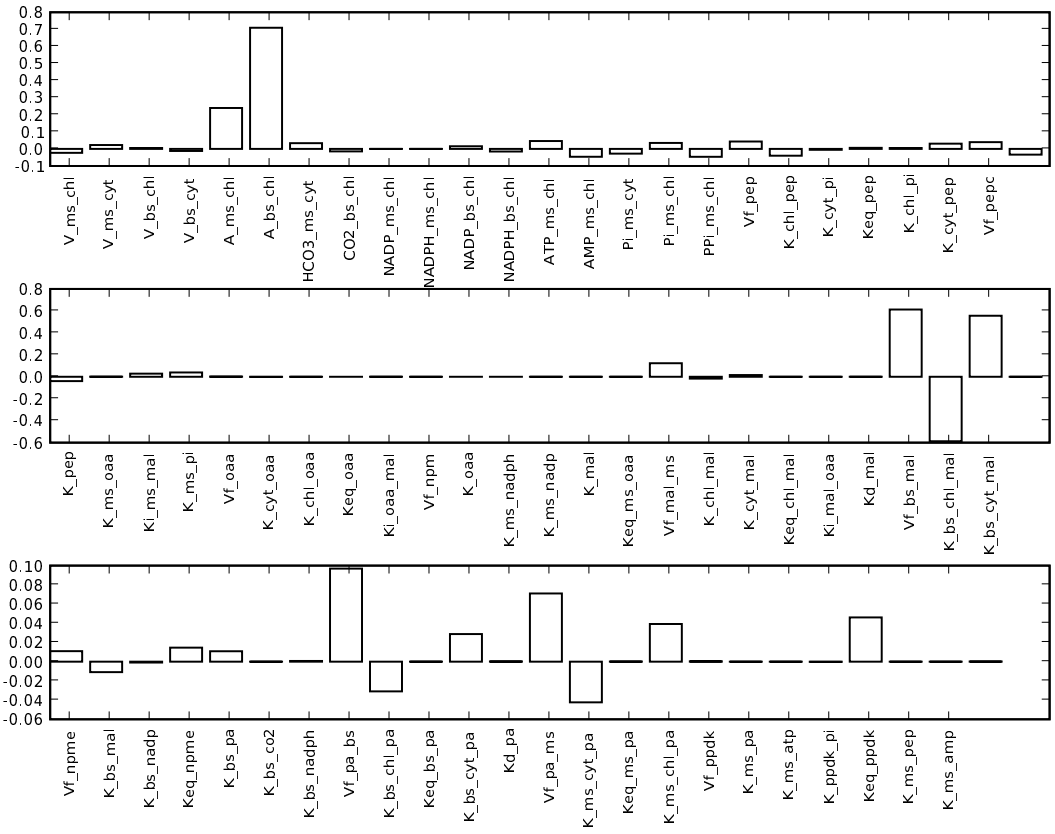

Figure 5.5: Response Coefficients (RC) in the Carbon Fixation Pathway with respect to the flux through NADP-ME. All response coefficients are in the order that are found in the PySCeS input file in B.1.

5.5.3 Response Coefficients

The response coefficient calculated and presented are from the flux through NADP-ME, the decarboxylating enzyme in the carbon fixation pathway (Figure 5.5). The response coefficient showing the highest amount of control include the surface area of the bundle sheath chloroplast. This is followed by the surface area of the mesophyll chloroplast, the V_{maxes} of the MAL and PA transporter in the bundle sheath and PA in the mesophyll. It further includes the saturation constants of MAL to the bundle sheath transporter, the saturation constant of PA of the mesophyll transporter as well as the equilibrium constant of PPDK.

5.6 Discussion

The above results begin to give an insight into the photosynthesising leaf. Metabolic control analysis is just the first step in the analysis of this model, although it is suggested that modifications are made for further analysis (Section 6.3). The study illustrates the change in metabolite concentration from time zero to steady-state whilst predicting the metabolite concentrations and flux of the system. It has further brought to light the flux and concentration control coefficients as well as the response coefficients.

The time-course and steady-state analysis highlight two metabolites, MAL and PA, having high concentration pools. Although, these levels are still physiologically plausible, they appear to drain or withhold from other pools in the carboxylating pathway. MAL in the mesophyll chloroplast has high concentrations, therefore affecting the OAA concentration in the mesophyll chloroplast and cytoplasm. PA in the mesophyll and bundle sheath chloroplast affect the levels of PEP in the mesophyll cytoplasm. The metabolite control coefficients and response coefficients emphasize the factors affecting these OAA and PEP levels. The factors affecting the OAA concentration include the OAA transporter and the MAL transporter in both the mesophyll and bundle sheath cells. However, the factors affecting PEP levels are the MAL transporter in the mesophyll and PEPCase. Therefore strategies for lowering MAL and PA in the model include targetting the MAL transporter in both compartments, OAA transporter and PEPCase. Information regarding the transporters in both the mesophyll and bundle sheath is extremely limited, therefore the model may be more accurately modelled as more experimental data becomes available.

Possible reasons for the discrepancy between the experimental and theoretical data include: (i) limited parameter data therefore the set of parameters may be based on other plant species, (ii) parameter data may have been collected under different physiological conditions (pH, temperature *etc*.), (iii) the validation data was collected from different C4 species and due to the lack of data, many of the concentrations had to estimated.

From the study, it is also apparent that the diffusion gradient between the mesophyll and bundle sheath is considerably small. As presented (Section 2.2.3), there

is a required 2 mM gradient between the mesophyll and bundle sheath. However, both PA and MAL have gradients in the region of 0.07mM. Possible ways of correcting this are discussed in Section 6.3.

The flux control analysis shows the highest control was found in the MAL transporter in the bundle sheath. Many of the other transporters also showed high control on the flux. However, as this data is still very limited, it suggested that a more reliable control of the flux may be via PEPCase, the only irreversible step in the carbon fixing pathway. Theoretical calculations show the flux control exerted by PEPase to be 0.03 whereas experimental determinations show it to be 0.26 [14]. The flux control coefficients show possible targets for manipulation to increase the flux through the carbon fixation pathway.

The response coefficients (RC) describe a combination of the control coefficients and elasticities in a system

$$\mathrm{R}_p^y = C_{\nu_i}^y \times \epsilon_p^{\nu_i}$$

where $C_{\nu_i}^y$ is the control coefficient and $\epsilon_p^{\nu_i}$ is elasticity coefficient defined as the relative change in reaction rate (ν_i) caused by any parameter (p) i.e.

$$\frac{\mathrm{d}\ \ln \nu_i}{\mathrm{d}\ \ln p}$$

The control coefficient indicates the control of the local reaction rate on either the flux or concentration whereas the elasticities show the effect of the parameter on the enzyme activity. These RCs generally show the parameter which has the largest effect on the whole system and hence the sensitivity of the system to a parameter. Therefore, as shown above, the PEP transporter, the area of the mesophyll chloroplast, the half saturation constant of P_i to the PEP transporter and the concentration of P_i in the mesophyll cytoplasm have the largest response coefficients in the system. These RCs also indicate possible engineering targets in the system.

5.7 Conclusions

This study is paving the way for developing strategies for increasing the flux through the carbon fixation pathway. Parameters controlling the system (flux and metabolite concentrations) are highlighted and indicate possible targets for further study, not only experimentally but also theoretically. Although this work requires modification, the foundation of the model has been laid by the parameters that have been collected, the volumes of the compartments and the areas of the transporters have been incorporated into the model. Further, as it stands, the model is able to reach steady-state. This work is therefore just the first step in the kinetic investigation of photosynthesis in sugarcane. Further, the work also has many implications and future possibilities which are outlined in Chapter 6.

Chapter 6

Discussion and Future Work

The work covered in Chapters 4 and 5 has scope for improvement of both the structural and kinetic models. Below, model modification for each model (Sections 6.1 & 6.3) are discussed as well as proposed further analysis of the models (Sections 6.2 & 6.4). Future work on the sugarcane project is also discussed in Section 6.5.

6.1 Proposed Extentions to the Structural Model

As the structural model stands, the pathways are complete in representing sucrose production and accumulation in sugarcane. As kinetic data becomes available from the different pathways, it may be added to this model to form the basis for assembling a full kinetic model.

6.2 Proposed Further Analysis on the Structural Model

Elementary mode analysis has already been performed on the structural model, aiding in answering many questions regarding favoured pathways and energy consumption. Further analysis of the model may include extreme pathways (a subset of elementary modes) as well as flux balance analysis (Section 3.3.1). FBA will determine the flux distribution through the pathway and one can validate this using experimental flux data. This will have implications for targeting the main stream flux in order to manipulate fluxes that are of industrial importance (e.g. sucrose production in the leaf).

Further work on the model may include placing multiple structural models together so as to simulate different internodes, like the kinetic model by Uys [119] where internodes 3-10 were modelled. The sugarcane plant is unique in that there is only one leaf per internode, therefore building an 'internode model' will be as simple as placing one structural model on top of another. Younger internodes are generally characterised as having high levels of futile cycling and show degradation of sucrose to glucose and fructose. However, more mature internodes generally have much higher levels of sucrose and the synthesis thereof from glucose and fructose (Section 4.4). This model can also then be analysed using FBA, hopefully capturing the different metabolic states between the immature and mature internodes.

6.3 Proposed Extentions to the Kinetic Model

The goal of the kinetic model was to assemble a model that could reach steady-state. In the first step, we merely wanted to collate the kinetic data, incorporate the volumes of the compartments and areas of the transporters for their respective chloroplast into the model. However, the next step is to get the model to predict metabolite concentrations to match experimental concentrations. With this in mind, the following are proposed as extentions to the kinetic model:

- accurately characterising plasmodesmata frequency and surface area,
- modelling the adenylate pool using forcing functions,
- more accurate parameter values.

Characterising plasmodesmata frequency The diffusion in the model was modelled using basic diffusion coefficients mulitplied by the difference in the metabolite concentrations between the two compartments. The problem with this however, is that the surface area of the plasmodesmata between the two cell types is not taken into consideration. The orientation of the cells, together with the plasmodesmata frequency, will have a large effect on the overall diffusion of metabolites between the cells. Data of plasmodesmata and surface area between mesophyll and bundle cells is available which can be incorporated into the kinetic model [83, 95, 123].

Modelling the adenylate pool using forcing functions As discussed in Section 3.5, a more accurate discription of the adenylate pool can be captured using forcing functions. Many reactions produce and consume the adenylate pool but due to the nature of adenylate kinase, the adenylate pool is kept generally near equilibrium. The forcing function equations in Section 3.5, together with C_A = 1.39, P = 2.09 and K_{eq} (Adenylate kinase) = 0.83 can therefore be used in the kinetic model. Together with this, regeneration of inorganic phosphate and ATP need to be taken into account as well as a non-specific demand of ATP seen in Figure 6.1 [114].

More accurate parameter values Many of the parameter values are from many different plants within the NADP-ME subtype. This, may give possible reason for high levels of MAL and PA seen in the mesophyll. As more sugarcane data becomes available, this may be added to the parameters and validation data to develop a more accurate model. This is particularly applicable to the transporters in the C4 pathway.

6.4 Proposed Further Analysis on the Kinetic Model

Supply-Demand analysis can be performed on the overall model of the leaf and storage parenchyma on the linking metabolite, sucrose. However, this approach will be limited until kinetic data of sucrose in the phloem becomes available. It was first demonstrated that the production and accumulation of sucrose in sugarcane leaves inhibits photosynthesis during the day [31]. This was further investigated to establish a link between the accumulation of sucrose in the internodes and the rate of photosynthesis. Experimental evidence by McCormick *et al.* [73] shows that the photosynthetic sink regulates photosynthesis. Understanding this vital mechanism between sourse and sink could also be used as a genetic manipulating point for increasing sucrose accumulation.

6.5 Future Work on the Sugarcane Project

The 'sugarcane project' aims to represent the sugarcane plant as accurately as possible. To date, futile cycling and sucrose accumulation in internodes 3-10 have been investigated by our group, and now the carbon fixation pathway is being

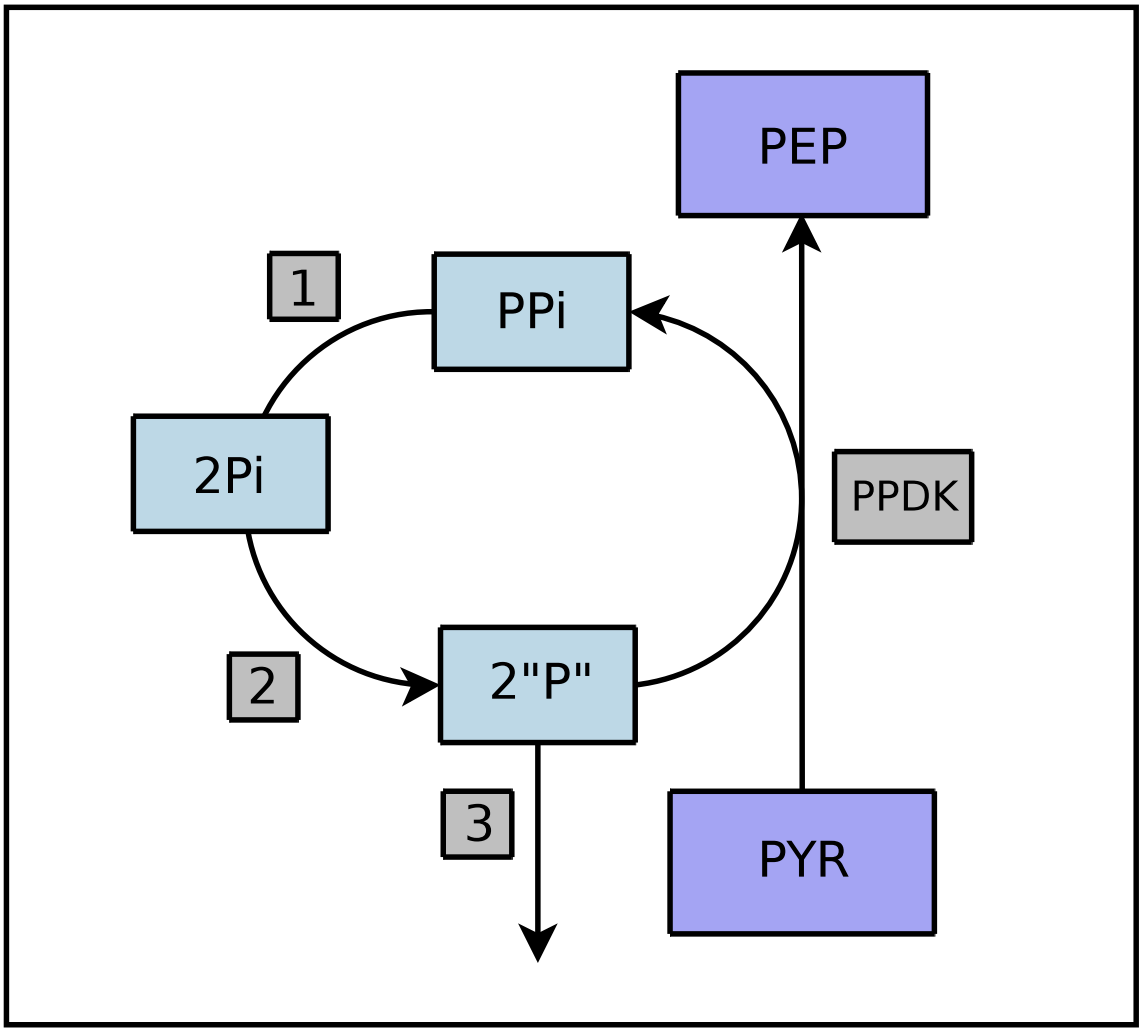

Figure 6.1: The proposed method of modelling adenylate kinase, pyrophosphatase and Pi in the PPDK step. Steps 1, 2, 3 represent pyrophosphatase, ATP regeneration (ATP synthase) and non-specific ATP demand respectively. This model assumes that adenylate kinase is in equilibrium. PPDK, Pyruvate,Orthophophate Dikinase; PA, Pyruvate; PEP, Phosphoenolpyruvate

investigated.

The C4 plant consists of leaf, stalk and root system. Possible future work on the project includes:

Including Sucrose Production in the Carbon Fixation Kinetic Model This will be the next step in kinetically modelling sucrose production in the leaf. The model will include the Calvin cycle, which has been modelled by Poolman *et al.* [92]. This may be used as a foundation and adapted to include sugarcane parameters. Further, the sucrose producing pathway in the mesophyll will need to be included. Doing metabolic control analysis on this model should shed more light on possible control of sucrose production during photosynthesis. This information can be collated to the supply-demand analysis of source and sink on sucrose in the phloem.

Modelling of the Root System The root system is a fundamental part of the plant and plays a vital role in the supply of nutrients and water to the plant. Possible components to be modelled in the roots system include: nitrogen fixation and amino acid synthesis. A suggested approach would be a structural model initially, followed by a kinetic model.

As seen from the above, the 'sugarcane project' has abundant potential for determining the control points in increasing sucrose production and accumulation, paving the way for identifying manipulation points in genetic engineering. An increased sucrose production and accumulation has profitable implications for improving sucrose yield in an already well established sugar industry.

Appendix A

A.1 PySCeS Input for Carbon Fixation

_ms: mesophyll, _s: stroma, _chl: chloroplast, _bs: bundle sheath cell
_vac: vacuole, _phl: phloem, _apo: apoplast, _com: companion cell
_stp: storage parenchyma, _cyt: cytoplasm: _sym: symplastic

FIX: CO2_air SUC_phl NADPH_ms_chl NADP_ms_chl NADP_bs_chl NADPH_bs_chl
ATP_ms_chl AMP_ms_chl Pi_ms_chl ATP_bs_chl ADP_bs_chl Pi_bs_chl ADP_ms_chl
UDP_ms_cyt UDP_bs_cyt Pi_bs_cyt UTP_ms_cyt UTP_bs_cyt Pi_ms_cyt

#CARBON FIXATION
R1:
    {1}CO2_air $\longrightarrow$ {1}HCO3_ms_cyt
    v_R1
v_R1 = 1
CO2_air = 1
HCO3_ms_cyt = 1

R2:
    {1}PEP_ms_chl $\longrightarrow$ {1}PEP_ms_cyt
    v_R2
v_R2 = 1
PEP_ms_chl = 1
PEP_ms_cyt = 1

R3:

{1}HCO3_ms_cyt + {1}PEP_ms_cyt ⟶ {1}OAA_ms_cyt + {1}Pi_ms_cyt

v_R3

v_R3 = 1

OAA_ms_cyt = 1

R4:

{1}OAA_ms_cyt ⟶ {1}OAA_ms_chl

v_R4

v_R4 = 1

OAA_ms_chl = 1

R5:

{1}OAA_ms_chl + {1}NADPH_ms_chl = {1}MAL_ms_chl + {1}NADP_ms_chl

v_R5

v_R5 = 1

MAL_ms_chl = 1

R6:

{1}MAL_ms_chl ⟶ {1}MAL_ms_cyt

v_R6

v_R6 = 1

MAL_ms_cyt = 1

R7:

{1}MAL_ms_cyt = {1}MAL_bs_cyt

v_R7

v_R7 = 1

MAL_bs_cyt = 1

R8:

{1}MAL_bs_cyt ⟶ {1}MAL_bs_chl

v_R8

v_R8 = 1

MAL_bs_chl = 1

R9:

{1}MAL_bs_chl + {1}NADP_bs_chl = {1}CO2_bs_chl + {1}PA_bs_chl + {1}NADPH_bs_chl

v_R9

v_R9 = 1

CO2_bs_chl = 1

PA_bs_chl = 1

R10:

{1}PA_bs_chl ⟶ {1}PA_bs_cyt

v_R10

v_R10 = 1

PA_bs_cyt = 1

R11:

{1}PA_bs_cyt = {1}PA_ms_cyt

v_R11

v_R11 = 1

PA_ms_cyt = 1

R12:

{1}PA_ms_cyt ⟶ {1}PA_ms_chl

v_R12

v_R12 = 1

PA_ms_chl = 1

R13:

{1}PA_ms_chl + {1}ATP_ms_chl + {1}Pi_ms_chl = {1}PEP_ms_chl + {1}AMP_ms_chl + {1}PPi_ms_chl

v_R13

v_R13 = 1

R14:

{1}PPi_ms_chl = {2}Pi_ms_chl

v_R14

v_R14 = 1

##PRODUCTION OF ASPARTATE AND ALANINE [4]

R15:
{1}OAA_ms_chl + {1}GLM_ms_chl = {1}ASP_ms_chl + {1}KGT_ms_chl
v_R15
v_R15 = 1
ASP_ms_chl = 1

R16:
{1}ASP_ms_chl ⟶ {1}ASP_ms_cyt
v_R16
v_R16 = 1
ASP_ms_cyt = 1

R17:
{1}ASP_ms_cyt = {1}ASP_bs_cyt
v_R17
v_R17 = 1
ASP_bs_cyt = 1

R18:
{1}ASP_bs_cyt ⟶ {1}ASP_bs_mit
v_R18
v_R18 = 1
ASP_bs_mit = 1

R19:
{1}ASP_bs_mit + {1}KGT_bs_mit = {1}OAA_bs_mit + {1}GLM_bs_mit
v_R19
v_R19 = 1
OAA_bs_mit = 1

R20:
{1}OAA_bs_mit ⟶ {1}OAA_bs_cyt

v_R20
v_R20 = 1
OAA_bs_cyt = 1

R21:
{1}OAA_bs_cyt ⟶ {1}OAA_bs_chl
v_R21
v_R21 = 1
OAA_bs_chl = 1

R22:
{1}OAA_bs_chl + {1}NADPH_bs_chl ={1} MAL_bs_chl + {1}NADP_bs_chl
v_R22
v_R22 = 1

R23:
{1}PA_bs_cyt + {1}GLM_bs_cyt = {1}ALA_bs_cyt + {1}KGT_bs_cyt
v_R23
v_R23 = 1
ALA_bs_cyt = 1

R24:
{1}ALA_bs_cyt = {1}ALA_ms_cyt
v_R24
v_R24 = 1
ALA_ms_cyt = 1

R25:
{1}ALA_ms_cyt ⟶ {1}ALA_ms_chl
v_R25
v_R25 = 1
ALA_ms_chl = 1

R26:
{1}ALA_ms_chl + {1}KGT_ms_chl = {1}PA_ms_chl + {1}GLM_ms_chl

v_R26
v_R26 = 1
R27:
{1}GLM_bs_mit = {1}GLM_bs_cyt
v_R27
v_R27 = 1

R28:
{1}KGT_bs_mit = {1}KGT_bs_cyt
v_R28
v_R28 = 1

#CALVIN CYCLE

R29:
{3}RUBP_bs_chl + {3}CO2_bs_chl ⟶ {6}G3P_bs_chl
v_R29
v_R29 = 1
RUBP_bs_chl = 1
G3P_bs_chl = 1

R30:
{6}G3P_bs_chl + {6}ATP_bs_chl = {6}GBP_bs_chl + {6}ADP_bs_chl
v_R30
v_R30 = 1
GBP_bs_chl = 1

R31:
{6}GBP_bs_chl + {6}NADPH_bs_chl = {6}TRP_bs_chl + {6}Pi_bs_chl + {6}NADP_bs_chl
v_R31
v_R31 = 1
TRP_bs_chl = 1

R32:
{2}TRP_bs_chl = {1}FRU16BP_bs_chl

v_R32
v_R32 = 1
FRU16BP_bs_chl = 1

R33:
{1}FRU16BP_bs_chl ⟶ {1}FRU6P_bs_chl + {1}Pi_bs_chl
v_R33
v_R33 = 1
FRU6P_bs_chl = 1

R34:
{1}FRU6P_bs_chl + {1}TRP_bs_chl = {1}XU5P_bs_chl + {1}ERTH4P_bs_chl
v_R34
v_R34 = 1
XU5P_bs_chl = 1
ERTH4P_bs_chl = 1

R35:
{1}ERTH4P_bs_chl + {1}TRP_bs_chl = {1}SEDH17BP_bs_chl
v_R35
v_R35 = 1
SEDH17BP_bs_chl = 1

R36:
{1}SEDH17BP_bs_chl = {1}SEDH7P_bs_chl + {1}Pi_bs_chl
v_R36
v_R36 = 1
SEDH7P_bs_chl = 1

R37:
{1}SEDH7P_bs_chl + {1}TRP_bs_chl = {1}XU5P_bs_chl + {1}RI5P_bs_chl
v_R37
v_R37 = 1
RI5P_bs_chl = 1

R38:

{1}RI5P_bs_chl = {1}RIBU5P_bs_chl

v_R38

v_R38 = 1

RIBU5P_bs_chl = 1

R39:

{2}XU5P_bs_chl = {2}RIBU5P_bs_chl

v_R39

v_R39 = 1

R40:

{3}RIBU5P_bs_chl + {3}ATP_bs_chl = {3}RUBP_bs_chl + {3}ADP_bs_chl

v_R40

v_R40 = 1

RUBP_bs_chl = 1

R41:

{1}TRP_bs_chl + {1}Pi_bs_cyt = {1}TRP_bs_cyt + {1}Pi_bs_chl

v_R41

v_R41 = 1

TRP_bs_cyt = 1

##TRANSITION OF G3P_calvincycle TO DHAP IN MS_chl

R42:

{1}G3P_bs_chl + {1}Pi_bs_cyt = {1}G3P_bs_cyt + {1}Pi_bs_chl

v_R42

v_R42 = 1

G3P_bs_cyt = 1

R43:

{1}G3P_bs_cyt = {1}G3P_ms_cyt

v_43

v_R43 = 1

G3P_ms_cyt = 1

R44:
{1}G3P_ms_cyt ⟶ {1}G3P_ms_chl
v_R44
v_R44 = 1
G3P_ms_chl = 1

R45:
{1}G3P_ms_chl + {1}ATP_ms_chl = {1}GBP_ms_chl + {1}ADP_ms_chl
v_R45
v_R45 = 1
GBP_ms_chl = 1

R46:
{1}GBP_ms_chl + {1}NADPH_ms_chl = {1}TRP_ms_chl + {1}NADP_ms_chl + {1}Pi_ms_chl
v_R46
v_R46 = 1
TRP_ms_chl = 1

R47:
{1}TRP_ms_chl ⟶ {1}TRP_ms_cyt
v_R47
v_R47 = 1
TRP_ms_cyt = 1

R48:
{1}TRP_ms_cyt = {1}TRP_bs_cyt
v_R48
v_R48 = 1
TRP_bs_cyt = 1

#PRODUCTION OF SUC IN MESOPHYLL FROM DHAP

R49:

{2}TRP_ms_cyt = {1}FRU16BP_ms_cyt

v_R49

v_R49 = 1

R50:

{1}FRU16BP_ms_cyt = {1}HEXP_ms_cyt + {1}Pi_ms_cyt

v_R50

v_R50 = 1

HEXP_ms_cyt = 1

R51:

{1}HEXP_ms_cyt + {1}UTP_ms_cyt = {1}UDPGLC_ms_cyt + {1}PPi_ms_cyt

v_R51

v_R51 = 1

UDPGLC_ms_cyt = 1

R52:

{1}PPi_ms_cyt = {2}Pi_ms_cyt

v_R52

v_R52 = 1

R53:

{1}HEXP_ms_cyt + {1}UDPGLC_ms_cyt = {1}SUC6P_ms_cyt + {1}UDP_ms_cyt

v_R53

v_R53 = 1

SUC6P_ms_cyt = 1

R54:

{1}SUC6P_ms_cyt ⟶ {1}SUC_ms_cyt + {1}Pi_ms_cyt

v_R54

v_R54 = 1

SUC_ms_cyt = 1

R55:

{1}SUC_ms_cyt ⟶ {1}SUC_bs_cyt

v_R55

v_R55 = 1

SUC_bs_cyt = 1

##PRODUCTION OF SUC IN BS FROM DHAP_calvincycle

R56:

{2}TRP_bs_cyt = {1}FRU16BP_bs_cyt

v_R56

v_R56 = 1

R57:

{1}FRU16BP_bs_cyt = {1}HEXP_bs_cyt + {1}Pi_bs_cyt

v_R57

v_R57 = 1

HEXP_bs_cyt = 1

R58:

{1}HEXP_bs_cyt + {1}UTP_bs_cyt = {1}UDPGLC_bs_cyt + {1}PPi_bs_cyt

v_R58

v_R58 = 1

UDPGLC_bs_cyt = 1

R59:

{1}PPi_bs_cyt = {2}Pi_bs_cyt

v_R59

v_R59 = 1

R60:

{1}HEXP_bs_cyt + {1}UDPGLC_bs_cyt = {1}SUC6P_bs_cyt + {1}UDP_bs_cyt

v_R60

v_R60 = 1

SUC6P_bs_cyt = 1

R61:

{1}SUC6P_bs_cyt ⟶ {1}SUC_bs_cyt + {1}Pi_bs_cyt

v_R61

v_R61 = 1

R62:

{1}SUC_bs_cyt = {1}SUC_phl

v_R62

v_R62 = 1

SUC_phl = 1

A.2 PySCeS Input for the Storage Parenchyma

```
# _ms: mesophyll, _s: stroma, _chl: chloroplast, _bs: bundle sheath cell
# _vac: vacuole, _phl: phloem, _apo: apoplast, _com: companion cell
# _stp: storage parenchyma, _cyt: cytoplasm: _sym: symplastic
FIX: SUC_phl SUC_stp_vac UTP_stp_cyt UDP_stp_cyt ATP_stp_cyt ADP_stp_cyt
PPi_stp_cyt Pi_stp_cyt NADplus_stp_cyt NADH_stp_cyt TRP_stp_cyt UDPGA_stp_cyt

R63:
    {1}SUC_phl ⟶ {1}SUC_apo_cyt
    v_R63
v_R63 = 1
SUC_apo_cyt = 1

R64:
    {1}SUC_phl = {1}SUC_stp_cyt
    v_R64
v_R64 = 1
SUC_stp_cyt = 1

R65:
    {1}SUC_apo_cyt ⟶ {1}GLC_apo_cyt + {1}FRU_apo_cyt
    v_R65
v_R65 = 1
SUC_apo_cyt = 1
GLC_apo_cyt = 1
FRU_apo_cyt = 1

R66:
    {1}SUC_apo_cyt ⟶ {1}SUC_stp_cyt
    v_R66
v_SUCuptake = 1

R67:
    {1}FRU_apo_cyt ⟶ {1}FRU_stp_cyt
    v_R67
```

v_R67 = 1
FRU_stp_cyt = 1

R68:
{1}GLC_apo_cyt ⟶ {1}GLC_stp_cyt
v_R68
v_R68 = 1
GLC_stp_cyt = 1

R69:
{1}GLC_stp_cyt + {1}ATP_stp_cyt = {1}HEXP_stp_cyt + {1}ADP_stp_cyt
v_R69
v_R69 = 1
HEXP_stp_cyt = 1

R70:
{1}FRU_stp_cyt + {1}ATP_stp_cyt = {1}HEXP_stp_cyt + {1}ADP_stp_cyt
v_R70
v_R70 = 1

R71:
{1}UDPGLC_stp_cyt + {1}HEXP_stp_cyt = {1}SUC6P_stp_cyt + {1}UDP_stp_cyt
v_R71
v_R71 = 1
SUC6P_stp_cyt = 1
UDPGLC_stp_cyt = 1

R72:
{1}SUC6P_stp_cyt ⟶ {1}SUC_stp_cyt + {1}Pi_stp_cyt
v_R72
v_R72 = 1
SUC_stp_cyt = 1

R73:
{1}UDPGLC_stp_cyt + {1}FRU_stp_cyt = {1}SUC_stp_cyt + {1}UDP_stp_cyt

v_R73
v_R73 = 1

R74:
{1}SUC_stp_cyt ⟶ {1}GLC_stp_cyt + {1}FRU_stp_cyt
v_R74
v_R74 = 1

Vacuole # Carbohydrate uptake

R75:
{1}SUC_stp_cyt ⟶ {1}SUC_stp_vac
v_R75
v_R75 = 1
SUC_stp_vac = 1
# Reactions inside the vacuole

R76:
{1}SUC_stp_vac ⟶ {1}GLC_stp_vac + {1}FRU_stp_vac
v_R76
v_R76 = 1
GLC_stp_vac = 1
FRU_stp_vac = 1

R77:
{1}GLC_stp_vac = {1}GLC_stp_cyt
v_R77
v_R77 = 1

R78:
{1}FRU_stp_vac = {1}FRU_stp_cyt
v_R78
v_R78 = 1

Glycolysis in the storage parenchyma

R79:

{1}HEXP_stp_cyt + {1}ATP_stp_cyt = {1}FRU16BP_stp_cyt + {1}ADP_stp_cyt

v_R79

v_R79 = 1

FRU16BP_stp_cyt = 1

R80:

{1}HEXP_stp_cyt + {1}PPi_stp_cyt = {1}FRU16BP_stp_cyt + {1}Pi_stp_cyt

v_R80

v_R80 = 1

PPi_stp_cyt = 1

R81:

{1}FRU16BP_stp_cyt ⟶ {2}TRP_stp_cyt

v_R81

v_R81 = 1

glycolysis = 1

Fibre formation

R82:

{1}UDPGLC_stp_cyt + {2}NADplus_stp_cyt ⟶ {1}UDPGA_stp_cyt + {2}NADH_stp_cyt

v_R82

v_R82 = 1

UDPGA_stp_cyt = 1

R83:

{1}UTP_stp_cyt + {1}HEXP_stp_cyt ⟶ {1}UDPGLC_stp_cyt + {1}PPi_stp_cyt

v_R83

v_R83 = 1

UTP_stp_cyt = 1

A.3 Elementary Modes: Net Reaction Sequences for the Leaf.

E.M.	Reaction Sequence
1	(6 R46)⟶ -R30⟶ -R31 ⟶(6 R45)⟶ (-6 R41)⟶ (6 R43)⟶ (6 R42)⟶ (6 R48)⟶(6 R47)⟶ (6 R44)
2	(12 R24)⟶ (12 R17)⟶ (12 R14)⟶ (12 R15)⟶ (12 R13)⟶ (4 R40)⟶ (12 R19) ⟶ R58⟶ R59⟶ (4 R38)⟶ (4 R39)⟶ (4 R34)⟶ (4 R35)⟶ (4 R36)⟶ (4 R37) ⟶ (4 R30)⟶ (4 R31)⟶ (-12 R28)⟶ (12 R9)⟶ (12 R23)⟶ (2 R56)⟶ (12 R22)⟶ (2 R57)⟶ R62⟶ R60 ⟶ (4 R41)⟶ (4 R32)⟶ (12 R27)⟶ (12 R26)⟶ (4 R29)⟶ (12 R16)⟶ (12 R10)⟶ (12 R18) ⟶(12 R4)⟶ (12 R1)⟶ (12 R2)⟶ (12 R3)⟶ R61⟶ (12 R25)⟶ (4 R33)⟶ (12 R21)⟶ (12 R20)
3	(12 R14)⟶ (12 R13)⟶ (12 R11)⟶ (4 R40)⟶ R58⟶ R59⟶ (4 R38)⟶ (4 R39)⟶ (4 R34)⟶ (4 R35)⟶ (4 R36)⟶ (4 R37)⟶ (4 R30)⟶ (4 R31)⟶ (12 R5)⟶ (12 R7)⟶ (12 R9)⟶ (2 R56)⟶ (2 R57)⟶ R62⟶ R60 ⟶(4 R41) ⟶(4 R32)⟶ (4 R29)⟶ (12 R12)⟶ (12 R10)⟶ (12 R4)⟶ (12 R6)⟶ (12 R1)⟶ (12 R2)⟶ (12 R3)⟶ (12 R8)⟶ R61⟶ (4 R33)
4	(12 R24)⟶ (4 R46)⟶ (12 R17)⟶ (12 R14) ⟶ (12 R15) ⟶ (12 R13)⟶ (4 R40)⟶ (12 R19)⟶ (4 R38)⟶ (4 R39) ⟶ (4 R34)⟶ (4 R35)⟶ (4 R36)⟶ (4 R37)⟶ (3.33333 R30) ⟶ (3.33333 R31) ⟶ (-12 R28)⟶ (12 R9)⟶ R52⟶ R53⟶ (12 R23)⟶ (2 R50)⟶ R51 ⟶ (12 R22)⟶ (4 R45)⟶ R62⟶ (4 R32)⟶ (4 R43)⟶ (4 R42)⟶ (12 R27)⟶ (12 R26)⟶ (2 R49)⟶ (4 R29)⟶ (12 R16)⟶ (12 R10) ⟶ (4 R47) ⟶ (12 R18)⟶ R54 ⟶ R55⟶ (12 R4)⟶ (12 R1)⟶ (12 R2)⟶ (12 R3)⟶ (4 R44)⟶ (12 R25) ⟶ (4 R33) ⟶ (12 R21) ⟶ (12 R20)
5	(12 R24)⟶ (4 R46)⟶ (12 R17)⟶ (12 R14) ⟶ (12 R15)⟶ (12 R13)⟶ (4 R40)⟶ (12 R19)⟶ R58⟶ R59 ⟶ (4 R38)⟶ (4 R39) ⟶ (4 R34)⟶ (4 R35)⟶ (4 R36) ⟶

	(4 R37)⟶ (3.33333 R30) ⟶ (3.33333 R31)⟶ (-12 R28)⟶ (12 R9)⟶ (12 R23)⟶ (2 R56)⟶ (12 R22)⟶ (2 R57)⟶ (4 R45)⟶ R62⟶ R60 ⟶ (4 R32) ⟶ (4 R43)⟶ (4 R42)⟶ (12 R27)⟶ (12 R26)⟶ (4 R48)⟶ (4 R29)⟶ (12 R16) ⟶ (12 R10)⟶ (4 R47)⟶ (12 R18)⟶ (12 R4) ⟶ (12 R1)⟶ (12 R2) ⟶(12 R3)⟶ (4 R44)⟶ R61⟶ (12 R25)⟶ (4 R33)⟶ (12 R21)⟶ (12 R20)
6	(4 R46)⟶ (12 R14)⟶ (12 R13)⟶ (12 R11)⟶ (4 R40)⟶ (4 R38)⟶ (4 R39) ⟶ (4 R34)⟶ (4 R35)⟶ (4 R36)⟶ (4 R37)⟶ (3.33333 R30)⟶ (3.33333 R31)⟶ (12 R5)⟶ (12 R7) ⟶ (12 R9)⟶ R52⟶ R53⟶ (2 R50) ⟶ R51⟶ (4 R45)⟶ R62 ⟶ (4 R32)⟶ (4 R43) ⟶ (4 R42)⟶ (2 R49)⟶ (4 R29) ⟶ (12 R12)⟶ (12 R10)⟶ (4 R47)⟶ R54 ⟶ R55⟶ (12 R4)⟶ (12 R6)⟶ (12 R1)⟶ (12 R2)⟶ (12 R3)⟶ (12 R8)⟶ (4 R44)⟶ (4 R33)
7	(4 R46) ⟶ (12 R14)⟶ (12 R13)⟶ (12 R11)⟶ (4 R40)⟶ R58⟶ R59⟶ (4 R38)⟶ (4 R39)⟶ (4 R34) ⟶ (4 R35)⟶ (4 R36)⟶ (4 R37)⟶ (3.33333 R30)⟶ (3.33333 R31)⟶ (12 R5)⟶ (12 R7)⟶ (12 R9)⟶ (2 R56)⟶ (2 R57)⟶ (4 R45)⟶ R62 ⟶ R60⟶ (4 R32)⟶ (4 R43) ⟶ (4 R42)⟶ (4 R48) ⟶ (4 R29)⟶ (12 R12)⟶ (12 R10)⟶ (4 R47)⟶ (12 R4)⟶ (12 R6)⟶ (12 R1)⟶ (12 R2)⟶ (12 R3)⟶ (12 R8) ⟶ (4 R44) ⟶ R61 ⟶ (4 R33)
8	(12 R24)⟶ (12 R17)⟶ (12 R14)⟶ (12 R15)⟶ (12 R13) ⟶ (4 R40)⟶ (12 R19)⟶ (4 R38)⟶ (4 R39) ⟶ (4 R34)⟶ (4 R35)⟶ (4 R36)⟶ (4 R37) ⟶ (4 R30)⟶ (4 R31)⟶ (-12 R28)⟶ (12 R9)⟶ R52⟶ R53⟶ (12 R23)⟶ (2 R50)⟶ R51⟶ (12 R22)⟶ R62⟶ (4 R41)⟶ (4 R32)⟶ (12 R27)⟶ (12 R26)⟶ (2 R49)⟶ (-4 R48)⟶ (4 R29)⟶ (12 R16)⟶ (12 R10) ⟶ (12 R18) ⟶ R54 ⟶ R55⟶ (12 R4)⟶ (12 R1)⟶ (12 R2)⟶ (12 R3)⟶ (12 R25)⟶ (4 R33)⟶ (12 R21)⟶ (12 R20)
9	(12 R14)⟶ (12 R13) ⟶ (12 R11) ⟶ (4 R40) ⟶ (4 R38)⟶ (4 R39)⟶ (4 R34)⟶ (4 R35)⟶ (4 R36)⟶ (4 R37) ⟶ (4 R30) ⟶ (4 R31)⟶ (12 R5)⟶ (12 R7) ⟶ (12 R9) ⟶

	R52⟶ R53 ⟶ (2 R50)⟶ R51⟶ R62⟶ (4 R41)⟶ (4 R32)⟶ (2 R49)⟶ (-4 R48)⟶ (4 R29)⟶ (12 R12)⟶ (12 R10) ⟶ R54⟶ R55⟶ (12 R4) ⟶ (12 R6)⟶ (12 R1) ⟶ (12 R2) ⟶ (12 R3) ⟶ (12 R8)⟶ (4 R33)
10	(12 R24)⟶ (24 R46)⟶ (12 R17)⟶ (12 R14)⟶ (12 R15)⟶ (12 R13)⟶ (4 R40)⟶ (12 R19)⟶ (4 R38) ⟶ (4 R39)⟶ (4 R34) ⟶ (4 R35)⟶ (4 R36)⟶ (4 R37)⟶ (-12 R28)⟶ (12 R9)⟶ R52⟶ R53⟶ (12 R23)⟶ (2 R50)⟶ R51 ⟶ (12 R22)⟶ (24 R45)⟶ R62⟶ (-20 R41)⟶ (4 R32)⟶ (24 R43)⟶ (24 R42) ⟶ (12 R27)⟶ (12 R26)⟶ (2 R49)⟶ (20 R48)⟶ (4 R29)⟶ (12 R16)⟶ (12 R10)⟶ (24 R47)⟶ (12 R18)⟶ R54⟶ R55 ⟶ (12 R4) ⟶ (12 R1)⟶ (12 R2)⟶ (12 R3)⟶ (24 R44)⟶ (12 R25) ⟶ (4 R33) ⟶ (12 R21)⟶ (12 R20)
11	(12 R24)⟶ (24 R46)⟶ (12 R17)⟶ (12 R14)⟶ (12 R15) ⟶ (12 R13)⟶ (4 R40) ⟶ (12 R19) ⟶ R58⟶ R59⟶ (4 R38)⟶ (4 R39)⟶ (4 R34) ⟶ (4 R35)⟶ (4 R36) ⟶ (4 R37)⟶ (-12 R28)⟶ (12 R9)⟶ (12 R23)⟶ (2 R56)⟶ (12 R22) ⟶ (2 R57)⟶ (24 R45)⟶ R62⟶ R60⟶ (-20 R41)⟶ (4 R32)⟶ (24 R43)⟶ (24 R42)⟶ (12 R27)⟶ (12 R26) ⟶ (24 R48) ⟶ (4 R29) ⟶ (12 R16) ⟶ (12 R10)⟶ (24 R47) ⟶ (12 R18)⟶ (12 R4)⟶ (12 R1)⟶ (12 R2)⟶ (12 R3) ⟶ (24 R44) ⟶ R61⟶ (12 R25) ⟶ (4 R33)⟶ (12 R21)⟶ (12 R20)
12	(24 R46)⟶ (12 R14)⟶ (12 R13)⟶ (12 R11)⟶ (4 R40)⟶ (4 R38)⟶ (4 R39) ⟶ (4 R34) ⟶ (4 R35)⟶ (4 R36)⟶ (4 R37)⟶ (12 R5)⟶ (12 R7)⟶ (12 R9)⟶ R52⟶ R53⟶ (2 R50)⟶ R51⟶ (24 R45)⟶ R62 ⟶ (-20 R41)⟶ (4 R32)⟶ (24 R43)⟶ (24 R42)⟶ (2 R49)⟶ (20 R48) ⟶ (4 R29) ⟶ (12 R12)⟶ (12 R10)⟶ (24 R47) ⟶ R54⟶ R55⟶ (12 R4)⟶ (12 R6)⟶ (12 R1)⟶ (12 R2)⟶ (12 R3)⟶ (12 R8)⟶ (24 R44)⟶ (4 R33)
13	(24 R46)⟶ (12 R14)⟶ (12 R13) ⟶ (12 R11) ⟶ (4 R40) ⟶ R58 ⟶ R59⟶ (4 R38)⟶ (4 R39)⟶ (4 R34)⟶

	(4 R35)⟶ (4 R36)⟶ (4 R37)⟶ (12 R5)⟶ (12 R7)⟶ (12 R9)⟶ (2 R56)⟶ (2 R57) ⟶ (24 R45) ⟶ R62 ⟶ R60 ⟶ (-20 R41)⟶ (4 R32)⟶ (24 R43) ⟶ (24 R42)⟶ (24 R48)⟶ (4 R29)⟶ (12 R12) ⟶ (12 R10)⟶ (24 R47) ⟶ (12 R4)⟶ (12 R6)⟶ (12 R1)⟶ (12 R2)⟶ (12 R3)⟶ (12 R8)⟶ (24 R44)⟶ R61 ⟶ (4 R33)

Table A.1: Net reactions of elementary modes in the leaf. All modes are irreversible and the PySCeS input file can be found in A1.

A.4 Elementary Modes: Net Reaction Sequences for the Storage Parencyma

E.M.	Reaction Sequence
1	R64⟶R75
2	-R64⟶ R63⟶ R66
3	R63⟶ R66⟶ R75
4	R70 ⟶R71⟶ -R73⟶R72
5	-R79⟶ R80
6	R73⟶ R69⟶ R83 ⟶R74
7	R70⟶ R71⟶ R69⟶ R83⟶ R72⟶ R74
8	-R64 ⟶R73 R⟶77⟶ R78 ⟶R69 ⟶R83⟶R76
9	-R64⟶ R73⟶ R69⟶ R65⟶ R83 ⟶R63 ⟶R67⟶R68
10	R73⟶ R77⟶ R78⟶ R69⟶R83⟶ R76⟶ R75
11	R73⟶ R69 ⟶R65⟶ R83⟶ R63 ⟶R67⟶ R68⟶ R75
12	R64⟶ R70⟶ -R73 ⟶R83⟶ (2 R82)
13	-R64⟶ R70⟶ R71⟶ R77⟶ R78⟶ R69⟶ R83⟶ R72⟶ R76
14	-R64⟶ R70⟶ R71 ⟶R69⟶ R65⟶ R83⟶ R63⟶ R72⟶ R67 ⟶ R68
15	R70⟶ -R73⟶ R83⟶ (2 R82)⟶ R63⟶ R66
16	R70⟶ R77⟶ R78⟶ R69 ⟶(2 R83)⟶ (2 R82) ⟶R76
17	R70 ⟶R71⟶ R77⟶ R78 ⟶R69⟶ R83⟶ R72⟶ R76⟶ R75
18	R70⟶ R69⟶ R65⟶ (2 R83)⟶ (2 R82)⟶ R63 ⟶R67⟶ R68
19	R70 ⟶R71⟶ R69⟶ R65⟶ R83⟶ R63⟶ R72⟶ R67⟶ R68 ⟶ R75
20	R64⟶ R70⟶ R69⟶ (2 R83)⟶ (2 R82)⟶ R74
21	R70⟶ R69⟶ (2 R83) ⟶(2 R82)⟶ R63⟶ R66⟶ R74
22	(2 R79)⟶ R70⟶ R77⟶ R78⟶ R69⟶ (2 R81)⟶ R76
23	(2 R79)⟶ R70⟶ R69⟶R65⟶ (2 R81)⟶ R63⟶ R67⟶ R68
24	R64⟶ (2 R79)⟶ R70⟶ R69⟶ (2 R81)⟶ R74
25	(2 R79)⟶ R70⟶ R69⟶ (2 R81)⟶ R63⟶ R66 ⟶R74
26	(2 R80)⟶ R70⟶ R77⟶ R78⟶ R69⟶(2 R81)⟶ R76
27	(2 R80)⟶ R70⟶ R69⟶ R65⟶(2 R81)⟶ R63⟶ R67⟶ R68
28	R64 ⟶(2 R80)⟶ R70 ⟶R69 ⟶(2 R81)⟶ R74
29	(2 R80)⟶ R70⟶ R69⟶ (2 R81)⟶ R63⟶ R66⟶ R74
30	R64 ⟶R79⟶ R70 ⟶-R73⟶ R81 ⟶R82
31	R64⟶ R80⟶ R70⟶ -R73⟶ R81⟶ R82
32	R79⟶ R70⟶ -R73⟶ R81⟶ R82⟶ R63⟶ R66
33	R80⟶ R70 ⟶-R73⟶ R81⟶ R82⟶ R63⟶ R66

Table A.2: Elementary Modes of the Storage Parenchyma. All elementary modes are irreversible and the reactions can be found in Appendix A2.

Appendix B

B.1 PySCeS Input File for Kinetic Model of Carbon Fixation

FIX: HCO3_ms_cyt CO2_bs_chl NADPH_ms_chl NADP_ms_chl NADP_bs_chl NADPH_bs_chl Pi_ms_cyt Pi_ms_chl AMP_ms_chl ATP_ms_chl PPi_ms_chl

TRANS_pep:

PEP_ms_chl + Pi_ms_cyt = PEP_ms_cyt + Pi_ms_chl

Vf_pep∗A_ms_chl/(K_chl_pep∗K_cyt_pi)∗(PEP_ms_chl∗Pi_ms_cyt/V_ms_chl - PEP_ms_cyt∗Pi_ms_chl/(Keq_pep∗V_ms_cyt))/((1+PEP_ms_chl/(K_chl_pep∗V_ms_chl) + PEP_ms_cyt/(K_cyt_pep∗V_ms_cyt))∗(1 + Pi_ms_cyt/K_cyt_pi + Pi_ms_chl/K_chl_pi))

PEPCase:

HCO3_ms_cyt + PEP_ms_cyt $\longrightarrow$ OAA_ms_cyt + Pi_ms_cyt

Vf_pepc∗V_ms_cyt/(K_hco∗K_pep)∗(HCO3_ms_cyt∗PEP_ms_cyt/V_ms_cyt) /((1 + HCO3_ms_cyt/K_hco + MAL_ms_cyt/(Ki_ms_mal∗V_ms_cyt) + OAA_ms_cyt/(K_ms_oaa∗V_ms_cyt))∗(1 + PEP_ms_cyt/(K_pep∗V_ms_cyt) + Pi_ms_cyt /K_ms_pi))

TRANS_oaa_ms:

OAA_ms_cyt = OAA_ms_chl

Vf_oaa∗A_ms_chl/K_cyt_oaa∗(OAA_ms_cyt/V_ms_cyt - OAA_ms_chl/(Keq_oaa∗V_ms_chl))/(1 + OAA_ms_cyt/(K_cyt_oaa∗V_ms_cyt) + MAL_ms_cyt/(Ki_oaa_mal∗V_ms_cyt) + OAA_ms_chl/(K_chl_oaa∗V_ms_chl))

NPMDH:

OAA_ms_chl + NADPH_ms_chl = MAL_ms_chl + NADP_ms_chl

Vf_npm∗V_ms_chl/(K_oaa∗K_ms_nadph)∗(OAA_ms_chl∗NADPH_ms_chl/V_ms_chl
- MAL_ms_chl∗NADP_ms_chl/(Keq_ms_oaa∗V_ms_chl))/((1 + OAA_ms_chl/
(K_oaa∗V_ms_chl) + MAL_ms_chl/(K_mal∗V_ms_chl))∗(1 + NADPH_ms_chl/
K_ms_nadph + NADP_ms_chl/K_ms_nadp))

TRANS_mal_ms:
MAL_ms_chl = MAL_ms_cyt
Vf_mal_ms∗A_ms_chl/K_chl_mal∗(MAL_ms_chl/V_ms_chl - MAL_ms_cyt/(Keq_chl_mal∗
V_ms_cyt))/(1 + MAL_ms_chl/(K_chl_mal∗V_ms_chl) + OAA_ms_chl/
(Ki_mal_oaa∗V_ms_chl) + MAL_ms_cyt/(K_cyt_mal∗V_ms_cyt))

DIF_mal_bs:
MAL_ms_cyt = MAL_bs_cyt
Kd_mal∗(MAL_ms_cyt/V_ms_cyt - MAL_bs_cyt/V_bs_cyt)

TRANS_mal_bs:
MAL_bs_cyt = MAL_bs_chl
Vf_bs_mal∗A_bs_chl/K_bs_chl_mal∗(MAL_bs_cyt/V_bs_cyt - MAL_bs_chl/(Keq_bs_mal∗
V_bs_chl))/(1 + MAL_bs_cyt/(K_bs_cyt_mal∗V_bs_cyt) + MAL_bs_chl/(K_bs_chl_mal∗
V_bs_chl))

NPME:
MAL_bs_chl + NADP_bs_chl = CO2_bs_chl + PA_bs_chl + NADPH_bs_chl
Vf_npme∗V_bs_chl/(K_bs_mal∗K_bs_nadp)∗(MAL_bs_chl∗NADP_bs_chl/V_bs_chl
-
CO2_bs_chl∗PA_bs_chl∗NADPH_bs_chl/(Keq_npme∗V_bs_chl))/
((1 + MAL_bs_chl/(K_bs_mal∗V_bs_chl) + _bs_chl/(K_bs_pyr∗V_bs_chl) +
CO2_bs_chl/K_bs_co2)∗(1 + NADP_bs_chl/K_bs_nadp + NADPH_bs_chl/K_bs_nadph))

TRANS_pyr_bs:
_bs_chl = _bs_cyt
Vf_pyr_bs∗A_bs_chl/K_bs_chl_pyr∗(_bs_chl/V_bs_chl - _bs_cyt/(Keq_bs_pyr∗
V_bs_cyt))/(1 + _bs_chl/(K_bs_chl_pyr∗V_bs_chl) + _bs_cyt/(K_bs_cyt_pyr∗
V_bs_cyt))

```
DIF_bs_ms:
    PA_bs_cyt = PA_ms_cyt
Kd_pyr*(PA_bs_cyt/V_bs_cyt - PA_ms_cyt/V_ms_cyt)

TRANS_pyr_ms:
    PA_ms_cyt = PA_ms_chl
Vf_pyr_ms*A_ms_chl/K_ms_cyt_pa*(PA_ms_cyt/V_ms_cyt - PA_ms_chl/
(Keq_ms_pa*V_ms_chl))/(1 + _ms_cyt/(K_ms_cyt_pa*V_ms_cyt) +
PA_ms_chl/(K_ms_chl_pa*V_ms_chl))

PPDK:
    PA_ms_chl + ATP_ms_chl + Pi_ms_chl = PEP_ms_chl + PPi_ms_chl + AMP_ms_chl
(Vf_ppdk*V_ms_chl/(K_ms_pyr*K_ms_atp*K_ppdk_pi))*(PA_ms_chl*
ATP_ms_chl*Pi_ms_chl/V_ms_chl - PEP_ms_chl*AMP_ms_chl*PPi_ms_chl/(Keq_ppdk*
V_ms_chl))/((1 + PA_ms_chl/(K_ms_pa*V_ms_chl) + PEP_ms_chl/(K_ms_pep*
V_ms_chl))*(1 + ATP_ms_chl/K_ms_atp + AMP_ms_chl/K_ms_amp)*(1 + Pi_ms_chl
/K_ppdk_pi + PPi_ms_chl/K_ms_ppi))

#Compartmental volumes are in uL, which means our molar amounts must be
in nmoles in order for concentrations to be in mM
#Since all Vmaxes are expressed as umoles/min/mg chlorophyll we need to use
a reference volume 25 uL equiv to 1 mg chlorophyll

V_ms_chl = 25.0*1.0*1.17
V_ms_cyt = 25.0*2.7*1.17
V_bs_chl = 25.0*1.0 # equivalent to 1mg chlorophyl
V_bs_cyt = 25.0*2.7

A_ms_chl = 1.0
A_bs_chl = 1.11 # 24.71/22.25

#External Concentrations (mM)
HCO3_ms_cyt = 0.041
CO2_bs_chl = 0.7
NADP_ms_chl = 1.37
```

NADPH_ms_chl = 0.48
NADP_bs_chl = 0.29 #previously modelled value
NADPH_bs_chl = 0.21 #previously modelled value
ATP_ms_chl = 0.85
AMP_ms_chl = 0.15
Pi_ms_cyt = 10.0
Pi_ms_chl = 15.0
PPi_ms_chl = 10.0

#Trans_pep
Vf_pep = 10.0
K_chl_pep = 0.086
K_cyt_pi = 0.045
Keq_pep = 1000.0
K_chl_pi = 0.05
K_cyt_pep = 0.8

#PEPCase
Vf_pepc = 27.5
K_hco = 0.027
K_pep = 8.7
K_ms_oaa = 0.25 #random
Ki_ms_mal = 0.97
K_ms_pi = 0.06 #random

#Trans_oaa
Vf_oaa = 1.5
K_cyt_oaa = 0.053
K_chl_oaa = 0.053
Keq_oaa = 1000.0
Ki_oaa_mal = 7.5

#NPMDH
Vf_npm = 9.5
K_oaa = 0.056

K_ms_nadph = 0.024
K_ms_nadp = 0.073
K_mal = 32.0
Keq_ms_oaa = 30000

#Trans_mal_ms
Vf_mal_ms = 0.7
K_chl_mal = 0.5
K_cyt_mal = 0.5
Keq_chl_mal = 1000.0
Ki_mal_oaa = 0.3 #random

#Diffusion of malate from ms to bs
Kd_mal = 10.0

#Trans_mal_bs
Vf_bs_mal = 0.6
K_bs_chl_mal = 0.4
K_bs_cyt_mal = 0.4
Keq_bs_mal = 1000.0

#NPME
Vf_npme = 10.7
K_bs_mal = 0.12
K_bs_nadp = 0.0046
Keq_npme = 51 #(mM)
K_bs_pa = 0.04
K_bs_co2 = 1.1
K_bs_nadph = 0.045

#Trans_pyr_bs
Vf_pa_bs = 0.8
K_bs_chl_pa = 0.6
Keq_bs_pa = 1000.0
K_bs_cyt_pa = 0.6

#Diffusion of pyr from bs to ms
Kd_pa = 10.0

#Trans_pyr_ms
Vf_pa_ms = 1.5
K_ms_cyt_pa = 0.85
Keq_ms_pa = 1000.0
K_ms_chl_pa = 1.5

#PPDK
Vf_ppdk = 6.5
K_ms_pyr = 0.11
K_ms_atp = 0.009
K_ppdk_pi = 0.56
Keq_ppdk = 0.0002
K_ms_pep = 0.11
K_ms_amp = 0.13
K_ms_ppi = 0.32

#Initial values
PEP_ms_chl = 0.0
PEP_ms_cyt = 4800 # nmoles, which in 25 uL gives 100.0 mM
OAA_ms_cyt = 0.0
OAA_ms_chl = 0.0
MAL_ms_cyt = 0.0
MAL_ms_chl = 0.0
MAL_bs_chl = 0.0
MAL_bs_cyt = 0.0
PA_bs_cyt = 0.0
PA_bs_chl = 0.0
PA_ms_cyt = 0.0
PA_ms_chl = 0.0

B.2 The Set of Steady-State Metabolite Concentrations

A comparative study of the predicted steady-state values when PEP or MAL are initialise as 4800 nmoles (150mM) respectively whilst the other metabolites are initialised as zero. There is only one flux running through the conserved cycle therefore, regardless of the starting points, the same steady-state values are obtained.

Metabolite & Compartment	PEP initialised (mM)	PA initialised (mM)
PEP_ms_chl_ss	0.03	0.03
PEP_ms_cyt_ss	2.68	2.68
OAA_ms_cyt_ss	0.07	0.07
OAA_ms_chl_ss	0.01	0.01
MAL_ms_chl_ss	47.45	47.45
MAL_ms_cyt_ss	6.99	6.99
MAL_bs_cyt_ss	6.93	6.93
MAL_bs_chl_ss	0.32	0.32
PA_bs_chl_ss	18.19	18.19
PA_bs_cyt_ss	7.92	7.92
PA_ms_cyt_ss	7.86	7.86
PA_ms_chl_ss	18.97	18.97

Table B.1: The steady-state data of metabolite concentration when PEP in the mesophyll is initialised as the only metabolite having a initial value. These steady-state values are alike when PEP in the mesophyll cytoplasm is set to zero and PA in the bundle sheath chloroplast is initialised as 4800 nmoles.

B.3 Flux Control Coefficients

The control of the enzymes or transporters on the steady-state flux through the decarboxylating enzyme, NADP-malic enzyme.

'JNPME'	
cc$\{JNPME\}\{PPDK\}$	0.000335
cc$\{JNPME\}\{TRANS_pa_ms\}$	0.070930
cc$\{JNPME\}\{PEPCase\}$	0.039553
cc$\{JNPME\}\{TRANS_oaa_ms\}$	0.002036
cc$\{JNPME\}\{NPMDH\}$	0.000008
cc$\{JNPME\}\{TRANS_mal_ms\}$	0.123270
cc$\{JNPME\}\{DIF_mal_bs\}$	0.000444
cc$\{JNPME\}\{TRANS_mal_bs\}$	0.612160
cc$\{JNPME\}\{NPME\}$	0.010945
cc$\{JNPME\}\{TRANS_pa_bs\}$	0.096802
cc$\{JNPME\}\{DIF_bs_ms\}$	0.000269
cc$\{JNPME\}\{TRANS_pep\}$	0.043252

Table B.2: The Flux Control Coefficients in the Carbon Fixation Pathway. The control coefficients will remain the same for each of the enzyme or transporters as this is a moiety-conserved cycle.

Bibliography

[1] L. Acerenza and H. Kacser. Enzyme kinetics and metabolic control. *Biochem. J.*, 269:697–707, 1990.

[2] C.S. Andreo, D.H. Gonzalez, and A.A. Iglesias. Higher plant phosphoenolpyruvate carboxylase. *FEBS LETTERS*, 213:1–8, 1987.

[3] N. Aoki and R. Kanai. Reappraisal of the role of sodium in the light-dependent active transport of pyruvate into mesophyll chloroplasts of C4 plants. *Plant Cell Physiol.*, 38(11):1217–1225, 1997.

[4] A.P. Arkin. Simulac & deduce. 2001.

[5] R. S. Bandurski. Further studies on the enzymatic synthesis of oxalacetate from phosphorylenolpyruvate and carbon dioxide. *J. Biol. Chem.*, 217:137–150, 1955.

[6] H. Bauwe. An efficient method for the determination of K_m values of HCO_3^- of phosphoenolpyruvate carboxylase. *Planta*, 169:356–360, 1986.

[7] C. Bell, J. Jones, G.F. Milford, and R.A Leigh. The effects of crop nutrition on sugar beet quality. *Aspects Appl. Biol.*, 32:29–26, 1992.

[8] Tim Bray, Jean Paoli, and C. M. Sperberg-McQueen. Extensible Markup Language (XML) 1.0 - W3C recommendation 10-february-1998. Technical Report REC-xml-19980210, 1998.

[9] J.N. Burnell and M.D. Hatch. Low bundle sheath carbonic anhydrase is apparently essential for effective C4 pathway operation. *Plant Physiol.*, 86:1252–1256, 1988.

[10] K.S.R. Chapman, J.A. Berry, and M.D. Hatch. Photosynthetic metabolism in bundle sheath cells of C4 species *Zea mays*: Sources of ATP and NADPH

and the contribution of photosystem ii. *Archives of Biochemistry and Biophysics*, 202:330–341, 1980.

[11] J.R. Coleman. *Photosynthesis: Physiology and Metabolism*, pages 353–367. Kluwer Academic Publishers, 2000.

[12] Athel Cornish-Bowden. *Fundamentals of Enzyme Kinetics*. Portland Press, London, 1995.

[13] D. Day and M.D. Hatch. Dicarboxylate transport in maize mesophyll chloroplasts. *Archives of Biochemistry and Biophysics*, 211:738–742, 1981.

[14] L. Dever, K. Bailey, R. Leegood, and P. Lea. Control of photosynthesis in *Amaranthus edulis* mutants with reduced amounts of PEP Carboxylase. *Aust. J. Plant Physiol.*, 24:468–476, 1997.

[15] J. Edelman, A. I. Schoolar, and W.B. Bonnor. Permeability of sugarcane chloroplasts to sucrose. *Journal of Experimental Botany*, 22:524–545, 1971.

[16] G. E. Edwards, V. R. Franceschi, M. S. B. Ku, E. V. Voznesenskaya, V. I. Pyankov, and C. S. Andreo. Compartmentation of photosynthesis in cells and tissues of C4 plants. *J. Exp. Bot.*, 52:577–590, 2001.

[17] G. E. Edwards and D.A. Walker. *C3, C4: Mechanisms, and environmental regulation of photosynthesis.* Blackwell Scientific, Oxford, 1983.

[18] G.E. Edwards and C.S. Andreo. NADP-malic enzyme from plants. *Phytochemistry*, 31:1845–1857, 1992.

[19] G.E. Edwards, R.M. Lilley, S. Craig, and M.D. Hatch. Isolation of intact and functional chloroplasts from mesophyll and bundle sheath protoplasts of the C4 plant *Panicum miliceum*. *Plant Physiol.*, 63:821–827, 1979.

[20] H. Edwards, G.E.and Nakamoto, J.N. Burnell, and M.D. Hatch. Pyruvate, Pi dikinase and NADP-malate dehydrogenase in C4 photosynthesis:properties and mechanism of light/dark regulation. *Annu.Rev.Plant Physiol.*, 36:255–286, 1985.

[21] U. Flugge, M. Stitt, and H. Heldt. Light-driven uptake of pyruvate into mesophyll chloroplasts from maize. *FEBS LETTERS*, 183:335–339, 1985.

[22] U.-I. Flugge and H.W. Heldt. Metabolite translocators of the chloroplast envelope. *Annu. Rev. Plant Physiol. Plant Mol. Biol.*, 42:129–144, 1991.

[23] J. Frank, J. Vater, and J.F. Holzwarth. Kinetics and equilibrium binding of phosphoenolpyruvate to phosphoenolpyruvate carboxylase from *Zea mays*. *Phys. Chem. Chem. Phys*, 1:455–461, 1999.

[24] L.E. Fridlyand and R. Scheibe. Regulation of the calvin cycle for CO_2 fixation as an example for general control mechanisms in metabolic cycles. *BioSystems*, 51:79–93, 1999.

[25] R.T. Furbank and M.D. Hatch. Mechanism of C4 photosynthesis: Size and composition of the inorganic carbon pool in bundle sheath cells. *Plant Physiol.*, 85:958–964, 1987.

[26] R.T. Furbank and M.D. Hatch. Mechanism of C4 photosynthesis: The size and composition of the inorganic carbon pool in bundle sheath cells. *Plant Physiol.*, 85:958–964, 1987.

[27] K.T. Glasziou. Accumulation and transformation of sugars in sugarcane stalks. *Plant Physiol.*, pages 895–901, 1960.

[28] K.T. Glasziou and K.R. Gayler. Sugar transport: Occurrence of trehalase activity in sugar cane. *Planta*, 85:299–02, 1969.

[29] A.J. Hanekom, J-H.S. Hofmeyr, J.L. Snoep, and J.M. Rohwer. Experimental evidence for the allosteric modifier saturation as predicted by the bisubstrate hill equation. *IEE Proc.-Syts. Biol.*, 153:342–345, 2006.

[30] I. Harary, S. Korey, and S. Ochoa. Biosynthesis of dicarboxylic acids by carbon dioxide fixation. *J. Biol.Chem.*, 203:595–604, 1953.

[31] C.E. Hartt, H.P. Kortschak, A.J. Forbes, and G.O. Burr. Translocation of C^{14} in sugarcane. *Plant Physiology*, 38:305–318, 1963.

[32] M.D. Hatch. The C4-pathway of photosynthesis: evidence for an intermediate pool of carbon dioxide and the identity of the donor C4-dicarboxylic acid. *Biochem J.*, 125:425–432, 1971.

[33] M.D. Hatch. Properties and regulation of adenylate kinase from *Zea mays* leaf operating in C4 pathway photosynthesis. *Aust. J. Plant Physiol.*, 9:287–296, 1982.

[34] M.D. Hatch. C4 photosynthesis: a unique blend of modified biochemistry, anatomy and ultrastructure. *Biochimica et Biophysica Acta*, 895:81–106, 1987.

[35] M.D. Hatch, L. Droscher, U.I. Flugge, and H.W. Heldt. A specific translocator for oxaloacetate transport in chloroplasts. *FEBS LETTERS*, 178:15–19, 1984.

[36] M.D. Hatch and K.T. Glasziou. Direct evidence for translocation of sucrose in sugarcane leaves and stems. *Plant Physiology*, pages 180–184, 1963.

[37] M.D. Hatch and T. Kagawa. Photosynthetic activities of isolated bundle sheath cells in relation to differing mechanisms of C4 pathway photosynthesis. *Archives of Biochemistry and Biophysics*, 175:39–53, 1976.

[38] M.D. Hatch, T. Kagawa, and S. Craig. Subdivision of C4 pathway species based on differing C4 acid decarboxylating systems and ultrastructural features. *Aust. J. Plant Physiol.*, 2:111–28, 1975.

[39] M.D. Hatch and C.B. Osmond. *Encyclopedia of Plant Physiology: Transport in plants III*, pages 144–184. Springer Verlag, Berlin, 1976.

[40] M.D. Hatch, J.A. Sacher, and K.T. Glasziou. Sugar accumulation cycle in sugar cane. I. studies on enzymes of the cycle. *Plant Physiol.*, pages 338–343, 1962.

[41] M.D. Hatch and C.R. Slack. Photosynthesis by sugar-cane leaves. *Biochemical Journal*, 101:103–111, 1966.

[42] M.D. Hatch and C.R. Slack. A new enzyme for the interconversion of pyruvate and phosphopyruvate and its role in the C4 dicarboxylic acid pathway of photosynthesis. *Biochem J.*, 106:141–146, 1968.

[43] M.D. Hatch and C.R. Slack. Pyruvate, pi dikinase from leaves. *Methods Enzymol.*, 42C:212–219, 1975.

[44] U. Heber. Metabolite exchange between chloroplasts and cytoplasm. *Ann. Rev. Plant Physiol.*, 25:393–421, 1974.

[45] H.W. Heldt. *Intracellular interactions and transport processes*, volume 3 of *Encyclopedia of Plant Physiology*, pages 137–143. Springer-Verlag Berlin, 1976.

[46] A.V. Hill. The possible effects of the aggregation of molecules of haemoglobin on its dissociation curves. *J. Physiol.(London)*, 40:iv–vii, 1910.

[47] J-H. S. Hofmeyr. Metabolic control analysis in a nutshell. In *Proceedings of the 2nd International Conference on Systems Biology*, 2001.

[48] J.-H.S. Hofmeyr and J.M. Rohwer. Computational systems biology, 2002.

[49] S. Hoops, S. Sahle, R. Gauges, C. Lee, J. Pahle, N. Simus, M. Singhal, L. Xu, P. Mendes, and U. Kummer. COPASI-a COmplex PAthway Simulator. *Bioinformatics*, 22:3067–3074, 2006.

[50] M. Hucka, A. Finney, H.M. Sauro, H. Bolouri, J. Doyle, and H. Kitano. The ERATO systems biolody workbench: enabling interaction and exchange between software tools for computational biology. In *Pacific Symposium on Biocomputing*, 2002.

[51] M. Hucka, A. Finney, H.M. Sauro, H. Bolouri, J.C. Doyle, H. Kitano, A.P. Arkin, B.J. Bornstein, D. Bray, A. Cornish-Bowden, A.A. Cuellar, S. Dronov, E.D. Gilles, M. Ginkel, V. Gor, I.I. Goryanin, W.J. Hedley, T.C. Hodgman, J.-H. Hofmeyr, P.J. Hunter, N.S. Juty, J.L. Kasberger, A. Kremling, U. Kummer, N. Le Novere, L.M. Louw, D. Lucio, P. Mendes, E. Minch, E.D. Mjolsness, Y. Nakayama, M.R. Nelson, P.F. Nielsen, T. Sakurada, J.C. Schaff, B.E. Shapiro, T.S. Shimizu, H.D. Spence, J. Stelling, K. Takahashi, M. Tomita, J. Wagner, and J. Wang. The systems biology markup language (SBML): a medium for representing and exchange of biochemical network models. *Bioinformatics*, 19:524–531, 2003.

[52] A. A. Iglesias. NADP-dependent malate dehydrogenase (decarboxylating) from sugar cane leaves. kinetic properties of different oligomeric structures. *European Journal of Biochemistry*, 192:729–733, 1990.

[53] C.L.D. Jenkins, J.N. Burnell, and M.D. Hatch. Form of inorganic carbon involved as a product and as an inhibitor of C4 acid decarboxylases operating in C4 photosythesis. *Plant Physiol.*, 85:952–957, 1987.

[54] C.L.D Jenkins, R.T. Furbank, and M.D. Hatch. Inorganic carbon diffusion between C4 mesophyll and bundle sheath cells: Direct bundle sheath CO_2 assimilation in intact leaves in the presence of an inhibitor of the C4 pathway. *Plant Physiol.*, 91:1356–1363, 1989.

[55] C.L.D. Jenkins, R.T. Furbank, and M.D. Hatch. Mechanism of C4 photosynthesis: A model describing the inorganic carbon pool in bundle sheath cells. *Plant Physiol.*, 91:1372–1381, 1989.

[56] C.L.D. Jenkins and M.D. Hatch. Properties and reaction mechanism of C4 leaf pyruvate, Pi dikinase. *Arch. Biochem. Biophys.*, 239:53–62, 1985.

[57] H.S. Johnson and M.D. Hatch. Properties and regulation of leaf nicotinamide-adenine dinucleotide phosphate-malate dehydrogenase and 'malate' enzyme in plants with the C4-dicarboxylic acid pathway of Photosynthesis. *Biochem. J.*, 119:273–280, 1970.

[58] H. Kacser and J.A. Burns. The control of flux. *Symp. Soc. Exp. Biol.*, 27:65–104, 1973.

[59] T. Kagawa and P.L. Bruno. NADP-malate dehydrogenase from leaves of Zea mays:purification and physical, chemical and kinetic properties. *Arch. Biochem. Biophys.*, 260:674–695, 1988.

[60] R. Kanai and G.E. Edwards. *The Biochemistry of C4 Photosynthesis*, chapter 3, pages 49–88. Academic Press, 1999.

[61] K.J. Kauffman, P. Prakash, and J.S. Edwards. Advances in flux balance analysis. *Current Opinion in Biotechnology*, 14:491–496, 2003.

[62] M.U.F. Kirschbaum, C. Kuppers, M. Schneider, C. Giersch, and S. Noe. Modelling photosynthesis in fluctuating light with inclusion of stomatal conductance, biochemical activation and pools of key photosynthetic intermediates. *Planta*, 204:16–26, 1998.

[63] E. Komor, M. Thom, and A. Maretzki. The mechanism of sugar uptake by sugarcane suspension cells. *Planta*, 153:181–192, 1981.

[64] A. Laisk and G.E. Edwards. A mathematical model of C4 photosynthesis: The mechanism of concentrating CO_2 in NADP-malic enzyme type species. *Photosynthesis Research*, 66:199–224, 2000.

[65] N. Le Novere and T. S. Shimizu. STOCHSIM: modelling of stochastic biomolecular processes. *Bioinformatics*, 17(6):575–576, 2001.

[66] R.C. Leegood. The intercellular compartmentation of metabolites in leaves of *Zea mays* L. *Planta*, 164:163–171, 1985.

[67] R.C. Leegood. *Photosynthesis:Physiology and Metabolism*, volume 9, pages 459–469. Kluwer Academic Publishers, 2000.

[68] R.C. Leegood and R.P. Walker. *C4 Plant Biology*, page 103. Academic Press, San Diego, 1999.

[69] L.M. Loew and J.C. Schaff. The Virtual Cell: a software environment for computational cell biology. *TRENDS in Biotechnology*, 19:401–406, 2001.

[70] J. E. Lunn and R. T. Furbank. Tansley Review no. 105 sucrose biosynthesis in C4 plants. *New Phytologist*, 143:221–237, 1999.

[71] A.A. Lushnikov, T. Ahonen, T. Vesala, E. Juurola, E. Nikinmaa, and P. Hari. Modelling of light-driven RuBP regeneration, carboxylation and CO2 diffusion for leaf photosynthesis. *J. theor. Biol.*, 188:143–151, 1997.

[72] B.C. Mayne, A.M. Dee, and G.E. Edwards. Photosynthesis in mesophyll protoplasts and bundle sheath cells of various types of C4 plants. III. fluorescence emission spectra, delayed light emission, and P700 content. *Z. Pflanzenphysiol. Bd*, 74:275–291, 1974.

[73] A.J. McCormick, M.D. Cramer, and D.A. Watt. Sink strength regulates photosynthesis in sugarcane. *New Phytologist*, 2006.

[74] G.A.L. McNaughton, C.A. Fewson, M.B. Wilkins, and H.G. Nimmo. Purification, oligomerization state and malate sensitivity of maize leaf phosphoenolpyruvate carboxylase. *Biochem. J.*, 261:349–355, 1989.

[75] P. Mendes. GEPASI: a software package for modelling the dynamics, steady-states and control of biochemical and other systems. *Comput. Appl. Biosci.*, 9:563–571, 1993.

[76] J. Monod, J. Wyman, and J.-P. Changeux. On the nature of allosteric conditions: A plausible model. *J. Mol. Biol.*, 12:88–118, 1965.

[77] J.A. Morgan and D. Rhodes. Mathematical modeling of plant metabolic pathways. *Metabolic Engineering*, 4:80–89, 2002.

[78] J. Murmu, B. Chinthapalli, and A.S. Raghavendra. Light inactivation of NADP-malic enzyme in leaves of maize: Marginal increase in activity, but marked change in regulatory properties of enzyme. *J. Plant. Physiol.*, 160:51–56, 2003.

[79] N. Ogawa, T. Kai, N. Yabuta, and K. Izui. Phosphoenolpyruvate carboyxlase of maize leaves: an improved method for purification and reduction of the inhibitory effect of malate by ethylene glycol and bicarbonate. *Plant Cell Physiol.*, 38:76–80, 1997.

[80] J. Ohnishi, U.I. Flugge, and H.W. Heldt. Phosphate translocator of mesophyll and bundle sheath chloroplasts of a C4 plant, panicum miliaceum l. *Plant Physiol.*, 91:1507–1511, 1989.

[81] J-I. Ohnishi and R. Kanai. Pyruvate uptake by mesophyll and bundle sheath chloroplasts of a C4 plant, *Panicum miliaceum* l. *Plant Cell. Physiol.*, 28:1–10, 1987.

[82] M.H. O'Leary. Phosphoenolpyruvate carboxylase: An enzymologist's view. *Ann. Rev. Plant Physiol.*, 33:297–315, 1982.

[83] P. Olesen. Plasmodesmata between mesophyll and bundle sheath cells in relation to the exchange of C4-acids. *Planta*, 123:199–202, 1975.

[84] B.G. Olivier, J.M. Rohwer, and J.-H.S. Hofmeyr. Modelling cellular systems with PySCes. *Bioinformatics*, 21(4):560–561, 2005.

[85] C.B. Osmond. Metabolite transport in C4 photosynthesis. *Aust. J. Biol. Sci.*, 24:159–163, 1971.

[86] B.O. Palsson, N.D. Price, and J.A. Papin. Development of network-based pathway definitions: the need to analyze real metabolic networks. *TRENDS in Biotechnology*, 21:195–198, 2003.

[87] J.A. Papin, Price N.A., S.J. Wiback, D.A. Fell, and B.O. Palsson. Metabolic pathways in the post-genome era. *TRENDS in Biochemical Sciences*, 28:250–259, 2003.

[88] G. Pettersson and U. Ryde-Pettersson. A mathematical model of the calvin photosynthetic cycle. *Eur. J. Biochem.*, 175:661–672, 1988.

[89] T. Pfeiffer, I. Sánchez-Valdenebro, J. C. Nuño, F. Montero, and S. Schuster. METATOOL: for studying metabolic networks. *Bioinformatics*, 15:251–257, 1999.

[90] Mark G. Poolman, Hulya Olcer, Julie C. Lloyd, Christine A. Raines, and David A. Fell. Computer modelling and experimental evidence for two steady states in the photosynthetic calvin cycle. *Eur J Biochem*, 268:2810–2816, 2001.

[91] M.G. Poolman, D.A. Fell, and C.A. Raines. Elementary modes analysis of photosynthate metabolism in the chloroplast stroma. *Eur. J. Biochem.*, 270:430–439, 2003.

[92] M.G. Poolman, D.A. Fell, and S. Thomas. Modelling photosynthesis and its control. *Journal of Experimental Botany*, 51:319–328, 2000.

[93] N.D. Price, I. Famili, D.A. Beard, and B. Palsson. Letter to the editor. extreme pathways and Kirchhoff's Second Law. *Biophysical Journal*, 83:2879–2882, 2002.

[94] A.L. Rae, C.P.L. Grof, R.E. Casu, and G.D. Bonnett. Sucrose accumulation in the sugarcane stem:pathways and control points for transport and compartmentation. *Field Crops Research*, 92:159–168, 2005.

[95] K. Robinson-Beers and R.F. Evert. Ultrastructure of and plasmodesmatal frequency in mature leaves of sugarcane. *Planta*, 184:291 – 306, 1991.

[96] J.M. Rohwer and F.C. Botha. Analysis of sucrose accumulation in the sugar cane culm on the basis of *in vitro* kinetic data. *Biochem. J.*, 358:437–445, 2001.

[97] J.M. Rohwer, A.J. Hanekom, C. Crous, J.L. Snoep, and J.-H.S. Hofmeyr. Evaluation of a simplified generic bi-substrate rate equation for computational systems biology. *IEE Proc.-Syst. Biol.*, 153:338–341, 2006.

[98] J.A. Sacher, M.D. Hatch, and K.T. Glasziou. Sugar accumulation cycle in sugar cane. iii physical & metabolic aspects of cycle in immature storage tissues. *Plant Physiol.*, 38:348–354, 1962.

[99] C. Schilling, D. Letscher, and B. Palsson. Theory for the systematic definition of metabolic pathways and their use in interpreting metabolic function from a pathway-oriented perspective. *J. theor. Biol.*, 203:229–248, 2000.

[100] S. Schuster, T. Dandekar, and D.A. Fell. Detection of elementary flux modes in biochemical networks:a promising tool for pathway analysis and metabolic engineering. *TIBTECH*, 17:53–60, 1999.

[101] S. Schuster, D.A. Fell, and T. Dandekar. A general definition of metabolic pathways usful for systematic organization and analysis of complex metabolic networks. *Nature America Inc*, 18:326–332, 2000.

[102] S. Schuster and C. Hilgetag. On elementary flux modes in biochemical reaction systems at steady state. *J. Biol. Syst.*, 2:165–182, 1994.

[103] J-M. Schwartz and M. Kanehisa. Quantitative elementary mode analysis of metabolic pathways: the example of yeast glycolysis. *BMC Bioinformatics*, 7:186, 2006.

[104] I.S. Sheoran and R. Singh. *Concepts in Photobiology. Photosynthesis and photomorphogenesis.*, pages 430–473. Kluwer Academic Publishers, 1999.

[105] R. G. Shulman. Hard days in the trenches. *FASEB J.*, 12:255–258, 1998.

[106] J. L. Snoep, F. Bruggeman, B. G. Olivier, and H. V. Westerhoff. Towards building the silicon cell: a modular approach. *BioSystems*, 83(2-3):207–216, 2006.

[107] N.G. Soros, C.L. an Dengler. Quantitative leaf anatomy of C3 and C4 cyperaceae and comparisons with the poaceae. *Int. J. Plant Sci.*, 159:480–491, 1998.

[108] L. Stelling. Mathematical models in microbial systems biology. *Current Opinion in Microbiology*, 7:513–518, 2004.

[109] R. Steuer, A. N. Nesi, A. R. Fernie, T. Gross, B. Blasius, and J. Selbig. From structure to dynamics of metabolic pathways: application to the plant mitochondrial tca cycle. *Bioinformatics*, 23:1378–1385, 2007.

[110] R.A. Steuer, T. Gross, and B. Selbig, J.and Bllasius. Structural kinetic modelling of metabolic networks. *Proc. Nat. Acad. Sci.USA*, 103:11868–11873, 2006.

[111] JR Stiles and TM. Bartol. *Monte Carlo methods for simulating realistic synaptic microphysiology using MCell.*, pages 87–127. Computational Neuroscience: Realistic Modeling for Experimentalists., (2001).

[112] J.R. Stiles, D. Van Helden, T. Bartol, E. Salpeter, and M. Salpeter. Miniature endplate current rise times less than 100 μs from improved dual recordings can be modeled with passive acetylcholine diffusion from a synaptic vesicle. *Proc. Natl. Acad. Sci. USA*, 93:5747–5752, 1996.

[113] T. Sugiyama. Purification, molecular and catalytic properties of pyruvate dikinase from the maize leaf. *Biochemistry*, 12:2862–2868, 1973.

[114] B. Teusink, J. Paasarge, C.A. Reijenga, E. Esgalhado, C. van der Weijden, M. Schepper, M. Walsh, B. Bakker, K. van Dam, H. Westerhoff, and J. Snoep. Can yeast glycoloysis be understood in terms of *in vitro* kinetics of the constituent enzymes? testing biochemistry. *Eur. J. Biochem.*, 267:5313–5329, 2000.

[115] M. Tomita, K. Hashimoto, K. Takahashi, T. Simon Shimizu, Y. Matsuzaki, F. Miyoshi, K. Saito, S. Tanida, K. Yugi, J. Craig Venter, and C.A. Hutchison III. E-CELL: software environment for whole-cell simulation. *Bioinformatics*, 15:72–84, 1999.

[116] K. Uedan and T. Sugiyama. Purification and characterization of phosphoenolpyruvate carboxylase from maize leaves. *Plant Physiol.*, 57:906–910, 1976.

[117] H. Usuda. Nonaqueous purification of maize mesophyll chloroplasts. *Plant Physiol.*, 87:427–430, 1988.

[118] H. Usuda, M.S.B. Ku, and G.E. Edwards. Activation of NADP-malate dehydrogenase, pyruvate,Pi dikinase and fructose 1,6-bisphosphate in relation to photosynthetic rate in maize. *Plant Physiol.*, 76:238–243, 1984.

[119] L. Uys, F.C. Botha, J.-H. S. Hofmeyr, and J.M. Rohwer. Kinetic model of sucrose accumulation in maturing sugarcane culm tissue. *Phytochemistry*, 2007.

[120] D. Voet and J.G. Voet. *Biochemistry*. John Wiley & Sons, Inc., 1995.

[121] S. von Caemmerer and R.T. Furbank. *Modeling C4 Photosynthesis*, chapter 6, pages 173–211. Academic Press, San Diego, 1999.

[122] J. Vu, L. Allen Jr, and R. Gesch. Up-regulation of photosynthesis and sucrose metabolism enzymes in young expanding leaves of sugarcane under elevated growth CO_2. *Plant Science*, 171:123–131, 2006.

[123] H. Weiner, J.N. Burnell, I.E. Woodrow, H.W. Heldt, and M.D. Hatch. Metabolite diffusion into bundle sheath cells from C4 plants: Relation to C4 photosynthesis and plasmodesmata function. *Plant Physiol.*, 88:815–822, 1988.

[124] H. Weiner and H.W. Heldt. Inter- and intracellular distribution of amino acids and other metabolites in maize (*Zea mays* l.) leaves. *Planta*, 187:242–246, 1992.

[125] G. E. Welbaum and F.C. Meinzer. Compartmentation of solutes and water in developing sugarcane stalk tissue. *Plant Physiol.*, 93:1147–1153, 1990.

[126] G.B. West, J.H. Brown, and B.J. Enquist. A general model for the structure and allometry of plant vascular systems. *Nature*, 400:664–667, 1999.

[127] A. Whittaker and F. C. Botha. Carbon partitioning during sucrose accumulation in sugarcane internodal tissue. *Plant Physiol.*, 115:1651–1659, 1997.

[128] S.J. Wiback, R. Mahadevan, and B. Palsson. Reconstructing metabolic flux vectors from extreme pathways: defining the alpha-spectrum. *Journal of Theorectical Biology*, 224:313–324, 2003.

[129] I. Ziegler. Malate dehydrogenase in *Zea mays*: Properties and inhibition by sulfite. *Biochimica et Biophysica Acta*, 364:28–37, 1974.